FINITE DIFFERENCE APPROACH FOR PREDICTING PROBABILISTIC LIFE OF A COMPOSITE CYLINDER SUBJECTED TO THERMAL RANDOM LOADS

by

Vu Ngoc Con

Dissertation submitted to the Graduate Faculty of the
Virginia Polytechnic Institute and State University
in partial fulfillment of the requirements for the degree of
DOCTOR OF PHILOSOPHY
in
Engineering Mechanics

APPROVED:

R. A. Heller, Chairman

L. Meirovitch

M. P. Singh

D. T. Mook

C. B. Ling

M. P. Kamat

March, 1979

Blacksburg, Virginia

ACKNOWLEDGEMENTS

The author wishes to express his sincere appreciation to his advisor, Professor R. A. Heller, for his guidance and support during the course of this study. Special thanks are extended to Dr. M. P. Kamat for some of his ideas on the finite difference part and to Dr. M. P. Singh for his suggestions and ideas. The author is also thankful to Professors L. Meirovitch, D. Mook and C. B. Ling for their encouragements and suggestions during the course of this investigation.

This work has been supported by the U.S. Army Missile Readiness Command, Redstone Arsenal through Contract No. DAA1101-78-R-0847.

Appreciation is extended to Mrs. Peggy Epperly for her excellence in typing this work and to Tim Crooks for his expertise in preparing some of the drawings.

Last, but not least, the author wishes to express his deepest appreciation to his wife, Nguyen Lan Huong, and sister, Vu Thi Tuyet Le for their patience and encouragements and many sacrifices they have made during this endeavor.

TABLE OF CONTENTS

LIST OF FIGURES

LIST OF TABLES

LIST OF SYMBOLS

a	absorptivity
D	diameter of the cylinder, in
E	modulus of elasticity, psi
h	heat convection coefficient, Btu/hr-ft^2-°F
I	incident radiation, Btu/ft^2-hr
i	index for motor layers, i = 1,2,3,4,5
K_i	thermal conductivity, Btu/ft-hr-°F
P_f	probability of failure
p	probability density function
Q_a	heat flux resulting from long-wave radiation emitted by the atmosphere, Btu/ft^2-hr
Q_g	heat flux by conduction into the cylinder, Btu/ft^2-hr
Q_h	heat flux resulting from evaporation, condensation, transpiration and sublimation, But/ft^2-hr
Q_i	heat flux resulting from incident short-wave radiation, But/ft^2-hr
Q_ℓ	heat flux resulting from long-wave radiation emitted by the cylinder surface, Btu/ft^2-hr
Q_r	heat flux resulting from reflected short-wave radiation, Btu/ft^2-hr
R_s,R_e	strength and strain capacity
r_i	radius
T	temperature, °F
T_{air}	ambient temperature
T_m	average of the air temperature and pavement surface temperature

T_{sky}	effective temperature of the sky
V	average daily wind velocity, ft/sec
t	time
α_i	coefficient of thermal expansion
γ_i	thermal diffusivity, in^2/hr
$\Delta\nu_s, \Delta\nu_e$	safety range
Δr_i	space increment
Δt	time increment
Δ	volumetric unit
∂	differential
$\epsilon_r, \epsilon_\theta$	strain, in/in
ϵ	emissivity of the cylinder surface
ϵ_{as}	atmospheric emittance
μ	mean
ν_i	Poisson's ratio
π	3.1416
ζ_i	mass density, lbs sec^2/in^4
$\sigma_r, \sigma_\theta, \sigma_z$	stress, psi
σ	Stefan-Boltzmann constant, 0.1714×10^{-8} Btu/hr-ft^2-R^4

I. INTRODUCTION

Solid propellant rocket motors used for tactical missiles are usually stored for years without careful protection from the environment. The environmental changes include changes of the ambient temperature, solar radiation, wind speed, cloud cover, etc. These changes, of course, vary with location, time of day and season. As a result, over a period of several years, the motors may experience high thermal stresses and strains. Consequently, their useful service life may be terminated by overstress conditions. The purpose of this study is to obtain for given environmental conditions the temperature responses of the motors and using these temperatures to evaluate induced thermal stresses and strains in the propellant. These stresses and strains are then used in a probabilistic failure analysis from which a service life is calculated.

The solid propellant rocket motor considered in the present analysis is modeled as a cylinder consisting of a long hollow propellant layer and a thin steel case. This cylinder with case is placed inside an insulated container. The insulated container, of course, will help to protect the propellant from experiencing the rapid and severe changes in environmental conditions. This arrangement can be modeled as a composite cylinder with five layers as shown in Fig. 1.

Besides heat conduction which exists inside the cylinder, heat convection and solar radiation and the effect of outside wind speed

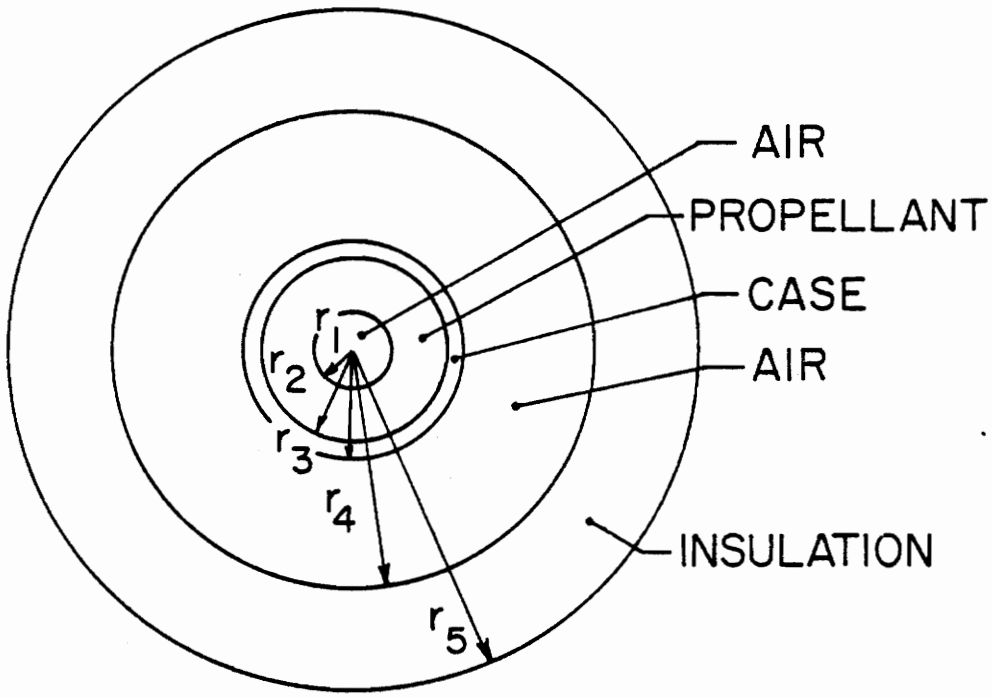

Figure 1. Physical model.

are also considered in the analysis. As will be discussed later, heat convection depends on several things in which the wind speed is considered to be very important. Records of hourly ambient temperature, solar radiation and wind speed measurements supplied by the U.S. National Oceanic and Atmospheric Administration are used for this investigation. Consequently, there will be three random inputs on the surface of the cylinder. The location of interest is Phoenix, Arizona.

It is quite obvious that the geometry of the structure is complicated and on the boundary surface there exist three forms of heat transfer: conduction, convection and radiation. An implicit finite difference scheme has been used in the present analysis to obtain heat transfer solutions, that is, temperature responses at various locations of the propellant. Once temperature responses are available, stress and strain responses are obtained through the use of appropriate expressions relating the stress and strain to temperature.

With the calculated stresses and strains, a probability analysis will be conducted to predict failure of the motor and hence determine its service life.

The following assumptions have been made in the analysis of this problem:

It is assumed that the propellant is an isotropic, homogeneous and continuous medium.

It is further assumed that materials treated in the present investigation have a linear elastic behavior. Also, all material properties are assumed to be time and temperature independent.

II. REVIEW OF LITERATURE

The heat conduction problem of a long cylinder was solved by Dahl back in 1924 [1] by using Bessel and Newman functions.

The state of stress in a long cylinder due to temperatures that vary with the radial coordinate only (axial symmetry) is well known. Kent [2] obtained the solution for both long solid and hollow cylinders with various modes of temperature inputs. The thermal stresses in two concentric joined cylinders where the coefficients of thermal expansion are different were discussed by Poritsky [3]. In a similar analysis, the behavior of composite cylinders was discussed by Gatewood [4].

In an effort to obtain the stress and strain for a hollow cylinder (propellant) with a thin case, Williams et al. [5] started out with the stress equilibrium equation and substituted appropriate boundary conditions to obtain expressions for stress and strain in terms of temperatures and material elastic constants. As will be seen later, this derivation will be presented and used in this study.

In a series of papers [6-11], Heller, Kamat and Singh have developed a probabilistic life prediction methodology for solid rocket motors. These motors were modeled as long hollow cylinders encased in a thin steel case and subjected to environmental temperatures. In references [6-9] the temperature was assumed to consist of an annual mean, a deterministic seasonal cycle and a random variation of the daily temperature. All material properties

were assumed to be elastic and to have a normal distribution except in references [10] and [11] where a Weibull distribution was assumed. In references [10,11] thermal loads are calculated with the use of actual, measured power spectra. Also, in reference [11] the material was treated as a pseudo-viscoelastic material. In this same reference, in addition to the ambient temperature, a simplified, deterministic, solar radiation model was included in the inputs.

Heller et al. analyzed the random process in the frequency domain. From the one-dimensional heat conduction differential equation, the method of separation of variables was used to obtain a Bessel differential equation and then the frequency response function was evaluated.

Using the theory of random process, Heller obtained the power spectral density for the temperature responses. Once the power spectral density is available, other statistical parameters of the output can be evaluated as well.

In a similar study, Cost [12] found the solution in the time domain by using a finite element scheme. The finite element technique helped to obtain the transient temperature throughout the rocket motor and numerical integrations were applied for evaluating the induced stress and strain. In order to obtain the probability distribution of various outputs, Cost used a Monte Carlo simulation technique.

Recently, Okono [13] solved the similar problem but the material was treated as nonlinear viscoelastic; again a finite element technique was employed to obtain the transient temperature throughout

the motor.

In all of the above mentioned references [6-12], the surface temperature of the cylinder is assumed to be identical to the ambient temperature.

III. HEAT EXCHANGE AT THE CYLINDER SURFACE

3.1 Formulation

The rocket motor can be considered as a long axisymmetric cylinder (plane strain problem). The heat flow within the cylinder may be modeled by the so-called one-dimensional heat conduction equation

$$\frac{\partial^2 T(r,t)}{\partial r^2} + \frac{1}{r}\frac{\partial T(r,t)}{\partial r} = \frac{1}{\gamma}\frac{\partial T(r,t)}{\partial t} \qquad (3.1)$$

in which

$T(r,t)$ = space and time dependent temperature

γ = thermal diffusivity

In reality, solar radiation and ambient temperature come into each part of the surface of the cylinder with different intensities and values around the circumference. It is quite obvious that, in the case of solar radiation, the complete surface of the cylinder does not absorb the same amount of solar radiation. In fact, only the upper half surface of the cylinder receives most of the solar radiation. In the present case, it is appropriate to assume that the cylinder receives the same amount of environmental input all around its circumference because the encased propellant is inside an insulated container which makes the propellant relatively insensitive to short term environmental variations. The change in temperature within the propellant is extremely slow as compared to the rapid change in input temperatures. This argument will become clearer in the latter

part of this study and justify the use of the one-dimensional heat conduction equation.

From Fig. 1, the boundary conditions are

B.C. 1 $$\left.\frac{\partial T}{\partial r}\right|_{r=0} = 0 \tag{3.2}$$

B.C. 2 $$T_1(r_1,t) = T_2(r_1,t) \tag{3.3}$$

B.C. 3 $$K_1 \frac{\partial T_1(r_1,t)}{\partial r} = K_2 \frac{\partial T_2(r_1,t)}{\partial r} \tag{3.4}$$

B.C. 4 $$T_2(r_2,t) = T_3(r_2,t) \tag{3.5}$$

B.C. 5 $$K_2 \frac{\partial T_2(r_2,t)}{\partial r} = K_3 \frac{\partial T_3(r_2,t)}{\partial r} \tag{3.6}$$

B.C. 6 $$T_3(r_3,t) = T_4(r_3,t) \tag{3.7}$$

B.C. 7 $$K_3 \frac{\partial T_3(r_3,t)}{\partial r} = K_4 \frac{\partial T_4(r_3,t)}{\partial r} \tag{3.8}$$

B.C. 8 $$T_4(r_4,t) = T_5(r_4,t) \tag{3.9}$$

B.C. 9 $$K_4 \frac{\partial T_4(r_4,t)}{\partial r} = K_5 \frac{\partial T_5(r_4,t)}{\partial r} \tag{3.10}$$

B.C. 10 $$K_5 \frac{\partial T(r_5,t)}{\partial r} + h(T - T_{air}) = aF(t) \tag{3.11}$$

where

r_i = inner radius of each layer (i=1,2,3,4,5)

h = coefficient of surface heat transfer

T_{air} = ambient temperature of the air

a = absorptivity ($0 < a < 1$)

$F(t)$ = normal component of heat flux entering the cylinder through the surface

K_i = thermal conductivity of each layer

Hence, the task is to solve the differential Eq. (3.1) with its associated boundary conditions (3.2-11). The last boundary condition makes it difficult to obtain a closed form solution of this problem. It becomes even more difficult, if not impossible, to obtain a closed form solution if the material properties are not linear elastic, but time and temperature dependent.

Given such a complex problem, it is appropriate to use a numerical scheme such as finite element or finite difference techniques to obtain solutions.

The finite difference method has been selected to analyze the problem.

3.2 Heat Balance Equation on the Surface of the Cylinder

It is quite obvious that the cylinder surface temperature and air temperature are related to one another. The nature of the relation is one of the most complex. On the cylinder surface there are three known forms of heat transfer, namely heat conduction, convection and solar radiation. Each form by itself is a complex phenomenon. Thus, there exists, on the surface of the cylinder, a fairly complicated boundary condition. In fact, as will be shown later, solar radiation renders the boundary condition nonlinear.

Transfer of heat between the cylinder surface and surrounding air is affected by evaporation and condensation of moisture, by wind

speed, ambient temperature, type of the surface, and by solar radiation.

Before probing into the nature of each of the above-mentioned phenomena it will prove fruitful to introduce the energy balance equation on the surface of the cylinder as follows [14]

$$Q_i - Q_r + Q_a - Q_\ell \pm Q_c \pm Q_h \pm Q_g = 0 \qquad (3.12)$$

where

Q_i = heat flux resulting from incident short-wave radiation, Btu/ft^2-hr;

Q_r = heat flux resulting from reflected; short-wave radiation, Btu/ft^2-hr;

Q_a = heat flux resulting from long-wave radiation emitted by the atmosphere, Btu/ft^2-hr;

Q_ℓ = heat flux resulting from long-wave radiation emitted by the cylinder surface, Btu/ft^2-hr;

Q_h = heat flux resulting from evaporation, condensation, transpiration and sublimation, Btu/ft^2-hr;

Q_g = heat flux by conduction into the cylinder, Btu/ft^2-hr;

Q_c = heat flux by convection, Btu/ft^2-hr.

Eq. (3.12) is nothing but an expression of the conservation of energy. In other words, total energy received by the surface will be transformed into different forms of heat transfer, no energy will be lost.

3.3 Thermal Radiation

It is of interest to discuss thermal radiation in general before discussing the structure of solar radiation.

Thermal radiation involves the transfer of heat from one body to another at lower temperature by electromagnetic waves passing through a separating medium. Most thermal radiation problems involve infrared rays. In the case of solar radiation, a significant amount of energy transfer occurs in the visible range of wave lengths.

Thermal radiation travels through a vacuum with the speed of light (186000 miles per second), travels in straight lines through a homogeneous medium, is converted to heat when it strikes any body which can absorb it, and is reflected and refracted according to the same rules as light.

Fig. 2 shows the changes which may occur when a ray of thermal radiation strikes a surface. Part of the incident radiation (I) may be reflected, part may be absorbed, and part may be transmitted.

3.4 Solar Radiation

It is known that besides the change in ambient temperature which affects the change in temperatures on the cylinder surface, solar radiation also plays an important role in changing surface temperatures.

Straub et al. [15] and Barber [16] have carried out studies of a pavement and measured the relative effect of radiation and air temperature. It was observed that solar radiation has a very

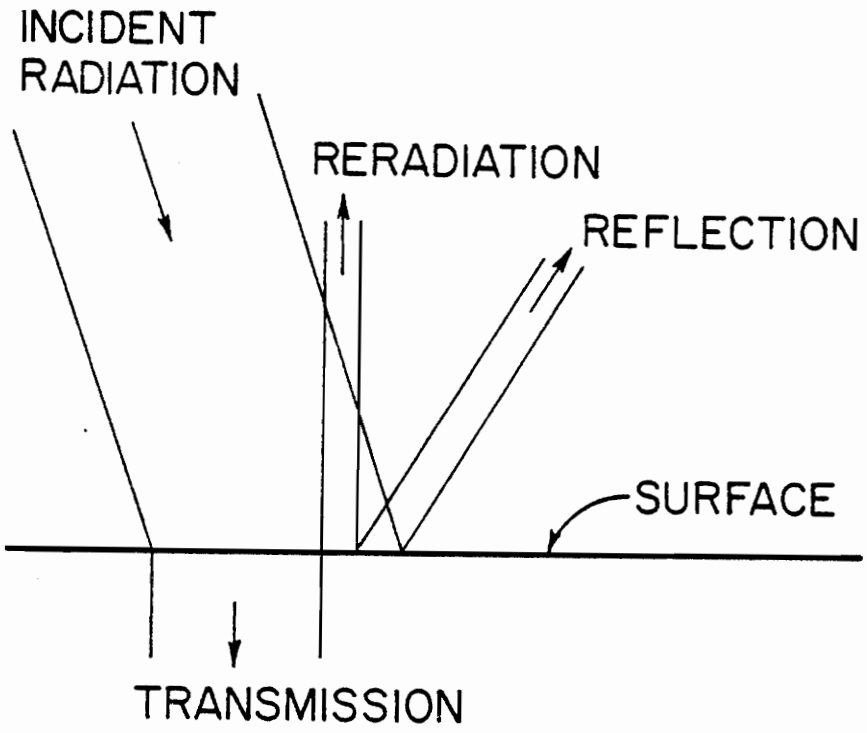

Figure 2. Typical radiation phenomenon on a surface.

significant, and sometimes greater effect than air temperature.

However, one cannot generalize these findings and conclude that, for all cases, solar radiation always has a greater effect than air temperature in heat transfer analysis.

In analyzing the temperature response for the problem at hand, it is however appropriate to consider the existence of solar radiation in the inputs.

3.4a Short-Wave Radiation

Short-wave radiation is regarded as that part of the spectrum of all solar radiation having wave lengths between 0.15 μ and 3.5 μ. Before reaching any object on earth, some solar radiation is absorbed and scattered as it passes through the 90-mile-thick layer of air, water vapor, carbon dioxide, and dust which surround the earth. The amount of solar radiation received by a body on earth depends on the time of the day, time of the year, locations. Figure 3 shows a typical amount of global solar radiation received on two consecutive days in summer in Phoenix, Arizona.

The short-wave radiation is made of two parts: direct and diffused solar radiation. Direct solar radiation is the part which is not reflected by clouds, absorbed or scattered by the atmosphere. On the other hand, the diffused solar radiation is the part which is reflected by clouds and absorbed or scattered by the atmosphere. The amount of both direct and diffused solar radiation reaching a horizontal surface is called global radiation. In the present study, several years of hourly observations of global radiation in Phoenix,

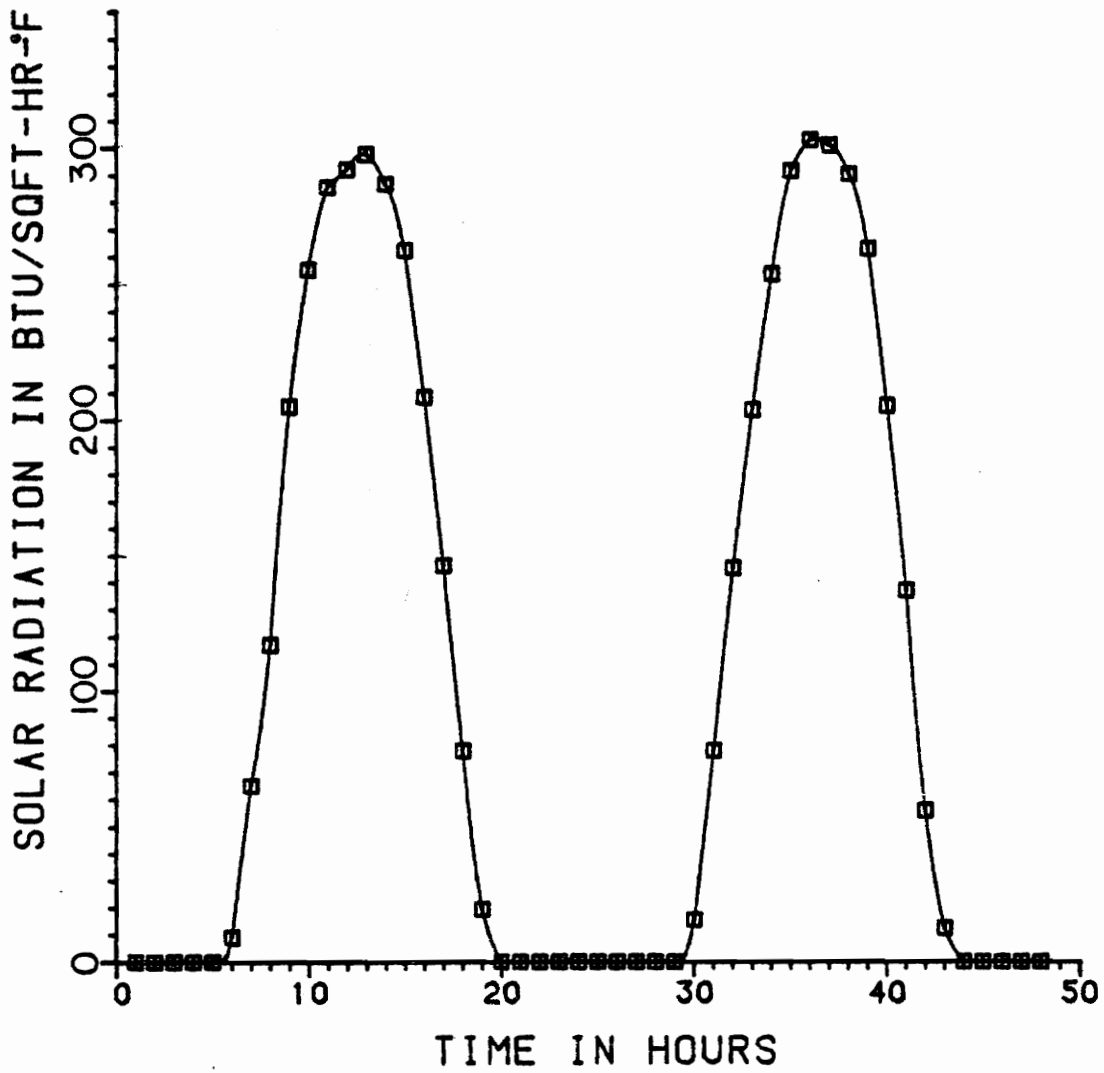

Figure 3. Typical solar radiation.

Arizona have been considered. These measurements were provided by the U.S. National Oceanic and Atmospheric Administration on magnetic tape.

Not all short-wave radiation will be absorbed by an object on earth. In fact, some of this radiation is reflected by the object. The amount of reflected radiation depends largely on the type and color of the surface.

In Eq. (3.12) Q_i represents the incident short-wave radiation (both direct and diffused radiation) and Q_r represents the reflected short-wave radiation. In fact, one can combine the above-mentioned radiations in the following equation:

$$Q_n = Q_i - Q_r = aQ_i \tag{3.13}$$

where

Q_n = absorbed short-wave radiation, Btu/ft^2-hr;

a = absorptivity (varies between 0 and 1)

3.4b Long-Wave Radiation

The long-wave radiation includes that part of the spectrum of radiation having wave lengths between 3.5 μ and 150 μ. This form of radiation exists as an exchange of heat energy between an object on the earth's surface and the sky. Long-wave radiation arises from the fact that all bodies emit radiation.

The long-wave radiation emitted from a unit area of the cylinder surface, denoted by Q_ℓ, is expressed as

$$Q_\ell = \sigma \epsilon T^4 \tag{3.14}$$

where σ = Stefan-Boltzmann constant, 0.1714×10^{-8}, Btu/hr-ft^2-R^4,

ϵ = emissivity of radiation by the cylinder surface

T = absolute surface temperature in degrees Rankine

The long-wave back radiation affecting the energy balance equation, Q_a, is the radiation going back to the earth from the atmosphere and can be written as [17]

$$Q_a = \sigma \epsilon \epsilon_{as} T_{air}^4 \tag{3.15}$$

where ϵ_{as} is the atmospheric emittance expressed in terms of the air temperature as

$$\epsilon_{as} = 1 - 0.261\ (-7.776 \times 10^{-4}\ T_{air}^2)$$

where T_{air} is in degrees Centigrade. Geiger [18] developed an empirical formula for this back radiation as follows

$$Q_a = T_{air}^4 \{G - J(10^{-\rho p})\} \tag{3.16}$$

Combining the works of several authors, Geiger assigned values for the constants in the above formula as follows

$G = 0.77$

$J = 0.28$

$\rho = 0.074$

and the vapor pressure, p, varies between 1 and 10 mm of mercury for the climate near the ground surface.

To simplify the calculations involved, Hunt and Cooke [19] combined both long-wave radiation emitted by the surface and back radiation by the atmosphere discussed earlier in a single equation

$$Q_{\ell w} = Q_{\ell} - Q_a = \epsilon\sigma(T^4 - T_{sky}^4) \tag{3.17}$$

where T and T_{sky} are the absolute temperatures of the surface and sky respectively.

They further used some approximations to obtain an even simpler relation. Their derivation is presented here.

The conduction and convection heat loss is approximated by

$$Q_{cv} = h_c(T - T_{air}) \tag{3.18}$$

where h_c is an experimental coefficient.

Eq. (3.17) can be written in the form

$$Q_{\ell w} = \epsilon\sigma(T^4 - T_{air}^4) + \epsilon\sigma(T_{air}^4 - T_{sky}^4) \tag{3.19}$$

This relation can also be expressed as

$$Q_{\ell w} = h_r(T - T_{air}) + \epsilon\sigma(T_{air}^4 - T_{sky}^4) \tag{3.20}$$

in which

$$h_r = \epsilon\sigma(T^2 + T_{air}^2)(T + T_{air}) \tag{3.21}$$

and h_r is sometimes referred to as radiation heat transfer coefficient. Now the equation on the boundary surface can be expressed as

$$-k\frac{dT}{dr} = (h_c + h_r)(T - T_{air}) + \epsilon\sigma(T_{air}^4 - T_{sky}^4) - aI_n \tag{3.22}$$

in which $h_c + h_r \simeq h$ and is sometimes referred to as heat convection coefficient. The value of h_r is determined by an iterative process

whereby the surface temperature is first assumed in Eq. (3.21) and is used to calculate an improved temperature from Eq. (3.22) (see Chapter 4). The process is repeated until a stabilized h_r is obtained.

Eq. (3.14) represents the so-called reradiation phenomenon which occurs continuously throughout the day and night. During the night time, since there is no short wave radiation, the reradiation acts to release the heat from the cylinder into the surrounding air. Such a phenomenon renders the surface temperature of the cylinder lower than the ambient temperature.

3.5 Heat Convection

The transfer of heat by convection is a process of energy transport by the combined action of heat conduction, mass transport and mixing motion between the cylinder surface and surrounding fluid such as air. It is beyond the scope of the present study to probe into the details of the nature of heat convection.

Heat transfer by convection, Q_c, between the cylinder surface and surrounding air is expressed by the following equation for a unit surface area

$$Q_c = h(T_{air} - T) \tag{3.23}$$

where T is the temperature of the cylinder surface and h is the coefficient of heat convection, $h = h_c + h_r$, which depends on wind velocity, the type of surface, and to a lesser extent on temperature.

Investigators have developed empirical formulas for h_c. For example, Vehrencamp [20] proposed the following equation used for a

flat surface

$$h_c = 122.93\{0.00144\ T_m^{0.3} V^{0.7} + 0.00097(T - T_{air})^{0.3}\} \qquad (3.24)$$

where T = surface temperature in degrees Centigrade

T_m = average of the air temperature and pavement surface temperature in Kelvin degrees and is calculated as follows

$$T_m = 273.0 + \frac{T + T_{air}}{2}$$

V = average daily wind velocity in m/s

Eq. (3.24) takes into consideration both the forced convection resulting from wind turbulence and free convection resulting from the buoyancy effect of air.

Also, for a flat surface, Alford, Ryan and Urban [21] proposed the following formula

$$h_c = 1.3 + 0.62V^{3/4} \qquad (3.25)$$

where V = wind speed in mph. This relation takes into account the forced convection and average reradiation as well.

In the present study, a relation proposed by Ulrich [22] will be used. This relation is applicable for a cylindral object and expressed in terms of wind speed and diameter of the object as follows

$$h_c = 0.6\left(\frac{V}{D}\right)^{0.5} \quad \text{if} \quad 6 \times 10^{-4} < VD < 6$$

or (3.26)

$$h_c = 1.0\left(\frac{V}{D}\right)^{0.5} \quad \text{if} \quad 6 < VD < 60$$

The next term to be discussed is Q_h in Eq. (3.12). This term represents transpiration, condensation, evaporation and sublimation. Scott [23] and Berg [24] indicated that heat transfer caused by transpiration, condensation, evaporation and sublimation may be neglected in the energy balance equation without large error. Even if one wishes to take these affects into account there is no available method or formula to obtain their numerical values. Borg [24], in an effort to obtain a formula, found the results to be highly varied and completely unpredictable.

3.6 Heat Conduction

Heat conduction is defined as a process by which heat flows from a region of high temperature to a region of low temperature within a medium which could be a solid, liquid or gas or between different media in direct contact. In the present case, the medium is a composite cylinder. Heat transfer within the cylinder by conduction can be determined, as proposed, by a finite difference scheme.

The discussion of this section can be illustrated in Figure 4 that shows how different forms of heat transfer come into the energy balance equation. Note that the surface in the figure is flat, but for a cylindrical surface the same phenomena are present.

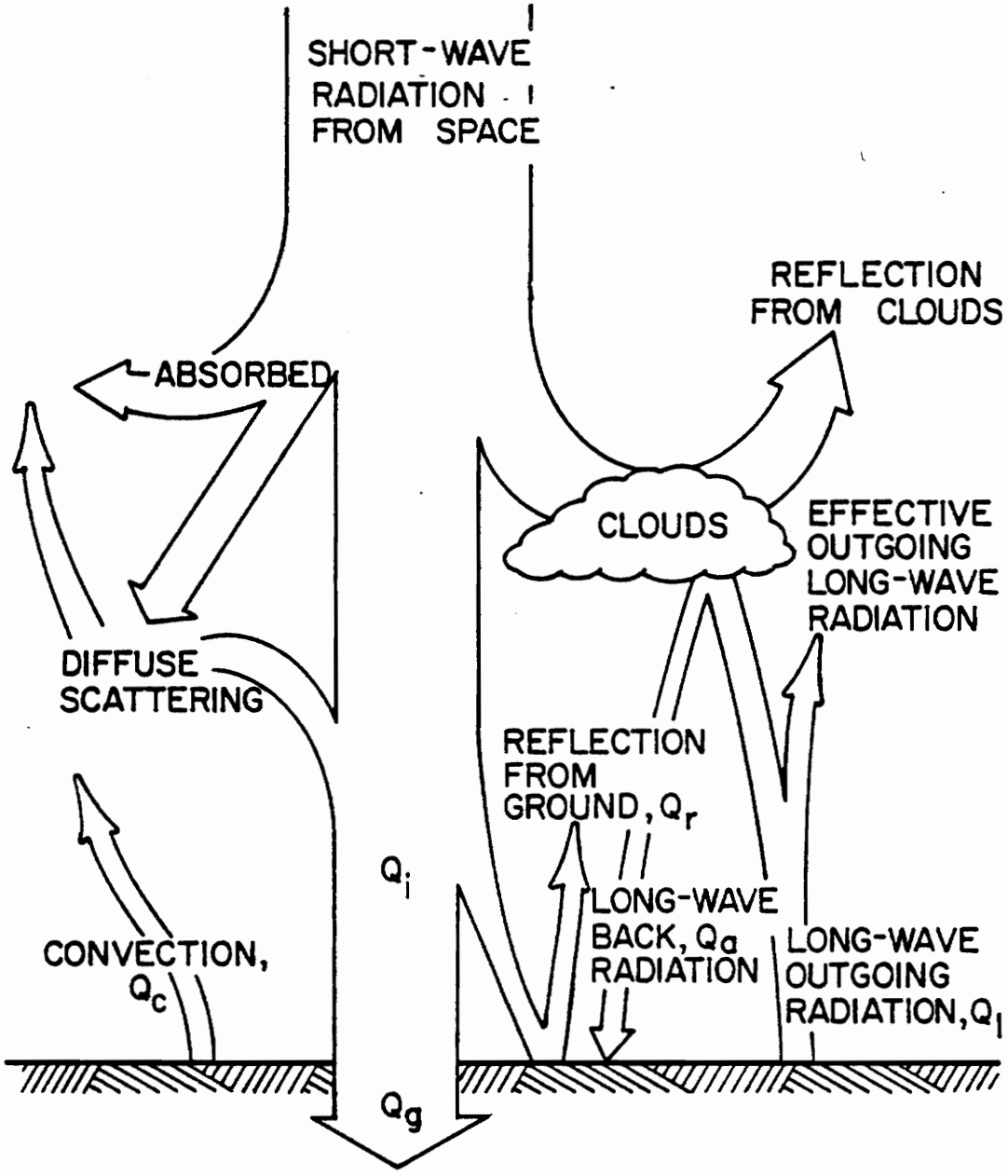

Figure 4. Heat transfer between pavement surface and air on a sunny day [14].

IV. FINITE DIFFERENCE SOLUTION

In finite difference analysis, one can approach a problem either by using the explicit or implicit scheme. In the explicit scheme one can easily set up a single algebraic relation between an unknown temperature at a location at some future time and known temperatures at some corresponding locations at the present time. One can evaluate temperatures at desired locations at any time by this single algebraic equation. In the explicit scheme, however, one has to take the stability condition into consideration. For a given space increment, denoted by Δr, the time increment, Δt, has to be selected in such a way that the stability condition will not be violated. For instance, for a one-dimensional heat transfer problem in Cartesian coordinates, it has been proven that Δt has to be such that [25]

$$\frac{\gamma \Delta t}{(\Delta r)^2} \leq \frac{1}{2}$$

where γ = diffusivity.

The stability considerations have restricted the size of time steps for a given Δr. If the space intervals are chosen rather small to improve accuracy and the calculations performed over a long period of time, say one year, computational problems become enormous. In such a case, the so-called implicit finite difference technique offers a better choice as will be seen shortly.

If one wishes to use the explicit scheme then for the present study where the thickness of each layer of the cylinder is relatively

small, (especially for the steel case: thickness = 0.060 in) Δt has to be very small. Thus the numerical analysis will not be efficient because the temperature response for one year is required. Consequently the implicit scheme has been adopted for this investigation.

In the implicit scheme one is not strictly restricted by the stability condition. Rigorous proofs are given in reference [26]. Because the restriction on the time increment is removed, one can choose a rather larger time increment and save considerable computational work. One drawback of the implicit technique, however, is its relatively complicated mathematical solution in which one has to set up a set of simultaneous algebraic equations whereas in the explicit technique one only needs to set up a single algebraic relation and uses it over and over again to obtain the solutions. As far as programming is concerned it is obvious that the implicit solution will be more involved. But, as will be seen later in the analysis, the set of algebraic equations can be arranged in a matrix form where the matrix coefficients will remain almost unchanged throughout the computation. As such the programming will not be all that complicated.

4.1 Formulation of the Finite Difference Equations

First the governing differential equation is re-written

$$\frac{\partial^2 T(r,t)}{\partial r^2} + \frac{1}{r}\frac{\partial T(r,t)}{\partial r} = \frac{1}{\gamma}\frac{\partial T(r,t)}{\partial t} \qquad (4.1)$$

Before actually deriving the finite difference expressions for the above differential equation some fundamental finite difference relations

will be discussed.

It was proved that by using a Taylor series expansion one can develop approximate finite difference expressions for the derivatives of a function.

The Taylor series expansion of a function T(r) about a point i is written as

$$T_{i+1} = T_i + \Delta r \left.\frac{\partial T}{\partial r}\right|_i + \frac{(\Delta r)^2}{2!} \left.\frac{\partial^2 T}{\partial r^2}\right|_i + \ldots \tag{4.2}$$

and

$$T_{i-1} = T_i - \Delta r \left.\frac{\partial T}{\partial r}\right|_i + \frac{(\Delta r)^2}{2!} \left.\frac{\partial^2 T}{\partial r^2}\right|_i - \ldots \tag{4.3}$$

Subtracting (4.3) from (4.2) to obtain

$$2\Delta r \frac{\partial T}{\partial r} = T_{i+1} - T_{i-1} + O(\Delta r^2)$$

or

$$\frac{\partial T}{\partial r} = \frac{T_{i+1} - T_{i-1}}{2\Delta r} + O(\Delta r^2) \tag{4.4}$$

So the first derivative of T(r) with respect to r has been expressed in the finite difference form. This form is called the central difference and the second term on the right hand side of Eq. (4.4) is the order of error due to truncating, which, in this case, has an order of Δr^2.

From Eq. (4.2)

$$\frac{\partial T}{\partial r} = \frac{T_{i+1} - T_i}{\Delta r} + O(\Delta r) \tag{4.5}$$

This is the so-called forward-difference expression of the first derivative.

Similarly Eq. (4.3) can be written

$$\frac{\partial T}{\partial r} = \frac{T_i - T_{i-1}}{\Delta r} + O(\Delta r) \tag{4.6}$$

which is called the backward difference equation. Note that in both the forward and backward difference equation above the error involved is of the order of Δr.

Similarly one can develop the finite difference expression for 2nd and higher order derivatives. The 2nd derivative becomes

$$\frac{\partial^2 T}{\partial r^2} = \frac{T_{i+1} - 2T_i + T_{i-1}}{\Delta r^2} + O(\Delta r^2) \tag{4.7}$$

Using finite difference technique, one always has to be concerned with the accuracy when developing the finite difference expressions for the differential equation of the problem. Of course, one wishes to have the error involved to be as small as possible. To this end, Crank-Nicolson [27] developed the finite difference expressions in which the error both in time (t) and space (r) is sufficiently small. Essentially, the 2nd derivative of a function T(r,t) can be approximated by the arithmetic average of its finite difference analogs at the points r_i, t_j and r_i, t_{j+1} as

$$\left(\frac{\partial^2 T}{\partial r^2}\right)_{i,j+\frac{1}{2}}$$

$$\approx \frac{1}{2}\left[\frac{T_{i+1,j+1} - 2T_{i,j+1} + T_{i-1,j+1}}{(\Delta r)^2} + \frac{T_{i+1,j} - 2T_{i,j} + T_{i-1,j}}{(\Delta r)^2}\right]$$

$$+ O(\Delta r^2) \tag{4.8}$$

and the second-order-correct expression for the time derivative at the point $r_i, t_{j+\frac{1}{2}}$ is [28]

$$\left(\frac{\partial T}{\partial t}\right)_{i,j+\frac{1}{2}} = \frac{T_{i,j+1} - T_{i,j}}{\Delta t} - \left(\frac{\partial^3 T}{\partial t^3}\right)_{i,j+\frac{1}{2}} \frac{(\Delta t)^2}{24} - \ldots \tag{4.9}$$

In order to derive the finite difference expression for Eq. (4.1), first Eq. (4.2) is multiplied by A and Eq. (4.3) by B with terms having Δr powered greater than 2 neglected

$$AT_{i+1} = AT_i + A\Delta r \frac{\partial T}{\partial r} + A \frac{(\Delta r)^2}{2!} \frac{\partial^2 T}{\partial r^2}$$

$$BT_{i-1} = BT_i - B\Delta r \frac{\partial T}{\partial r} + B \frac{(\Delta r)^2}{2!} \frac{\partial^2 T}{\partial r^2}$$

Adding the resulting equations to obtain

$$AT_{i+1} + BT_{i-1} = AT_i + BT_i + A\Delta r \frac{\partial T}{\partial r} - B\Delta r \frac{\partial T}{\partial r} + A \frac{\Delta r^2}{2!} \frac{\partial^2 T}{\partial r^2} + B \frac{\Delta r^2}{2!} \frac{\partial^2 T}{\partial r^2} \tag{4.10}$$

Simplifying Eq. (4.10)

$$(A - B)\, \Delta r \frac{\partial T}{\partial r} + (A + B) \frac{\Delta r^2}{2!} \frac{\partial^2 T}{\partial r^2} = A(T_{i+1} - T_i) + B(T_{i-1} - T_i) \tag{4.11}$$

is obtained. Now if the left hand side of Eq. (4.11) is to represent the left hand side of Eq. (4.1), then

$$(A - B)\Delta r = \frac{1}{r} \tag{4.12}$$

and

$$(A + B) \frac{\Delta r^2}{2} = 1 \tag{4.13}$$

Solving for A and B,

$$A = \frac{1}{\Delta r^2} + \frac{1}{2r\Delta r} \tag{4.14}$$

and

$$B = \frac{1}{\Delta r^2} - \frac{1}{2r\Delta r} \tag{4.15}$$

result.

Introducing Eqs. (4.14) and (4.15) in the right hand side of Eq. (4.11) to obtain

$$\frac{\partial^2 T}{\partial r^2} + \frac{1}{r}\frac{\partial T}{\partial r} = \left(\frac{1}{\Delta r^2} + \frac{1}{2r\Delta r}\right)(T_{i+1} - T_i) + \left(\frac{1}{\Delta r^2} - \frac{1}{2r\Delta r}\right)(T_{i-1} - T_i) \tag{4.16}$$

or

$$\frac{\partial^2 T}{\partial r^2} + \frac{1}{r}\frac{\partial T}{\partial r} = \frac{1}{\Delta r^2} T_{i+1} - \frac{1}{\Delta r^2} T_i + \frac{1}{2r\Delta r} T_{i+1} - \frac{1}{2r\Delta r} T_i$$

$$+ \frac{1}{\Delta r^2} T_{i-1} - \frac{1}{\Delta r^2} T_i - \frac{1}{2r\Delta r} T_{i-1} + \frac{1}{2r\Delta r} T_i \tag{4.17}$$

Simplifying Eq. (4.17)

$$\frac{\partial^2 T}{\partial r^2} + \frac{1}{r}\frac{\partial T}{\partial r} = \frac{1}{\Delta r}\left\{\frac{1}{2r} T_{i+1} + \frac{1}{\Delta r} T_{i+1} - \frac{2}{\Delta r} T_i - \frac{1}{2r} T_{i-1} + \frac{1}{\Delta r} T_{i-1}\right\} \tag{4.18}$$

results.

As indicated earlier, Crank-Nicolson used an averaging scheme for finite difference equations. More generally one can introduce a weighting factor θ into finite difference equations. For Crank-Nicholson, $\theta = 1/2$. As will be discussed later, θ can have other values.

Introducing θ in Eq. (4.18)

$$\frac{1}{\gamma}\frac{T_{i,j+1} - T_{i,j}}{\Delta t} = \frac{\theta}{\Delta r}\left\{\left(\frac{1}{\Delta r} - \frac{1}{2r}\right) T_{i-1,j+1} - \frac{2}{\Delta r} T_{i,j+1} + \left(\frac{1}{\Delta r} + \frac{1}{2r}\right)T_{i+1,j+1}\right\} + \frac{(1 - \theta)}{\Delta r}\left\{\left(\frac{1}{\Delta r} - \frac{1}{2r}\right)T_{i-1,j} - \frac{2}{\Delta r} T_{i,j} + \left(\frac{1}{\Delta r} + \frac{1}{2r}\right)T_{i+1,j}\right\} \tag{4.19}$$

where the error is of the order of $0(\Delta r^2)$ and $0(\Delta t^2)$.

For programming purposes, the above equation can further be written as

$$\frac{\theta}{\Delta r}\left(\frac{1}{2r} - \frac{1}{\Delta r}\right)T_{i-1,j+1} + \left(\frac{2\theta}{\Delta r^2} + \frac{1}{\gamma\Delta t}\right)T_{i,j+1} - \frac{\theta}{\Delta r}\left(\frac{1}{2r} + \frac{1}{\Delta r}\right)T_{i+1,j+1} = -\left(\frac{1-\theta}{\Delta r}\right)\left(\frac{1}{2r} - \frac{1}{\Delta r}\right)T_{i-1,j} - \left[\frac{2(1 - \theta)}{\Delta r^2} - \frac{1}{\gamma\Delta t}\right]T_{i,j} + \left(\frac{1-\theta}{\Delta r}\right)\left(\frac{1}{2r} + \frac{1}{\Delta r}\right)T_{i+1,j} \tag{4.20}$$

Next the finite difference equations for the boundary conditions will be developed.

As stated before, the boundary conditions involved consist of the boundary conditions at the center of the cylinder, across each interface and finally, on the surface of the cylinder.

Considering the boundary condition at the center first (r = 0), it is assumed that heat conduction is symmetrical with respect to the origin (center). In other words, there is no heat flux at the center

$$\left.\frac{\partial T}{\partial r}\right|_{r=0} = 0 \tag{4.21}$$

so that the 2nd term on the left hand side of Eq. (4.1) becomes

$$\frac{1}{r}\frac{\partial T}{\partial r} = \frac{0}{0} \tag{4.22}$$

Introducing Maclaurin's expansion

$$T'(r) = T'(0) + rT''(0) + \frac{1}{2} r^2 T'''(0) + \ldots \tag{4.23}$$

At the center, Eq. (4.23) becomes

$$\frac{\partial T}{\partial r} = r \frac{\partial^2 T}{\partial r^2}$$

So Eq. (4.1) can be written as

$$\frac{1}{\gamma}\frac{\partial T}{\partial t} = \frac{\partial^2 T}{\partial r^2} + \frac{\partial^2 T}{\partial r^2} = 2\frac{\partial^2 T}{\partial r^2} \tag{4.24}$$

Introducing the weighting factor θ in Eq. (4.24)

$$2\frac{\partial^2 T}{\partial r^2} = 2\left[\theta \frac{T_{1,j+1} - 2T_{0,j+1} + T_{-1,j+1}}{\Delta r^2} + (1-\theta)\frac{T_{1,j} - 2T_{0,j} + T_{-1,j}}{\Delta r^2}\right] \tag{4.25}$$

Due to symmetry $T_{-1} = T_1$ and changing the subscripts 0,1 to 1 and 2, for programming purposes, one can further write the following

$$2\frac{\partial^2 T}{\partial r^2} = 2\left[\theta\left(\frac{2T_{2,j+1} - 2T_{1,j+1}}{\Delta r^2}\right) + (1-\theta)\frac{2T_{2,j} - 2T_{1,j}}{\Delta r^2}\right]$$

or,

$$\frac{1}{\gamma}\frac{T_{1,j+1} - T_{1,j}}{\Delta t} = 2\left[\theta\left(\frac{2T_{2,j+1} - 2T_{1,j+1}}{\Delta r^2}\right) + (1-\theta)\frac{2T_{2,j} - 2T_{1,j}}{\Delta r^2}\right]$$

Finally

$$\frac{1}{\gamma}\frac{T_{1,j+1}}{\Delta t} - \frac{4\theta}{\Delta r^2}(T_{2,j+1} - T_{1,j+1}) = \frac{1}{\gamma\Delta t}T_{1,j} + \frac{4(1-\theta)}{\Delta r^2}(T_{2,j} - T_{1,j}) \tag{4.26}$$

results.

Next, the boundary conditions along the interfaces will be expressed in the finite difference form

$$-K_i\frac{\partial T}{\partial r} = K_{i+1}\frac{\partial T}{\partial r} \tag{4.27}$$

where i = 1, 2, 3, or 4.

One can employ a three point finite difference formula [25] to represent the above first derivative of the function T(r,t) along each interface

$$-K_i\left(\frac{T_{m-2} + 3T_m - 4T_{m-1}}{2\Delta r_i}\right) = K_{i+1}\left(\frac{T_{m+2} + 3T_m - 4T_{m+1}}{2\Delta r_{i+1}}\right) \tag{4.28}$$

where m is the point on the boundary.

For programming purposes, Eq. (4.28) can be rearranged as

$$-\frac{K_i}{2\Delta r_i}T_{m-2,j+1} + \frac{2K_i}{\Delta r_i}T_{m-1,j+1} - \left(\frac{3K_i}{2\Delta r_i} + \frac{3K_{i+1}}{2\Delta r_{i+1}}\right)T_{m,j+1} + \frac{2K_{i+1}}{\Delta r_{i+1}}T_{m+1,j+1} - \frac{K_{i+1}}{2\Delta r_{i+1}}T_{m+2,j+1} = 0 \tag{4.29}$$

Finally, for the boundary condition on the surface, the equation on the surface is rewritten as

$$K\frac{\partial T}{\partial r} + h(T - T_{air}) = aF(t) \tag{4.30}$$

where the term on the right hand side represents the solar radiation.

Multiplying Eq. (4.3) by A and Eq. (4.30) by B with terms having Δr powered higher than 2 neglected

$$AT_{i-1} = AT_i - A\Delta r \frac{\partial T}{\partial r} + A \frac{\Delta r^2}{2!} \frac{\partial^2 T}{\partial r^2} \tag{4.31}$$

$$B \frac{h}{K} (T_{air} - T) + B \frac{a}{K} F(t) = B \frac{\partial T}{\partial r} \tag{4.32}$$

Adding (4.31) and (4.32)

$$(-A\Delta r + B) \frac{\partial T}{\partial r} + \frac{A}{2} \Delta r^2 \frac{\partial^2 T}{\partial r^2} = A(T_{i-1} - T_i) + B\left[\frac{h}{K} (T_{air} - T_i) + \frac{a}{K} F(t)\right] \tag{4.33}$$

is obtained.

If Eq. (4.33) is to represent Eq. (4.1), then

$$-A\Delta r + B = \frac{1}{r} \tag{4.34}$$

$$\frac{A}{2} \Delta r^2 = 1 \tag{4.35}$$

Solving for A and B

$$A = \frac{2}{\Delta r^2} \tag{4.36}$$

$$B = \frac{1}{r} + \frac{2}{\Delta r} \tag{4.37}$$

results so that Eq. (4.33) can be written as

$$\frac{1}{r} \frac{\partial T}{\partial r} + \frac{\partial^2 T}{\partial r^2} = \frac{2}{\Delta r^2} (T_{i-1} - T_i) + \left(\frac{1}{r} + \frac{2}{\Delta r}\right)\left[\frac{h}{K} (T_{air} - T_i) + \frac{a}{K} F(t)\right] \tag{4.38}$$

where the last term on the right hand side represents the solar radiation. This term can be expressed as [19]

$$aF(t) = aI(t) - e\sigma(T_{air}^4 - T_{sky}^4) \tag{4.39}$$

in which a = absorptivity

$I(t)$ = short-wave radiation which includes both the direct and diffuse radiation

e = surface emissivity

σ = Stefan-Boltzman constant

T_{air} = absolute ambient temperature in Rankine degree

T_{sky} = absolute sky temperature in Rankine degree

It is often assumed that during day time $T_{air} \simeq T_{sky}$ in Eq. (4.39) [19] so that

$$aF(t) = aI(t)$$

However, at night no short wave radiation exists, i.e., $I(t) = 0$, hence

$$aF(t) = - e\sigma(T_{air}^4 - T_{sky}^4) \tag{4.40}$$

Eq. (4.40) represents the reradiation phenomenon existing during the night. Accordingly, at night the surface of the cylinder gives up heat to the air surrounding it, and acts as a black body radiating heat.

Next, introducing a weighting factor θ into Eq. (4.38) to obtain

$$\begin{aligned}\frac{1}{\gamma}\frac{T_{i,j+1} - T_{i,j}}{\Delta t} = {} & \frac{2}{\Delta r^2}\theta\,(T_{i-1,j+1} - T_{i,j+1}) + \frac{2}{\Delta r^2}(1-\theta)(T_{i-1,j} \\ & - T_{i,j}) + \left(\frac{1}{r} + \frac{2}{\Delta r}\right)\frac{h}{k}\,\theta(T_{air,j+1} - T_{i,j+1}) \\ & + \left(\frac{1}{r} + \frac{2}{\Delta r}\right)\frac{h}{k}\,(1-\theta)(T_{air,j} - T_{i,j}) \\ & + \left(\frac{1}{r} + \frac{2}{\Delta r}\right)\frac{a}{k}\,\theta\,F_{j+1} + \left(\frac{1}{r} + \frac{2}{\Delta r}\right)\frac{a}{k}\,(1-\theta)F_j \end{aligned} \tag{4.41}$$

Rearranging the equation and introducing a shape factor for the cylindrical surface as follows

$$
\begin{aligned}
&-\frac{2\theta}{\Delta r^2}\,T_{i-1,j+1}+\left[\frac{1}{\gamma\Delta t}+\frac{2\theta}{\Delta r^2}+\frac{h}{k}\,\theta\left(\frac{1}{r}+\frac{2}{\Delta r}\right)\right]T_{i,j+1}\\
&\quad=\frac{2}{\Delta r^2}\,(1-\theta)T_{i-1,j}+\left[\frac{1}{\gamma\Delta t}-\frac{2(1-\theta)}{\Delta r^2}-\left(\frac{1}{r}+\frac{2}{\Delta r}\right)(1-\theta)\,\frac{h}{k}\right]T_{i,j}\\
&\quad+\left(\frac{1}{r}+\frac{2}{\Delta r}\right)(1-\theta)\,\frac{h}{k}\,T_{air,j}+\left(\frac{1}{r}+\frac{2}{\Delta r}\right)\frac{h}{k}\,\theta\,T_{air,j+1}\\
&\quad+\frac{\theta}{k}\left(\frac{1}{r}+\frac{2}{\Delta r}\right)\left[asI_{n,j+1}-e\sigma\left(T_{air,j+1}^{4}-T_{sky}^{4}\right)\right]\\
&\quad+\frac{(1-\theta)}{k}\left(\frac{1}{r}+\frac{2}{\Delta r}\right)\left[asI_{n,j}-e\sigma\left(T_{air,j}^{4}-T_{sky}^{4}\right)\right]
\end{aligned}
\tag{4.42}
$$

where s is the shape factor.

T_{sky} was proposed and used by Ulrich [29] as

$$T_{sky}=T_{air}-20 \tag{4.43}$$

where T_{sky} and T_{air} are absolute temperatures.

4.2 Temperature Response via Finite Difference Scheme

Eqs. (4.20), (4.26), (4.29) and (4.42) provide a set of simultaneous algebraic equations, which can be solved by various techniques. In the present investigation, Gaussian elimination has been used.

In matrix form, the set of algebraic equations can be written as

$$AX=D \tag{4.44}$$

where A represents the coefficients of the matrix. X is a column matrix representing the unknown temperature at a time of interest, say

t_{j+1}, and the column matrix D includes the temperatures (known) at the present time, t_j. The complete expression of Eq. (4.44) will become

$$\begin{bmatrix}
a_{11} & a_{12} & 0 & 0 & 0 & 0 & \cdots & 0 \\
a_{21} & a_{22} & a_{23} & 0 & 0 & 0 & \cdots & 0 \\
0 & a_{32} & a_{33} & a_{34} & 0 & 0 & \cdots & 0 \\
\cdots & \cdots & \cdots & \cdots & \cdots & \cdots & \cdots & \cdots \\
\cdots & \cdots & \cdots & \cdots & \cdots & \cdots & \cdots & \cdots \\
\cdots & a_{i-1} & a_{ii} & a_{i+1} & \cdots & \cdots & \cdots & 0 \\
\cdots & a_{i,i-2} & a_{i,i-1} & a_{i,i} & a_{i,i+1} & a_{i,i+2} & \cdots & 0 \\
\cdots & \cdots & \cdots & \cdots & \cdots & \cdots & \cdots & 0 \\
0 & 0 & 0 & \cdots & \cdots & a_{n-1,n-2} & a_{n-1,n-1} & a_{n-1,n} \\
0 & 0 & 0 & \cdots & \cdots & 0 & a_{n,n-1} & a_{n,n}
\end{bmatrix}$$

$$\cdot \begin{bmatrix} T_{1,j+1} \\ T_{2,j+1} \\ T_{3,j+1} \\ \cdots \\ \cdots \\ \cdots \\ \cdots \\ \cdots \\ T_{n-1,j+1} \\ T_{n,j+1} \end{bmatrix} = \begin{bmatrix} D_{1,j} \\ D_{2,j} \\ D_{3,j} \\ \cdots \\ \cdots \\ \cdots \\ \cdots \\ \cdots \\ D_{n-1,j} \\ D_{n,j} \end{bmatrix} \qquad (4.45)$$

It is seen that the matrix of the coefficients has zeros everywhere except on the main diagonal and on the two diagonals (four diagonals for nodes on the interface) parallel to it on either side.

For a given initial temperature across the cylinder with n nodes, one then can obtain the temperature of these nodes at the next time step. Once this is done, one can use these new temperatures as known variables, and again by using Eq. (4.43) obtain temperatures of n nodes at yet another time step. The same procedure is repeated for other time steps. In a later part of this study, details of the finite difference solution will be discussed.

V. STRESS AND STRAIN ANALYSIS

It is generally known that when heat is added to or removed from a solid body, its energy content changes: a certain portion of the energy goes into thermal vibrations (kinetic energy) and appears as a rise or fall in temperature, the remainder goes into thermal expansion or contraction unless some structural change such as crystal transformation, vaporization, or melting takes place. In the present study such changes are assumed not to take place.

Changes in the environment and heat conduction in the motor produce thermal stresses and strains in the propellant. These are expected to follow the variations in environmental conditions with a time delay. In addition, the thermal expansion coefficient of the propellant is different from that of the case, so that the propellant grain is restrained from freely expanding or contracting by the case. As a result, stresses and strains build up along the interface of two materials.

The state of stress in a long cylinder due to temperatures which vary with the radial coordinate only is well known. The problem was initially solved by Duhamel in 1838 [30]. Recently, Williams et al. [5] developed appropriate equations used for evaluating stresses and strains for a cylinder within a thin case.

It is perhaps useful to present the derivation of these equations before attempting to use the calculated temperatures to obtain stresses and strains.

In cylinder coordinates r, θ, and z the equilibrium equations are

$$\frac{\partial \sigma_{rr}}{\partial r} + \frac{1}{r}\frac{\partial \sigma_{r\theta}}{\partial \theta} + \frac{\partial \sigma_{rz}}{\partial z} + \frac{\sigma_{rr} - \sigma_{\theta\theta}}{r} + R = 0$$

$$\frac{\partial \sigma_{rz}}{\partial r} + \frac{1}{r}\frac{\partial \sigma_{\theta z}}{\partial \theta} + \frac{\partial \sigma_{zz}}{\partial z} + \frac{\sigma_{rz}}{r} + Z = 0 \qquad (5.1)$$

$$\frac{\partial \sigma_{r\theta}}{\partial r} + \frac{1}{r}\frac{\partial \sigma_{\theta\theta}}{\partial \theta} + \frac{\partial \sigma_{\theta z}}{\partial z} + \frac{2\sigma_{r\theta}}{r} + \Theta = 0$$

In the present case, the plane strain and axisymmetrical condition reduce the above equations to

$$\frac{\partial \sigma_r}{\partial r} + \frac{\sigma_r - \sigma_\theta}{r} = 0 \qquad (5.2)$$

which is satisfied by the stress function ϕ,

$$\sigma_r = \frac{\phi}{r}$$

and

$$\sigma_\theta = \frac{\partial \phi}{\partial r}$$

Utilizing elastic stress-strain relations

$$\epsilon_r = \frac{1}{E}[\sigma_r - \nu(\sigma_\theta + \sigma_z)] + \alpha T$$

$$\epsilon_\theta = \frac{1}{E}[\sigma_\theta - \nu(\sigma_r + \sigma_z)] + \alpha T \qquad (5.3)$$

$$\epsilon_z = \frac{1}{E}[\sigma_z - \nu(\sigma_r + \sigma_\theta)] + \alpha T$$

in which E, ν, and α are modulus of elasticity, Poisson's ratio and linear thermal coefficient of expansion respectively.

Using the symbol Δ for the increase in unit volume, Δ then becomes

$$\Delta = \epsilon_r + \epsilon_\theta + \epsilon_z \tag{5.4}$$

$$\Delta = \frac{1 - 2\nu}{E} (\sigma_r + \sigma_\theta + \sigma_z) + 3\alpha T \tag{5.5}$$

From Eqs. (5.3) and (5.5), stress terms can be expressed as functions of strain terms

$$\begin{aligned}
\sigma_r &= \frac{E}{1 + \nu} \left(\epsilon_r + \frac{\nu}{1 - 2\nu} \Delta \right) - \frac{\alpha T E}{1 - 2\nu} \\
\sigma_\theta &= \frac{E}{1 + \nu} \left(\epsilon_\theta + \frac{\nu}{1 - 2\nu} \Delta \right) - \frac{\alpha T E}{1 - 2\nu} \\
\sigma_z &= \frac{E}{1 + \nu} \left(\epsilon_z + \frac{\nu}{1 - 2\nu} \Delta \right) - \frac{\alpha T E}{1 - 2\nu}
\end{aligned} \tag{5.5}$$

The compatability equation is written as [5]

$$r \frac{\partial \epsilon_\theta}{\partial r} + \epsilon_\theta - \epsilon_r = 0 \tag{5.6}$$

Hence, after substituting Eq. (5.3) into Eq. (5.6) the governing differential equation for long hollow cylinder with case (plane strain) is obtained.

$$\frac{\partial^2 \phi}{\partial r^2} + \frac{1}{r} \frac{\partial \phi}{\partial r} - \frac{\phi}{r^2} = - \frac{\alpha E}{1-\nu} \frac{\partial T}{\partial r} \tag{5.7}$$

The boundary conditions are

$$\sigma_r = 0 \quad \text{at} \quad r = r_1 \text{ and } r = r_3 \tag{5.8}$$

Eq. (5.7) can also be expressed as

$$\frac{\partial^2 \phi}{\partial r^2} + \frac{\partial}{\partial r} \left(\frac{\phi}{r} \right) = - \frac{\alpha E}{1-\nu} \frac{\partial T}{\partial r}$$

or

$$\frac{\partial}{\partial r} \left[\frac{1}{r} \frac{\partial}{\partial r} (r\phi) \right] = - \frac{\alpha E}{1-\nu} \frac{\partial T}{\partial r} \tag{5.9}$$

Integrating both sides:

$$\frac{1}{r}\frac{\partial}{\partial r}(r\phi) = -\frac{\alpha E}{1-\nu}T + C_1$$

Integrating both sides again

$$r\phi = -\frac{\alpha E}{1-\nu}\int_{r_1}^{r} Trdr + C_1\frac{r^2}{2} + C_2$$

or

$$\phi = \frac{-\alpha E}{1-\nu}\frac{1}{r}\int_{r_1}^{r} Trdr + \frac{C_1 r}{2} + \frac{C_2}{r} \tag{5.10}$$

Thus,

$$\sigma_r = \frac{\phi}{r} = -\frac{\alpha E}{1-\nu}\frac{1}{r^2}\int_{r_1}^{r} Trdr + \frac{C_1}{2} + \frac{C_2}{r^2} \tag{5.11}$$

in which T is the difference between the reference (manufacturing) and current temperature.

5.1 Stress and Strain in the Propellant

*At the bore: $r = r_1$

From the boundary condition Eq. (5.8), σ_r becomes

$$0 = \frac{C_1}{2} + \frac{C_2}{r_1^2}$$

$$C_1 = -\frac{2C_2}{r_1^2}$$

*At the interface $r = r_2$, then

$$-p' = \sigma_r = -\frac{\alpha_1 E_1}{1-\nu_1}\frac{1}{r_2^2}\int_{r_1}^{r_2} Trdr + \frac{C_1}{2} + \frac{C_2}{r_2^2}$$

where α_1, E_1, ν_1 are the linear thermal coefficient of expansion, modulus of elasticity and Poisson's ratio of the propellant.

or
$$p' = \frac{\alpha_1 E_1}{1-\nu_1}\frac{1}{r_2^2}\int_{r_1}^{r_2} Trdr + C_2\left(\frac{1}{r_1^2} - \frac{1}{r_2^2}\right) \tag{5.12}$$

Then
$$C_2 = \frac{p'}{\frac{1}{r_1^2} - \frac{1}{r_2^2}} - \frac{\alpha_1 E_1}{(1-\nu_1)r_2^2\left(\frac{1}{r_1^2} - \frac{1}{r_2^2}\right)}\int_{r_1}^{r_2} Trdr$$

$$C_2 = \frac{p'r_1^2r_2^2}{r_2^2 - r_1^2} - \frac{\alpha_1 E_1}{1-\nu_1}\left(\frac{r_1^2}{r_2^2 - r_1^2}\right)\int_{r_1}^{r_2} Trdr \tag{5.13}$$

Thus,
$$C_1 = -\frac{2C_2}{r_1^2} = -\frac{2p'r_2^2}{r_2^2 - r_1^2} + \frac{2\alpha_1 E_1}{1-\nu_1}\left(\frac{1}{r_2^2 - r_1^2}\right)\int_{r_1}^{r_2} Trdr \tag{5.14}$$

The value of p' will be determined later in this section. For the time being, stress and strain in the propellant can be evaluated and expressed as follows

*Radial stress

Eq. (5.11) can be written
$$\sigma_r = -\frac{\alpha_1 E_1}{1-\nu_1}\frac{1}{r^2}\int_{r_1}^{r} Trdr - \frac{p'r_2^2}{r_2^2 - r_1^2} + \frac{\alpha_1 E_1}{1-\nu_1}\left(\frac{1}{r_2^2 - r_1^2}\right)\int_{r_1}^{r_2} Trdr$$

$$+ \frac{p'r_1^2r_2^2}{r^2\left(r_2^2 - r_1^2\right)} - \frac{\alpha_1 E_1}{1-\nu_1}\frac{r_1^2}{\left(r_2^2 - r_1^2\right)r^2}\int_{r_1}^{r_2} Trdr$$

or

$$\sigma_r = -\frac{r_2^2 p'}{r_2^2-r_1^2}\left[1-\frac{r_1^2}{r^2}\right] + \frac{\alpha_1 E_1}{(1-\nu_1)(r_2^2-r_1^2)}\left[1-\frac{r_1^2}{r^2}\right]\int_{r_1}^{r_2} Trdr$$

$$-\frac{\alpha_1 E_1}{(1-\nu_1)r^2}\int_{r_1}^{r} Trdr \qquad (5.15)$$

*Tangential stress

From Eq. (5.10) tangential stress can be expressed as

$$\sigma_\theta = \frac{\partial\phi}{\partial r} = -\frac{\alpha_1 E_1 T}{1-\nu_1} + \frac{\alpha_1 E_1}{1-\nu_1}\frac{1}{r^2}\int_{r_1}^{r} Trdr + \frac{C_1}{2} - \frac{C_2}{r^2} \qquad (5.16)$$

Substituting C_1 and C_2 from Eqs. (5.13) and (5.14)

$$\sigma_\theta = \frac{-\alpha_1 E_1 T}{1-\nu_1} + \frac{\alpha_1 E_1}{1-\nu_1}\frac{1}{r^2}\int_{r_1}^{r} Trdr - \frac{p' r_2^2}{r_2^2-r_1^2} + \frac{\alpha_1 E_1}{1-\nu_1}\frac{1}{r_2^2-r_1^2}\int_{r_1}^{r_2} Trdr$$

$$+\frac{\alpha_1 E_1}{1-\nu_1}\frac{r_1^2}{r^2(r_2^2-r_1^2)}\int_{r_1}^{r_2} Trdr - \frac{p' r_1^2 r_2^2}{r^2(r_2^2-r_1^2)}$$

or

$$\sigma_\theta = -\frac{r_2^2 p'}{r_2^2-r_1^2}\left[1+\frac{r_1^2}{r^2}\right] + \frac{\alpha_1 E_1}{(1-\nu_1)(r_2^2-r_1^2)}\left[1+\frac{r_1^2}{r^2}\right]\int_{r_1}^{r_2} Trdr$$

$$+\frac{\alpha_1 E_1}{1-\nu_1}\frac{1}{r^2}\int_{r_1}^{r} Trdr - \frac{\alpha_1 E_1 T}{1-\nu_1} \qquad (5.17)$$

Also, the stress in the z-direction can be obtained as follows

$$\sigma_z = \nu_1(\sigma_r + \sigma_\theta) - \alpha_1 E_1 T \qquad (5.18)$$

Substituting σ_r and σ_θ from Eqs. (5.15) and (5.17)

$$\sigma_z = \frac{-2\nu_1 r_2^2 p'}{r_2^2 - r_1^2} + \frac{2\nu_1 \alpha_1 E_1}{(1-\nu_1)\left(r_2^2 - r_1^2\right)} \int_{r_1}^{r_2} Trdr - \frac{\alpha_1 E_1 T}{1-\nu_1} \qquad (5.19)$$

*Radial Strain

Rewriting the first part of Eq. (5.3)

$$\epsilon_r = \frac{1}{E_1} [\sigma_r - \nu_1(\sigma_\theta + \sigma_z)] + \alpha_1 T$$

In conjunction with Eq. (5.18) the above equation can be written as

$$\epsilon_r = \frac{1}{E_1} [\sigma_r - \nu_1(\sigma_\theta + \nu_1\sigma_r + \nu_1\sigma_\theta - \alpha_1 E_1 T)] + \alpha_1 T$$

or

$$\epsilon_r = \frac{1}{E_1} \left[\sigma_r\left(1 - \nu_1^2\right) - \sigma_\theta\left(\nu_1 + \nu_1^2\right)\right] + \alpha_1 T(1 + \nu_1)$$

$$\epsilon_r = \frac{1 + \nu_1}{E_1} \left[\sigma_r(1 - \nu_1) - \nu_1\sigma_\theta\right] + \alpha_1 T(1 + \nu_1) \qquad (5.20)$$

Substituting σ_r and σ_θ from Eqs. (5.15) and (5.17)

$$\epsilon_r = \frac{1 + \nu_1}{E_1} \left[- \frac{r_2^2 p'(1-\nu_1)}{r_2^2 - r_1^2} \left(1 - \frac{r_1^2}{r_2^2}\right) + \frac{\alpha_1 E_1}{r_2^2 - r_1^2} \left(1 - \frac{r_1^2}{r^2}\right) \int_{r_1}^{r_2} Trdr \right.$$

$$- \frac{\alpha_1 E_1}{r^2} \int_{r_1}^{r} Trdr + \frac{\nu_1 r_2^2 p'}{r_2^2 - r_1^2} \left(1 + \frac{r_1^2}{r^2}\right)$$

$$- \frac{\nu_1 \alpha_1 E_1}{(1-\nu_1)\left(r_2^2 - r_1^2\right)} \left(1 + \frac{r_1^2}{r^2}\right) \int_{r_1}^{r_2} Trdr - \frac{\nu_1 \alpha_1 E_1}{(1-\nu_1) r^2} \int_{r_1}^{r} Trdr$$

$$\left. + \frac{\alpha_1 E_1 \nu_1 T}{1-\nu_1} \right] + \alpha_1 T(1 + \nu_1)$$

$$e_r = -\frac{(1+\nu_1)r_2^2 p'}{E_1\left(r_2^2-r_1^2\right)}\left[(1-2\nu_1)-\frac{r_1^2}{r^2}\right]$$

$$+\frac{(1+\nu_1)\alpha_1}{(1-\nu_1)\left(r_2^2-r_1^2\right)}\left[(1-2\nu_1)-\frac{r_1^2}{r^2}\right]\int_{r_1}^{r_2} Trdr$$

$$-\frac{\alpha_1(1+\nu_1)}{(1-\nu_1)r^2}\int_{r_1}^{r} Trdr+\frac{1+\nu_1}{1-\nu_1}\alpha_1 T \qquad (5.21)$$

*Tangential Strain

The second part of Eq. (5.3) in conjunction with Eq. (5.18) gives

$$e_\theta = \frac{1}{E_1}\left[\sigma_\theta - \nu_1(\sigma_r + \nu_1\sigma_r + \nu_1\sigma_\theta) + \alpha_1\nu_1E_1T\right] + \alpha_1T$$

Simplifying

$$e_\theta = \frac{(1+\nu_1)}{E_1}\left[(1-\nu_1)\sigma_\theta - \nu_1\sigma_r\right] + \alpha_1T(1+\nu_1) \qquad (5.22)$$

Substituting σ_r and σ_θ from Eqs. (5.15) and (5.17) and simplifying to obtain

$$e_\theta = -\frac{(1+\nu_1)r_2^2 p'}{E_1\left(r_2^2-r_1^2\right)}\left[(1-2\nu_1)+\frac{r_1^2}{r^2}\right]$$

$$+\frac{(1+\nu_1)\alpha_1}{(1-\nu_1)\left(r_2^2-r_1^2\right)}\left[(1-2\nu_1)+\frac{r_1^2}{r^2}\right]\int_{r_1}^{r_2} Trdr$$

$$+\frac{1+\nu_1}{1-\nu_1}\left(\frac{\alpha_1}{r^2}\right)\int_{r_1}^{r} Trdr \qquad (5.23)$$

The strain-displacement relations in the cylindrical coordinates are

$$e_r = \frac{\partial U_r}{\partial r}$$

$$e_\theta = \frac{U_r}{r} + \frac{1}{r}\frac{\partial U_\theta}{\partial \theta} \tag{5.24}$$

$$\gamma_{r\theta} = \frac{1}{r}\frac{\partial U_r}{\partial \theta} + \frac{\partial U_\theta}{\partial r} - \frac{U_\theta}{r}$$

where U_r,U_θ are the displacements in the radial and tangential direction. In the present case, $U_\theta = 0$ because of the axisymmetric characteristic of the problem.

Eqs. (5.21) and (5.23) permit the evaluation of U_r are follows

$$U_r = -\frac{(1+\nu_1)r_2^2 p'}{E_1\left[r_2^2 - r_1^2\right]}\left[(1-2\nu_1)r + \frac{r_1^2}{r}\right] + \frac{\alpha_1(1+\nu_1)}{(1-\nu_1)r}\int_{r_1}^{r} Trdr$$

$$+ \frac{(1+\nu_1)\alpha_1}{(1-\nu_1)\left[r_2^2 - r_1^2\right]}\left[(1-2\nu_1)r + \frac{r_1^2}{r}\right]\int_{r_1}^{r_2} Trdr \tag{5.25}$$

5.2 Stress and Strain in the Case

From the differential equation (5.7), following the same steps described before (Eqs. 5.8-10) it is now possible to obtain

$$\sigma_r = \frac{\phi}{r} = -\frac{\alpha_2 E_2}{1-\nu_2}\frac{1}{r^2}\int_{r_2}^{r} Trdr + \frac{C_3}{2} + \frac{C_4}{r^2} \tag{5.26}$$

in which α_2, E_2, ν_2 are the linear thermal coefficient of expansion, modulus of elasticity and Poisson's ratio of the case respectively. Now, at the interface, $r = r_2$, Eq. (5.26) becomes

$$-p' = +\frac{C_3}{2} + \frac{C_4}{r_2^2} \tag{5.27}$$

At $r = r_3$

Eq. (5.26) becomes

$$0 = -\frac{\alpha_2 E_2}{1-\nu_2}\frac{1}{r_3^2}\int_{r_2}^{r_3} Trdr + \frac{C_3}{2} + \frac{C_4}{r_3^2}$$

$$C_3 = \frac{2\alpha_2 E_2}{1-\nu_2}\frac{1}{r_3^2}\int_{r_2}^{r_3} Trdr - \frac{2C_4}{r_3^2} \tag{5.28}$$

Substituting Eq. (5.28) into Eq. (5.27)

$$-p' = \frac{\alpha_2 E_2}{1-\nu_2}\frac{1}{r_3^2}\int_{r_2}^{r_3} Trdr + C_4\left(\frac{1}{r_2^2} - \frac{1}{r_3^2}\right)$$

Thus

$$C_4 = -p'\left(\frac{r_2^2 r_3^2}{r_3^2 - r_2^2}\right) - \frac{\alpha_2 E_2}{1-\nu_2}\frac{1}{r_3^2}\left(\frac{r_2^2 r_3^2}{r_3^2 - r_2^2}\right)\int_{r_2}^{r_3} Trdr \tag{5.29}$$

From Eq. (5.27) C_3 can be obtained

$$C_3 = 2\left[\frac{r_3^2 p'}{r_3^2 - r_2^2} + \frac{\alpha_2 E_2}{(1-\nu_2)\left(r_3^2 - r_2^2\right)}\int_{r_2}^{r_3} Trdr\right] \tag{5.30}$$

*<u>Stress in the Case</u>

Substituting Eqs. (5.28) and (5.30) into Eq. (5.26) and simplifying to obtain

$$\sigma_r = \frac{r_3^2 p'}{r_3^2 - r_2^2}\left(1 - \frac{r_3^2}{r^2}\right) + \frac{\alpha_2 E_2}{(1-\nu_2)\left(r_3^2 - r_2^2\right)}\left(1 - \frac{r_2^2}{r^2}\right)\int_{r_2}^{r_3} Trdr$$

$$- \frac{\alpha_2 E_2}{(1-\nu_2) r^2}\int_{r_2}^{r} Trdr \tag{5.31}$$

Similarly

$$\sigma_\theta = \frac{r_3^2 p'}{\left[r_3^2 - r_2^2\right]} \left[1 + \frac{r_3^2}{r^2}\right] + \frac{\alpha_2 E_2}{(1-\nu_2)\left[r_3^2 - r_2^2\right]} \left[1 + \frac{r_2^2}{r^2}\right] \int_{r_2}^{r_3} Trdr$$

$$+ \frac{\alpha_2 E_2}{1-\nu_2} \frac{1}{r^2} \int_{r_2}^{r} Trdr - \frac{\alpha_2 E_2 T}{1-\nu_2} \tag{5.32}$$

*Strain in the Case

Substituting Eq. (5.31,32) into Eq. (5.20) and simplifying to obtain

$$\epsilon_r = \frac{(1+\nu_2) r_3^2 p'}{E_2\left[r_3^2 - r_2^2\right]} \left[(1 - 2\nu_2) - \frac{r_3^2}{r^2}\right] - \frac{(1+\nu_2)}{(1-\nu_2)} \frac{\alpha_2}{r^2} \int_{r_2}^{r} Trdr$$

$$+ \frac{\alpha_2 (1+\nu_2)}{(1-\nu_2)\left[r_3^2 - r_2^2\right]} \left[(1 - 2\nu_2) - \frac{r_2^2}{r^2}\right] \int_{r_2}^{r} Trdr + \frac{(1+\nu_2)\alpha_2 T}{1-\nu_2} \tag{5.33}$$

From Eq. (5.22) one can obtain ϵ_θ

$$\epsilon_\theta = \frac{(1+\nu_2) r_3^2 p'}{E_2\left[r_3^2 - r_2^2\right]} \left[1 - 2\nu_2 + \frac{r_3^2}{r^2}\right]$$

$$+ \frac{(1+\nu_2)\alpha_2}{(1-\nu_2)\left[r_3^2 - r_2^2\right]} \left[1 - 2\nu_2 + \frac{r_2^2}{r^2}\right] \int_{r_2}^{r_3} Trdr$$

$$+ \frac{(1+\nu_2)\alpha_2}{(1-\nu_2) r^2} \int_{r_2}^{r} Trdr \tag{5.34}$$

The strain and displacement are related as follows

$$e_r = \frac{\partial U_r}{\partial r}$$

$$e_\theta = \frac{U_r}{r}$$

where U is the displacement. Then from Eqs. (5.33) and (5.34):

$$U_r = \frac{(1+\nu_2) r_3^2 p'}{E_2\left[r_3^2 - r_2^2\right]} \left[(1 - 2\nu_2) - \frac{r_3^2}{r^2}\right] r$$

$$+ \frac{(1+\nu_2)}{(1-\nu_2)} \frac{\alpha_2}{\left[r_3^2 - r_2^2\right]} \left[1 - 2\nu_2 + \frac{r_2^2}{r^2}\right] r \int_{r_2}^{r_3} Trdr$$

$$+ \frac{(1+\nu_2)\alpha_2}{(1-\nu_2) r^2} r \int_{r_2}^{r} Trdr$$

or

$$U_r = \frac{(1+\nu_2) r_2^2 p'}{E_2\left[r_3^2 - r_2^2\right]} \left[(1 - 2\nu_2) r + \frac{r_3^2}{r}\right] + \frac{(1+\nu_2)\alpha_2}{(1-\nu_2) r} \int_{r_2}^{r} Trdr$$

$$+ \frac{(1+\nu_2)}{(1-\nu_2)} \frac{\alpha_2}{\left[r_3^2 - r_2^2\right]} \left[(1 - 2\nu_2) r + \frac{r_2^2}{r}\right] \int_{r_2}^{r_3} Trdr \qquad (5.35)$$

From the boundary condition, there is a continuity in displacement across the interface of the propellant and case

$$U_r \Big|_{\substack{r=r_2 \\ \text{(propellant)}}} = U_r \Big|_{\substack{r=r_2 \\ \text{(case)}}}$$

Substituting Eqs. (5.25) and (5.35)

$$- \frac{(1+\nu_1)r_2^2 p'}{E_1\left(r_2^2-r_1^2\right)} \left[(1 - 2\nu_1)r_2 + \frac{r_1^2}{r_2}\right] + \frac{\alpha_1(1+\nu_1)}{(1-\nu_1)r_2} \int_{r_1}^{r_2} Trdr$$

$$+ \frac{(1+\nu_1)\alpha_1}{(1-\nu_1)\left(r_2^2-r_1^2\right)} \left[(1 - 2\nu_1)r_2 + \frac{r_1^2}{r_2}\right] \int_{r_1}^{r_2} Trdr$$

$$= \frac{(1+\nu_2)r_2^2 p'}{E_2\left(r_3^2-r_2^2\right)} \left[(1 - 2\nu_2)r_2 + \frac{r_3^2}{r_2}\right] + \frac{\alpha_2(1+\nu_2)}{(1-\nu_2)\left(r_3^2-r_2^2\right)} \left[(1 - 2\nu_2)r_2\right.$$

$$\left. + \frac{r_2^2}{r_2}\right] \int_{r_2}^{r_3} Trdr + \frac{(1+\nu_2)\alpha_2}{(1-\nu_2)r_2} \int_{r_2}^{r_2} Trdr \qquad (5.36)$$

The last term on the right hand side of Eq. 5.36 is equal to zero.

Dividing both sides of the above expression by r_2 to obtain

$$- \frac{(1+\nu_1)r_2^2 p'}{E_1\left(r_2^2-r_1^2\right)} \left[(1 - 2\nu_1) + \frac{r_1^2}{r_2^2}\right] + \frac{\alpha_1(1+\nu_1)}{(1-\nu_1)r_2^2} \int_{r_1}^{r_2} Trdr$$

$$+ \frac{(1+\nu_1)\alpha_1}{(1-\nu_1)\left(r_2^2-r_1^2\right)} \left[(1 - 2\nu_1) + \frac{r_1^2}{r_2^2}\right] \int_{r_1}^{r_2} Trdr$$

$$= \frac{(1+\nu_2)r_2^2 p'}{E_2\left(r_3^2-r_2^2\right)} \left[(1 - 2\nu_2) + \frac{r_3^2}{r_2^2}\right] + \frac{\alpha_2(1+\nu_2)}{(1-\nu_2)\left(r_3^2-r_2^2\right)} \left[(1 - 2\nu_2)\right.$$

$$\left. + \frac{r_2^2}{r_2^2}\right] \int_{r_2}^{r_3} Trdr \qquad (5.37)$$

Simplifying

$$p'\left[\frac{(1+\nu_2)r_2^2}{E_2\left(r_3^2-r_2^2\right)}\left(1-2\nu_2+\frac{r_3^2}{r_2^2}\right)+\frac{(1+\nu_1)r_2^2}{E_1\left(r_2^2-r_1^2\right)}\left(1-2\nu_1+\frac{r_1^2}{r_2^2}\right)\right]$$

$$=-\frac{\alpha_2(1+\nu_2)}{(1-\nu_2)\left(r_3^2-r_2^2\right)}\left[2(1-\nu_2)\right]\int_{r_2}^{r_3}Trdr+\frac{\alpha_1(1+\nu_1)}{(1-\nu_1)r_2^2}\int_{r_1}^{r_2}Trdr$$

$$+\frac{(1+\nu_1)\alpha_1}{(1-\nu_1)\left(r_2^2-r_1^2\right)}\left[(1-2\nu_1)+\frac{r_1^2}{r_2^2}\right]\int_{r_1}^{r_2}Trdr \qquad (5.38)$$

or

$$p'\left\{\frac{(1+\nu_2)}{E_2}\frac{\left[(1-2\nu_2)r_2^2+r_3^2\right]}{\left(r_3^2-r_2^2\right)}+\frac{(1+\nu_1)}{E_1}\frac{\left[(1-2\nu_1)r_2^2+r_1^2\right]}{\left(r_2^2-r_1^2\right)}\right\}$$

$$=-\frac{2\alpha_2(1+\nu_2)}{\left(r_3^2-r_2^2\right)}\int_{r_2}^{r_3}Trdr+\frac{(1+\nu_1)\alpha_1}{(1-\nu_1)\left(r_2^2-r_1^2\right)}\left[(1-2\nu_1)+\frac{r_1^2}{r_2^2}\right]\int_{r_1}^{r_2}Trdr$$

$$+\frac{\alpha_1(1+\nu_1)}{(1-\nu_1)r_2^2}\int_{r_1}^{r_2}Trdr \qquad (5.39)$$

Eq. (5.39) permits the evaluation of p', but before obtaining the complete expression for p' it is possible to simplify some terms in Eq. (5.39) by making use of the fact that the case is thin.

From Fig. 1 one can write

$$r_3 = r_2 + \Delta r$$

where $\Delta r = r_3 - r_2 \ll 1$

$$r_3^2 = r_2^2 + 2r_2\Delta r + \Delta r^2$$

Since Δr is very small

$$r_3^2 \simeq r_2^2 + 2r_2\Delta r$$

or

$$r_3^2 - r_2^2 \simeq 2r_2\Delta r \tag{5.40}$$

So that the first term on the left hand side of Eq. (5.39) is simplified as follows

$$\frac{1+\nu_2}{E_2}\frac{\left[(1-2\nu_2)r_2^2 + r_3^2\right]}{\left(r_3^2-r_2^2\right)} = \frac{1+\nu_2}{E_2\left(r_3^2-r_2^2\right)}\left[r_2^2 - 2\nu_2 r_2^2 + r_2^2 + 2r_2\Delta r\right]$$

$$= \frac{1+\nu_2}{E_2\left(r_3^2-r_2^2\right)}\left\{2r_2^2\left[(1-\nu_2) + \frac{\Delta r}{r_2}\right]\right\}$$

Since Δr is very small so $\frac{\Delta r}{r_2}$ can be neglected, also, substituting the relation (5.40) into the denominator to obtain

$$\frac{1+\nu_2}{E_2}\frac{\left[(1-2\nu_2)r_2^2 + r_3^2\right]}{\left(r_3^2-r_2^2\right)} \simeq \frac{1-\nu_2^2}{E_2}\frac{r_2}{\Delta r} \tag{5.41}$$

Next, the second term on the right hand side of Eq. (5.39) can be simplified as follows

$$\frac{\alpha_1(1+\nu_1)}{(1-\nu_1)\left[r_2^2-r_1^2\right]}\left[(1-2\nu_1)+\frac{r_1^2}{r_2^2}\right]\int_{r_1}^{r_2} Trdr$$

$$=\frac{\alpha_1(1+\nu_1)}{(1-\nu_1)\left[r_2^2-r_1^2\right]}\left[2(1-\nu_1)-\frac{\left[r_2^2-r_1^2\right]}{r_2^2}\right]\int_{r_1}^{r_2} Trdr$$

$$=\frac{2\alpha_1(1+\nu_1)}{r_2^2-r_1^2}\int_{r_1}^{r_2} Trdr-\frac{\alpha_1(1+\nu_1)}{(1-\nu_1)r_2^2}\int_{r_1}^{r_2} Trdr \qquad (5.42)$$

The simplified expression for the first term on the right hand side of Eq. (5.39) is obtained as follows

$$\frac{2\alpha_2(1+\nu_2)}{r_3^2-r_2^2}\int_{r_2}^{r_3} Trdr \simeq \frac{2\alpha_2(1+\nu_2)}{r_3^2-r_2^2}\,T(r_2)\,\frac{r_3^2-r_2^2}{2}$$

$$\simeq \alpha_2(1+\nu_2)T(r_2) \qquad (5.43)$$

Hence, p' can be obtained by substituting Eqs. (5.41), (5.42) and (5.43) into Eq. (5.39)

$$p'\left\{\frac{(1-\nu_2)^2}{E_2}\frac{r_2}{\Delta r}+\frac{(1+\nu_1)}{E_1}\frac{\left[(1-2\nu_1)r_2^2+r_1^2\right]}{\left[r_2^2-r_1^2\right]}\right\}$$

$$=-\alpha_2(1+\nu_2)T(r_2)+\frac{2\alpha_1(1+\nu_1)}{r_2^2-r_1^2}\int_{r_1}^{r_2} Trdr$$

or

$$p' = \frac{\dfrac{2\alpha_1(1+\nu_1)}{\left[r_2^2-r_1^2\right]}\int_{r_1}^{r_2} Trdr - \alpha_2(1+\nu_2)T(r_2)}{\dfrac{1+\nu_1}{E_1}\dfrac{\left[(1-2\nu_1)r_2^2+r_1^2\right]}{\left(r_2^2-r_1^2\right)} + \dfrac{(1-\nu_2)^2}{E_2}\dfrac{r_2}{\Delta r}} \tag{5.44}$$

Multiplying the numerator and denominator by $\left(r_2^2-r_1^2\right)$

$$p' = \frac{2\alpha_1(1+\nu_1)\int_{r_1}^{r_2} Trdr - \alpha_2(1+\nu_2)\left(r_2^2-r_1^2\right)T(r_2)}{\dfrac{1+\nu_1}{E_1}\left[(1-2\nu_1)r_2^2+r_1^2\right] + \dfrac{(1-\nu_2)^2 r_2\left[r_2^2-r_1^2\right]}{E_2\Delta r}}$$

Multiplying the numerator and denominator by E_1E_2

$$p' = \frac{E_1E_2\left[2\alpha_1(1+\nu_1)\int_{r_1}^{r_2} Trdr - \alpha_2(1+\nu_2)\left(r_2^2-r_1^2\right)T(r_2)\right]}{E_2(1+\nu_1)\left[(1-2\nu_1)r_2^2+r_1^2\right] + E_1(1-\nu_2)^2\dfrac{r_2\left[r_2^2-r_1^2\right]}{r_3-r_2}} \tag{5.45}$$

Eqs. (5.15), (5.17), (5.21) and (5.23) in conjunction with Eq. (5.45) enable one to obtain radial and tangential stresses and strains at various locations across the cross-sectional area of the propellant provided that temperatures at those locations are known. It is evident that some numerical scheme is needed to evaluate the integrand in each of the above-mentioned equations. In fact, temperatures obtained at various points in the propellant did not show significant variations, consequently, the curve of the product of T and r versus r as shown in Fig. 5 appears to be a straight line. As such,

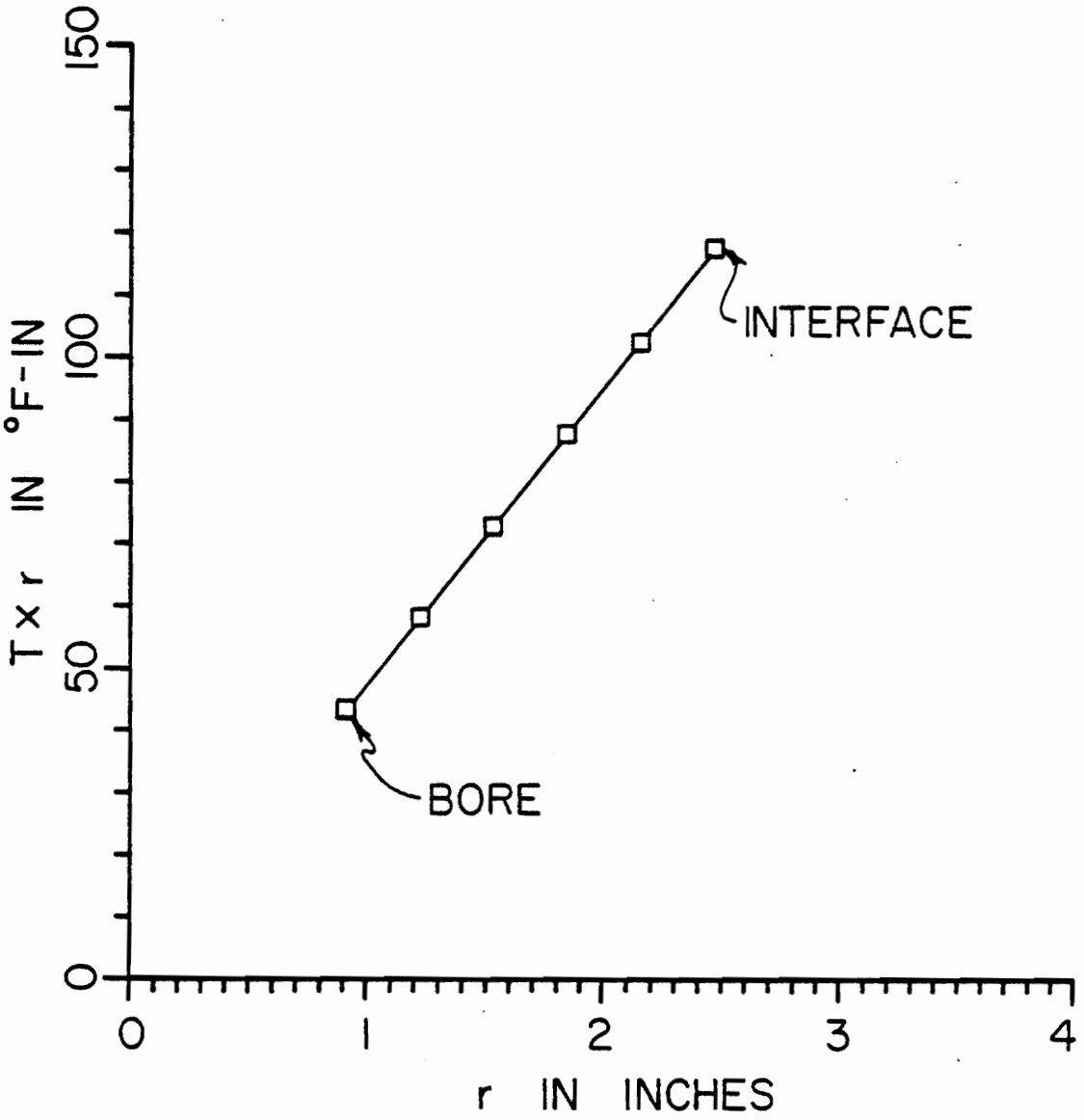

Figure 5. Product of temperature and radial distance across the propellant (thin cylinder).

to obtain the area under the curve one does not really need a large number of points. In fact, 2 or 3 points will be sufficient. This fact also justifies the use of fewer nodes for the propellant layer in the finite difference scheme without incurring large errors. In the present case, as will be shown later, 3 points were selected across the propellant and the case for the thin cylinder, while for the thicker cylinder the number of nodes used is 4. Hence the induced stresses and strains at the bore, the interface and between the bore and the interface can be evaluated. As will be shown later, the bore and the interface between the propellant and case are the critical locations.

5.3 Safety Analysis

The safety range in structural analysis is defined as

$$\Delta\nu_s = R_s - S \tag{5.46}$$

and

$$\Delta\nu_e = R_e - \epsilon \tag{5.47}$$

where $\Delta\nu_s$ and $\Delta\nu_e$ = safety ranges for stress and strain

R_s and R_e = strength and strain capacity of the material

Failure will occur whenever the strength and/or strain capacity of the structure is exceeded by the applied stress or strain. Several investigators [11,12] have discovered that for the case of a solid propellant motor, the critical locations are at the interface of the propellant and case and at the bore. It is expected that the greatest stresses or strains will occur at those locations. In fact, the greatest stress component will be either the tangential stress at the

bore or the radial stress at the interface and the largest strain is the tangential strain occurring at the bore. Hence the probability of failure, P_f, under a single load is the probability that $\Delta\nu_{s_\theta}(r_1)$, $\Delta\nu_{s_r}(r_2)$ or $\Delta\nu_{e_\theta}(r_1)$ are equal to or less than zero and is expressed as [11]

$$P_{f_1} = P_{f_{s_\theta}}(r_1) + P_{f_{e_\theta}}(r_1) + P_{f_{s_r}}(r_2) \tag{5.48}$$

In the present study, solutions have been sought in the time domain via the finite difference technique. In other words, values of stress and strain are available at the end of each time step (Δt = 1 hour) for a period of 24 hours which is considered as one load cycle, one can of course obtain the mean and standard deviation for one day by the following relations

*For stress:
$$\mu_s = \frac{\sum_{i=1}^{N} S_i}{N} \tag{5.49}$$

*For strain:
$$\mu_e = \frac{\sum_{i=1}^{N} e_i}{N} \tag{5.50}$$

*For stress:
$$\sigma_s = \frac{N \sum_{i=1}^{N} S_i^2 - \left[\sum_{i=1}^{N} S_i\right]^2}{N(N-1)} \tag{5.51}$$

$$\sigma_e = \frac{N \sum_{i=1}^{N} e_i^2 - \left[\sum_{i=1}^{N} e_i\right]^2}{N(N-1)} \tag{5.52}$$

where μ, σ stand for the mean and standard deviation respectively.

In order to obtain the probability of failure of a structure one needs to know the distribution of the responses of the structure, which in this case are the induced stresses and strains. By using the Chi-square test, Okono [12] has shown that the distribution of stress in the propellant is normal. In the present study, the normal distribution will be used to obtain various probabilities of failure.

It is useful to introduce some characteristics of a normal distribution before attempting to evaluate the probability of failure of the propellant.

The normal (or Gaussian) distribution is the best known and most widely used. The first order probability distribution function of a normal or Gaussian process x(t) has the following probability density function

$$p(x) = \frac{1}{\sqrt{2\pi}\,\sigma} \exp\left[-(x-\mu)^2/2\sigma^2\right] \tag{5.53}$$

where μ and σ are the mean and standard deviation of the process. Fig. 6 gives a typical sketch of a normal distribution.

Now, given that the stress and strain responses are normally distributed, one can readily evaluate the probability of failure as follows:

Introducing the following notation

$$\zeta = \Delta\nu_s = R_s - S \tag{5.54}$$

The function $p(\zeta)$ is defined as the difference density of $p(R_s)$ and $p(S)$. If both $p(R_s)$ and $p(S)$ are normally distributed then $p(\zeta)$ will also be normally distributed and its probability density

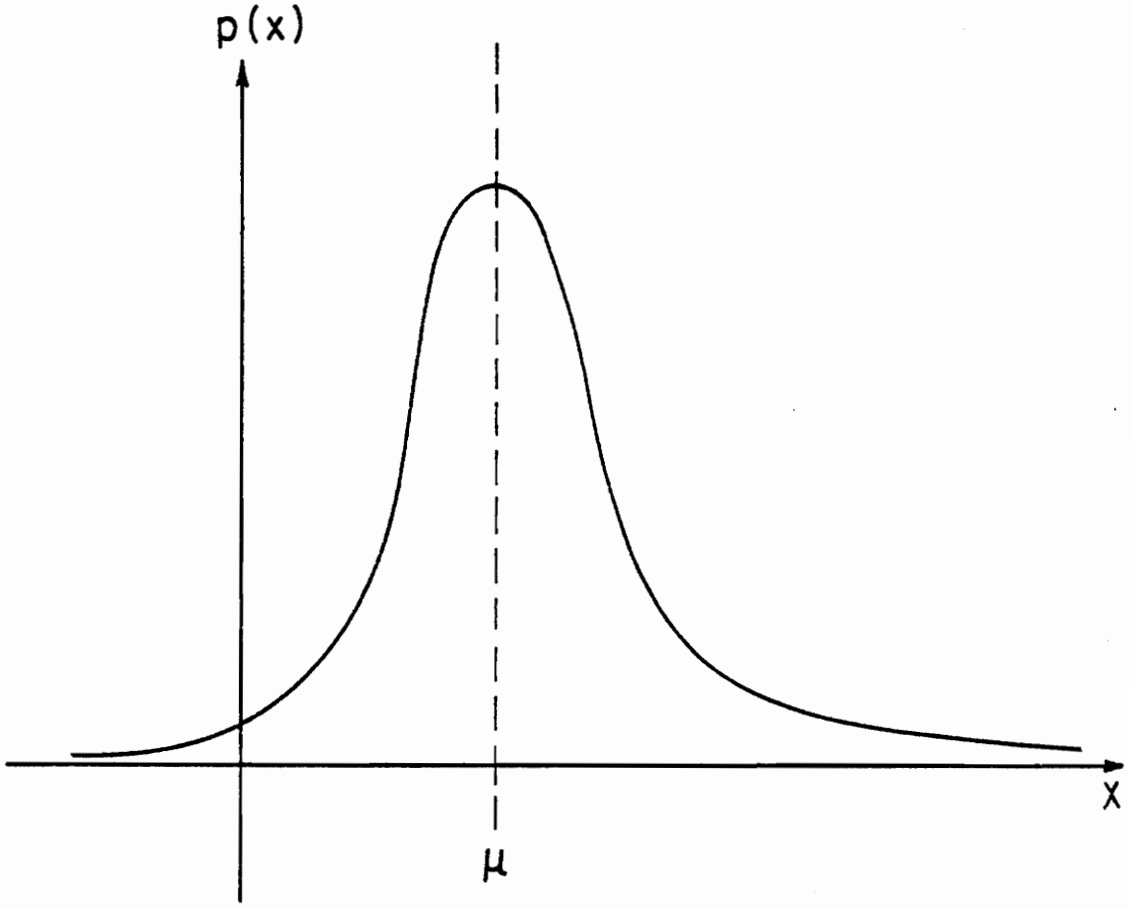

Figure 6. Probability density function of a Gaussian process.

function is written as

$$p(\zeta) = \frac{1}{\sigma_\zeta \sqrt{2\pi}} \exp\left[-\frac{1}{2}\left(\frac{\zeta - \bar{\zeta}}{\sigma_\zeta}\right)^2\right] \tag{5.55}$$

where

$$\bar{\zeta} = \bar{R}_s - \bar{S} \tag{5.56}$$

and

$$\sigma_\zeta = \sqrt{\sigma_{R_s}^2 + \sigma_s^2} \tag{5.57}$$

The reliabiiity P(s) can be written as

$$P(s) = \int_{-\infty}^{s} p(\zeta)d\zeta = \frac{1}{\sigma_\zeta \sqrt{2\pi}} \int_{-\infty}^{s} \exp\left[-\frac{1}{2}\left(\frac{\zeta - \bar{\zeta}}{\sigma_\zeta}\right)^2\right]d\zeta \tag{5.58}$$

Eq. (5.58) in conjunction with Eq. (5.48) will permit the evaluation of the probability of failure for one cycle of load.

The probability of failure for one year (365 load cycles) can be computed as

$$P_f(365) = 1.0 - \prod_{i=1}^{365} [1.0 - P_f(i)] \tag{5.59}$$

Hence, the service life of the motor in years could be obtained by the following relation

$$X \text{ (years)} = \frac{P_{f_{max}}}{P_f(365)} \tag{5.60}$$

where $P_{f_{max}}$ is the specified maximum acceptable probability of failure for the life of cylinder. In addition, if $P_f(i) << 1$, Eq. (5.59) can further be simplified as

$$P_f(365) = \sum_{i=1}^{365} P_f(i) \tag{5.61}$$

VI. ANALYSIS OF RESULTS

6.1 Temperature Response

It is generally known that, as discussed earlier, in setting up the finite difference model the error is minimized by selecting as small a mesh size as is applicable. As the mesh size is reduced the number of points increases and so does the number of equations. It is a frequent practice to start with some reasonable mesh size and then increase or reduce this size while observing the convergence.

Even though the implicit finite difference scheme helps to remove the stability problem which poses serious difficulties to the explicit finite difference scheme, it has been found that the Crank-Nicolson technique may produce some oscillations in the solution. To eliminate this problem, instead of using a weighting factor of $\theta = 1/2$ (as discussed in part IV), the so-called "Galerkin Technique" selects $\theta = 2/3$; other authors have also tried $\theta = 7/8$ [31].

In the present analysis all three weighting factors have been examined. It is found that the solutions obtained by Crank-Nicolson ($\theta = 1/2$) for a given sinusoidal temperature input with and without radiation and constant heat convective coefficient compared relatively well with Galerkin's method ($\theta = 2/3$). However, Galerkin's weighting factor has been used throughout the rest of this study.

Table I lists all physical parameters used in the present investigation.

TABLE I. Physical parameters.

Strain free temperature	130°F
Diffusivity of air	$3.00 \times 10^{-2} \frac{in^2}{sec}$
Diffusivity of propellant	$1.56 \times 10^{-4} \frac{in^2}{sec}$
Diffusivity of casing	$1.36 \times 10^{-2} \frac{in^2}{sec}$
Diffusivity of insulation	$3.43 \times 10^{-4} \frac{in^2}{sec}$
Thermal conductivity of air	$.014 \frac{Btu}{Hr\ ft\ °F}$
Thermal conductivity of propellant	$.155 \frac{Btu}{Hr\ ft\ °F}$
Thermal conductivity of casing	$14.6 \frac{Btu}{Hr\ ft\ °F}$
Thermal conductivity of insulation	$0.0158 \frac{Btu}{Hr\ ft\ °F}$
Thin cylinder (see figure 1)	
r_1	0.925 in
r_2	2.47 in
r_3	2.50 in
r_4	6.00 in
r_5	9.00 in
Thick cylinder (see figure 1)	
r_1	2.5 in
r_2	7.91 in
r_3	8.00 in
r_4	11.50 in
r_5	14.50 in

TABLE I (continued).

Modulus of elasticity for propellant	320 psi
Modulus of elasticity for casing	30×10^{6} psi
Poisson's ratio for propellant	.49
Poisson's ratio for casing	.25
Coefficient of thermal expansion of propellant	$8.5 \times 10^{-5} \frac{\text{in}}{\text{in } °F}$
Coefficient of thermal expansion of casing	$6.5 \times 10^{-6} \frac{\text{in}}{\text{in } °F}$
Mean strength capacity for propellant	72 psi
Standard deviation for the strength capacity of propellant	7.2 psi
Absorptivity of case (uninsulated)	0.7
Emissivity of case (uninsulated)	0.6
Absorptivity of insulation	0.5
Emissivity of insulation	0.5

Notes: In Fig. 20, the following values were used for the insulation:

Diffusivity	$5.6 \times 10^{-4} \frac{\text{in}^2}{\text{sec}}$
Thermal conductivity	$0.025 \frac{\text{Btu}}{\text{Hr ft } °F}$
Absorptivity	0.5
Emissivity	0.6

Although it is a fact that by using the implicit finite difference scheme one has flexibility in selecting the time step for a given mesh size, the small time step tends to give better solutions, of course at the expense of computation time. In the present analysis, initially a time step $\Delta t = 0.5$ hr was selected and then increased to $\Delta t = 1$ hr. It is found that for a sinusoidal ambient temperature input, with different mesh sizes, the two time steps do not show any significant differences in the solutions. Hence, $\Delta t = 1$ hr has been selected for the present investigation.

To decide on the best mesh size, a sinusoidal ambient temperature is used for the input, the heat convection coefficient is kept constant, h = 2 Btu/hr-ft^2-°F, even though in the actual situation, as mentioned earlier, it varies with the wind speed and type of surface. The system being investigated is a linear one. Hence, as expected, for a given sinusoidal input one should be able to obtain a sinusoidal output. This has been found to be the case in the present study.

To start the finite difference analysis, a mesh size with 21 nodes is used to obtain temperature responses at various locations across the cylinder. The mesh size is then reduced to 16 and finally to 11. Figure 7 illustrates these mesh sizes. For the thin cylinder it is found that, for a sinusoidal input temperature, the solutions for 3 mesh sizes are also sinusoidal with the same frequency as the input and the solutions do not show significant differences. However, for the thicker cylinder, there is a noticeable difference in the temperature responses. Figs. 8, 9, 10 and 11 illustrate these cases.

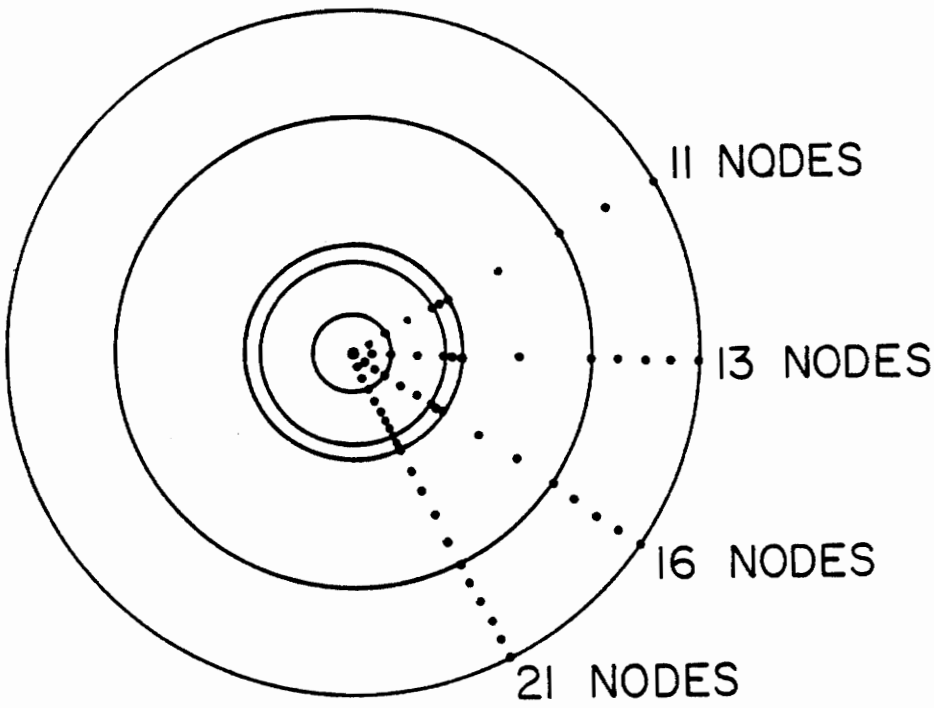

Figure 7. Finite difference model (4 different mesh sizes).

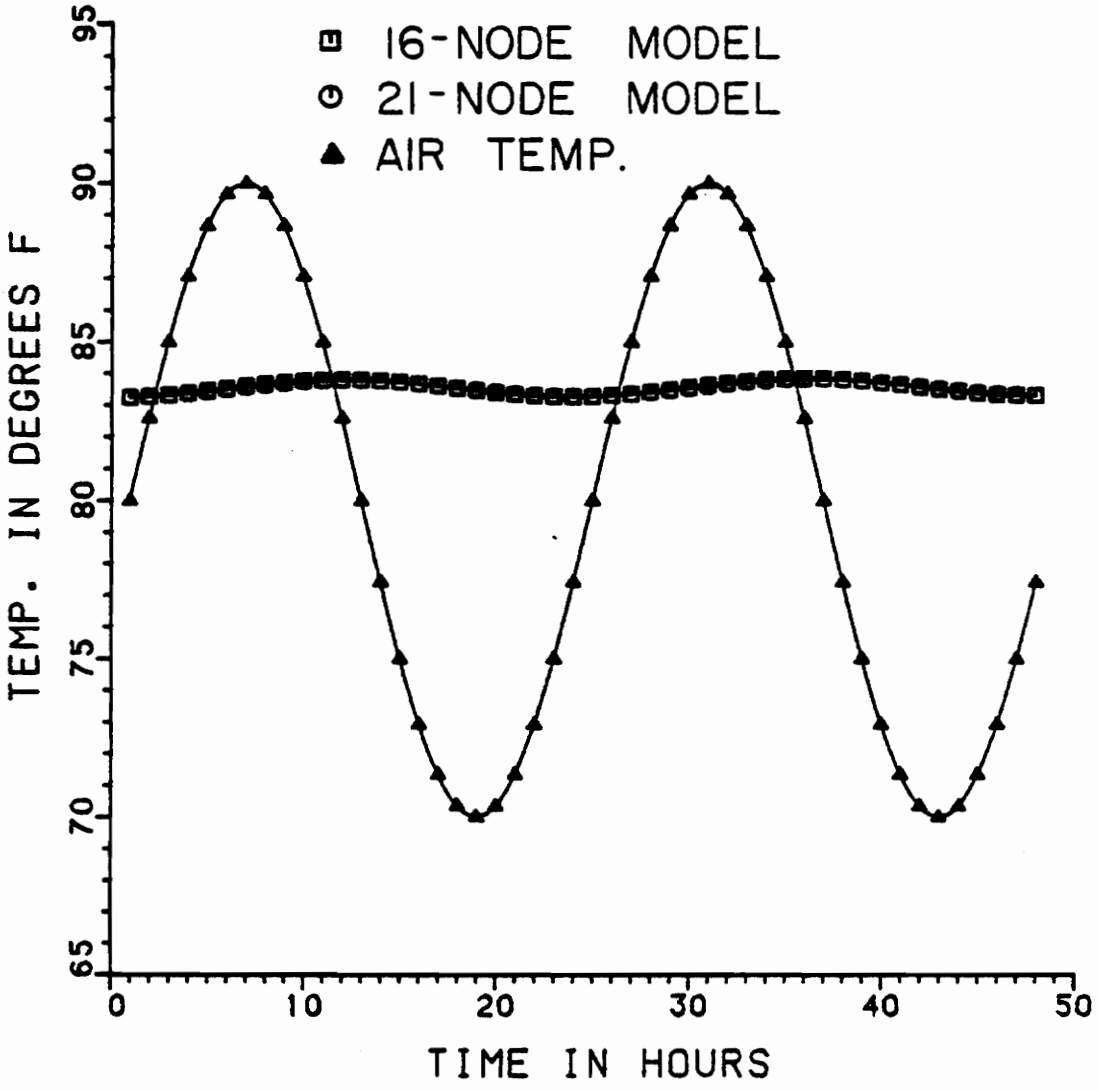

Figure 8. Temperature response at the bore of the thin cylinder (sinusoidal input).

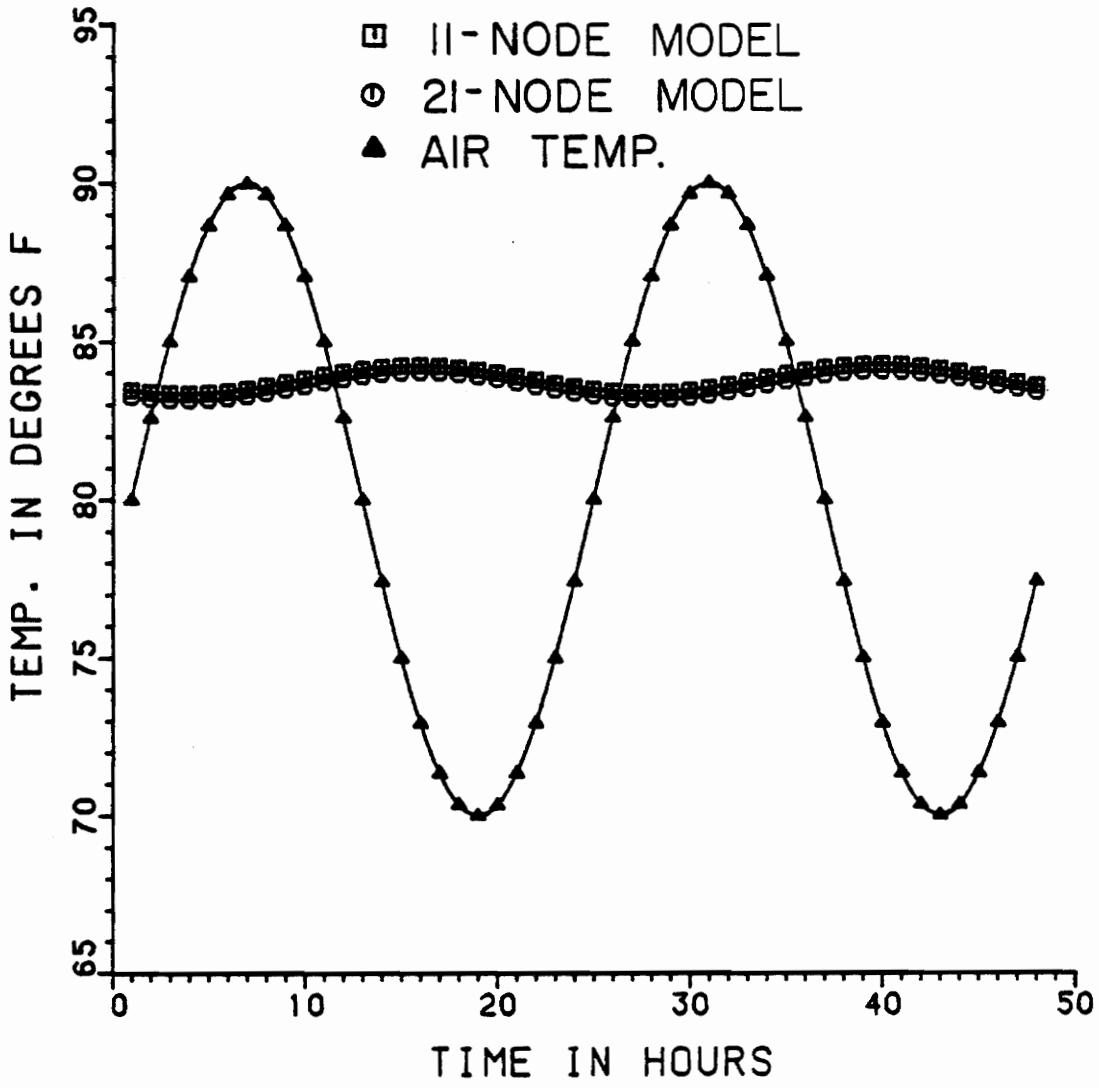

Figure 9. Temperature response at the bore of the thin cylinder (sinusoidal input).

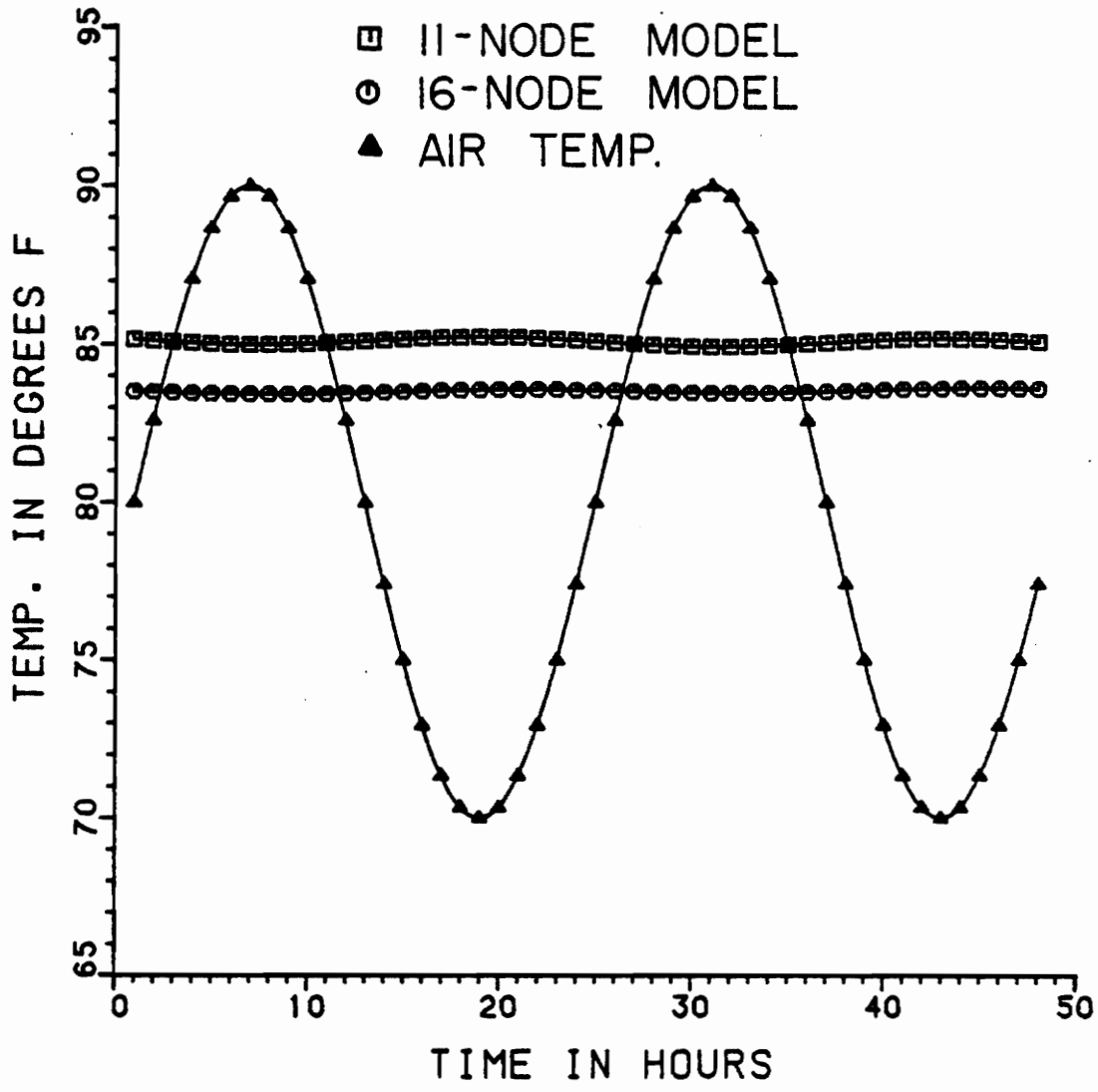

Figure 10. Temperature response of the bore of the thick cylinder (sinusoidal input).

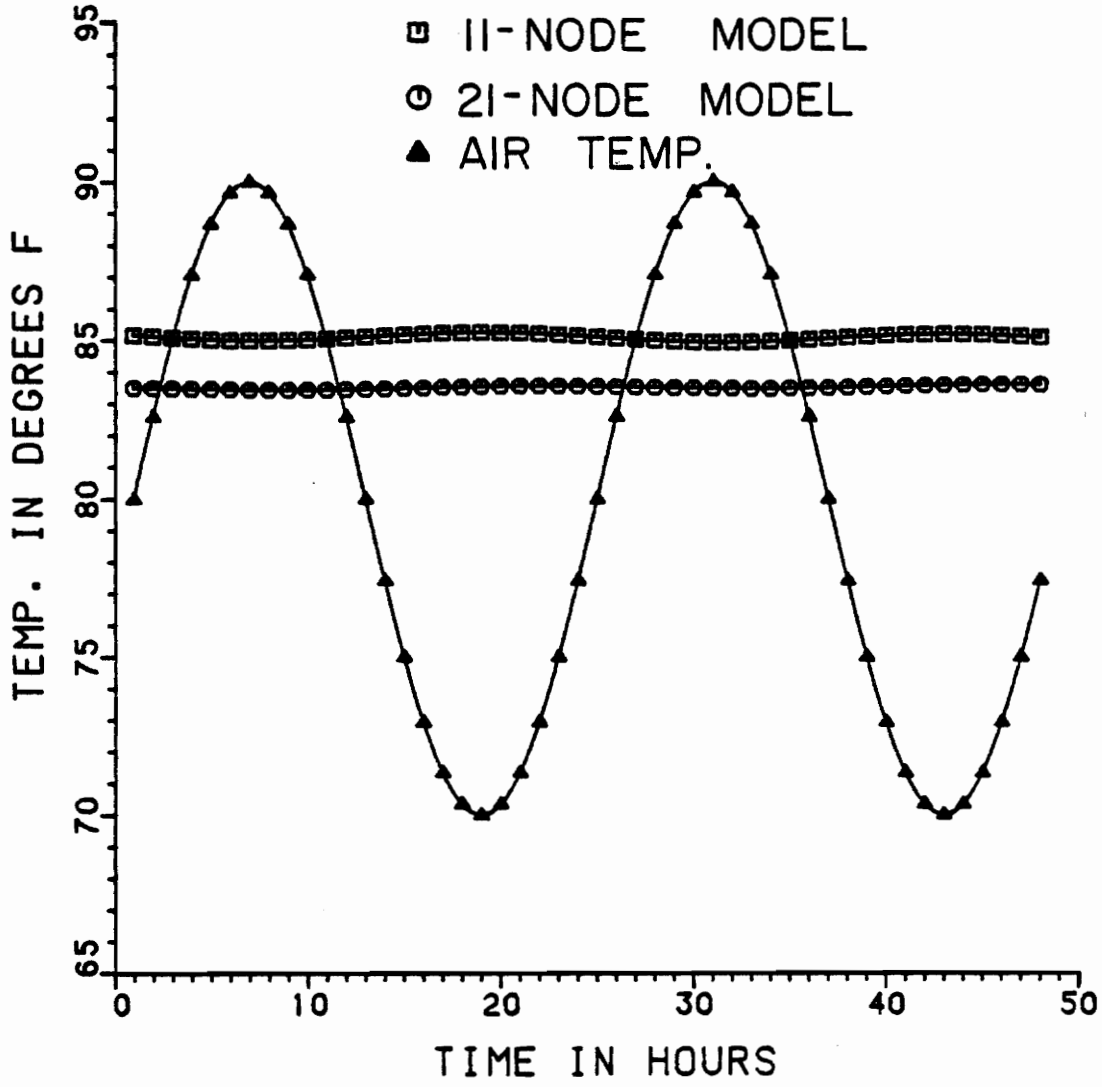

Figure 11. Temperature response at the bore of the thick cylinder (sinusoidal input).

Figs. 12 and 13 show temperature responses at four different times in a day across a 21-node model (thin cylinder) and 16-node model (thicker cylinder). It is seen that the temperatures in the cavity, the propellant and the steel layer remain almost uniform. But temperatures in the outside air and insulation layers show rapid variations. For the outside air layer, however, a linear trend appears across the layer. In the insulation there is a definite non-linearity of temperature distribution. This fact suggests that more nodes (finer mesh) should be used for the insulated layer. This is a usual practice in modeling a continuous system. It is, of course, possible to extend the fine network to the entire solution domain, but this would cause unnecessary expenditure of time and effort in the solution. The fact that temperatures inside the cylinder show a uniform or linear response suggests that large errors are not expected to be generated by choosing a rather larger mesh size. Mathematically, as explained before, the finite difference technique basically seeks to approximate the derivative terms of the partial differential equation. The smaller the chosen space interval the better the approximation, especially if the dependent variable, in this case the temperature response, has a nonlinear trend. In the present case, since the temperature does not show a nonlinear trend in four of the five layers, it is appropriate to select a rather larger space interval to approximate the differential equation.

Thus, for the thin cylinder, a 13-node model is used in which the mesh size of the insulation is relatively fine. But for the thick cylinder, since the inside air and the propellant layer are much

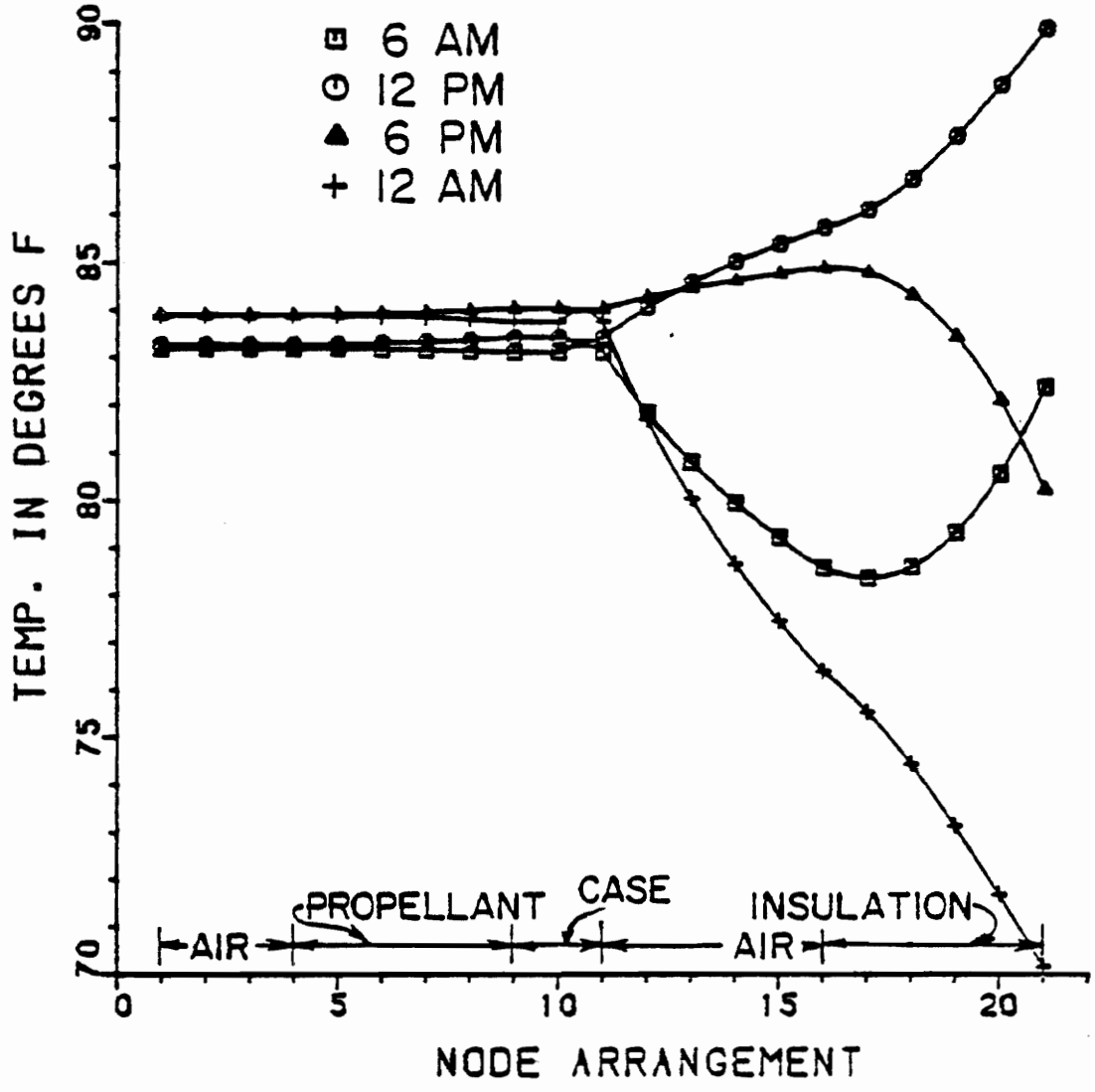

Figure 12. Temperature response of a 21-node model at 4 different times of the thin cylinder (for input see Fig. 8).

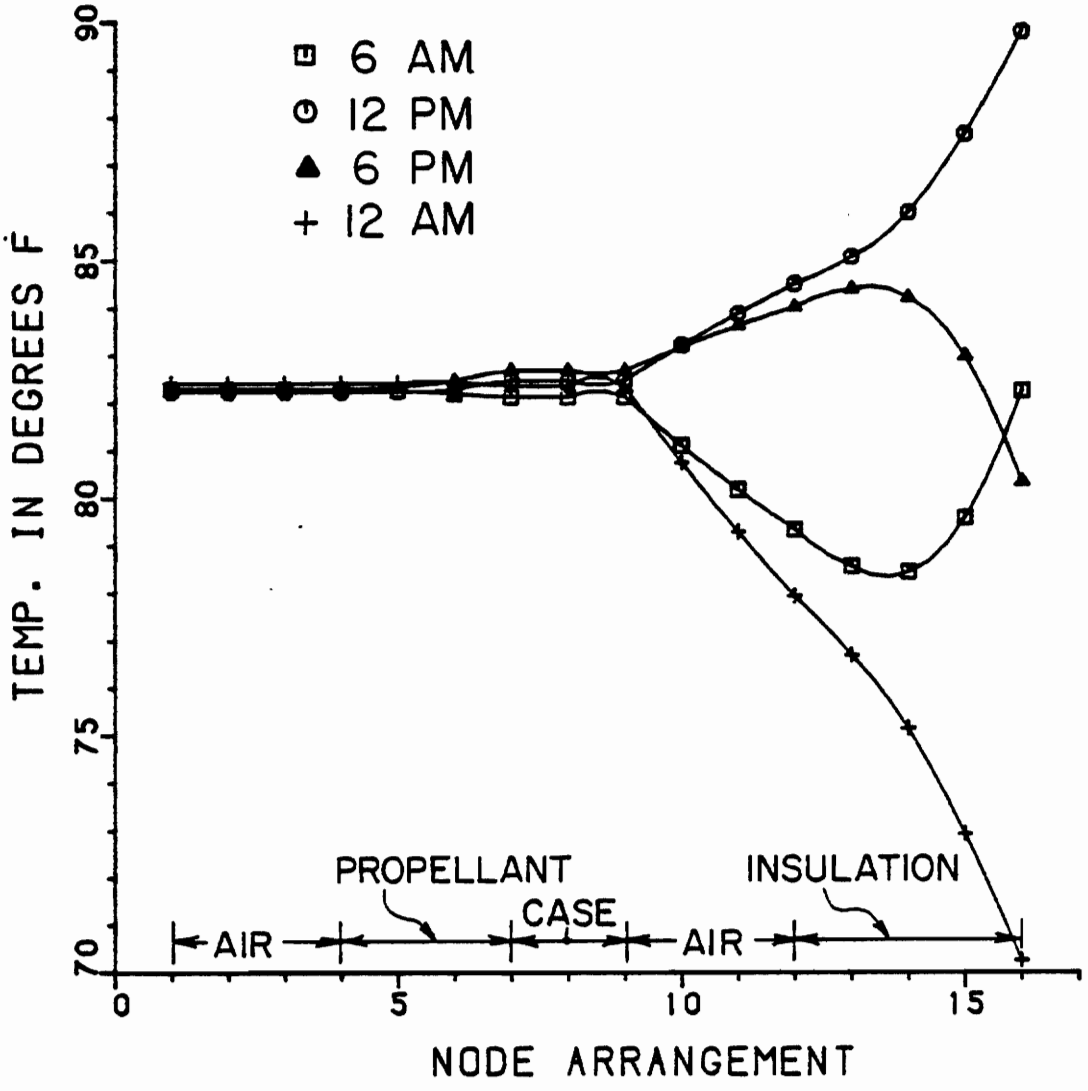

Figure 13. Temperature response of a 16-node model at 4 different times of the thick cylinder (for input see Fig. 8).

thicker, it is advisable to have more nodes in these layers in order to reduce truncation errors. Hence, a 16-node model is selected for the thicker cylinder. Figure 7 shows different finite difference models used and tested thus far.

The solutions for both cylinders have the same frequency as the input temperature, and exhibit an expected time delay in the solutions. At locations closer to the center of the cylinder, the time delay is larger. It should also be pointed out that the response in the propellant of the thicker cylinder is very slow; the change in temperatures from one hour to the next is quite small compared to outside temperature changes. Figs. 14 and 15 show temperature responses of the interface of the thin and thicker cylinders respectively.

It is also interesting to note that, without solar radiation, the surface temperature and the ambient temperature are almost identical for a given heat convection coefficient. Figure 16 illustrates this behavior.

To assure the accuracy of the finite difference model it is of great importance to compare its solution with an available closed form solution. To this end, the case of an encased propellant without insulation is used. With reference to Fig. 7, it is seen that there are only three layers in this cylinder: the inside air, the propellant and the steel layers. The same finite difference model developed for 5 layers can be used in this case by having two more artificial layers in the propellant which, in effect, renders the present system identical to the actual 5-layer model. If the finite difference scheme works for the actual 5-layer model it should also work for the

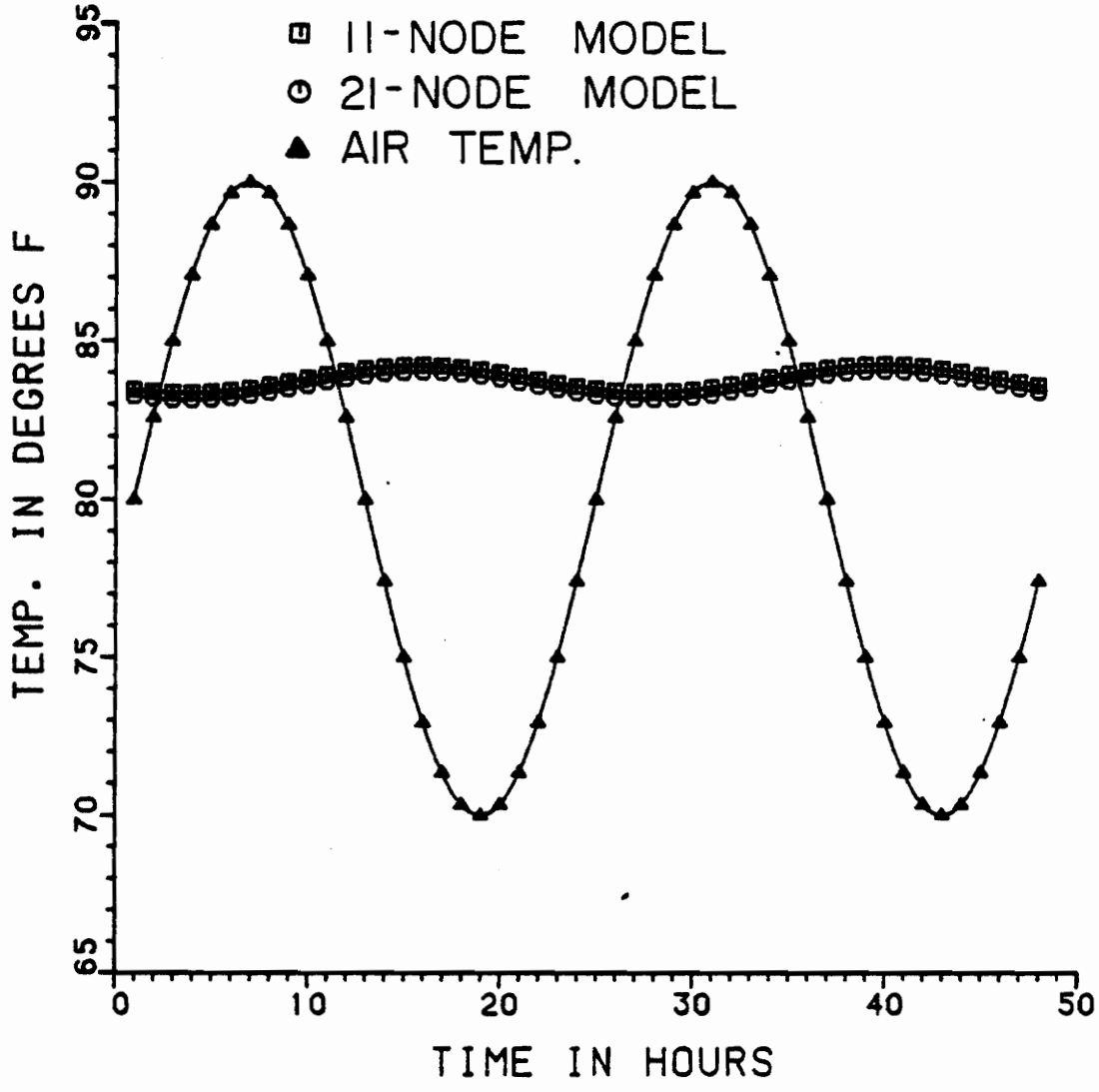

Figure 14. Temperature response at the interface (thin cylinder) of 2 different mesh sizes (sinusoidal input).

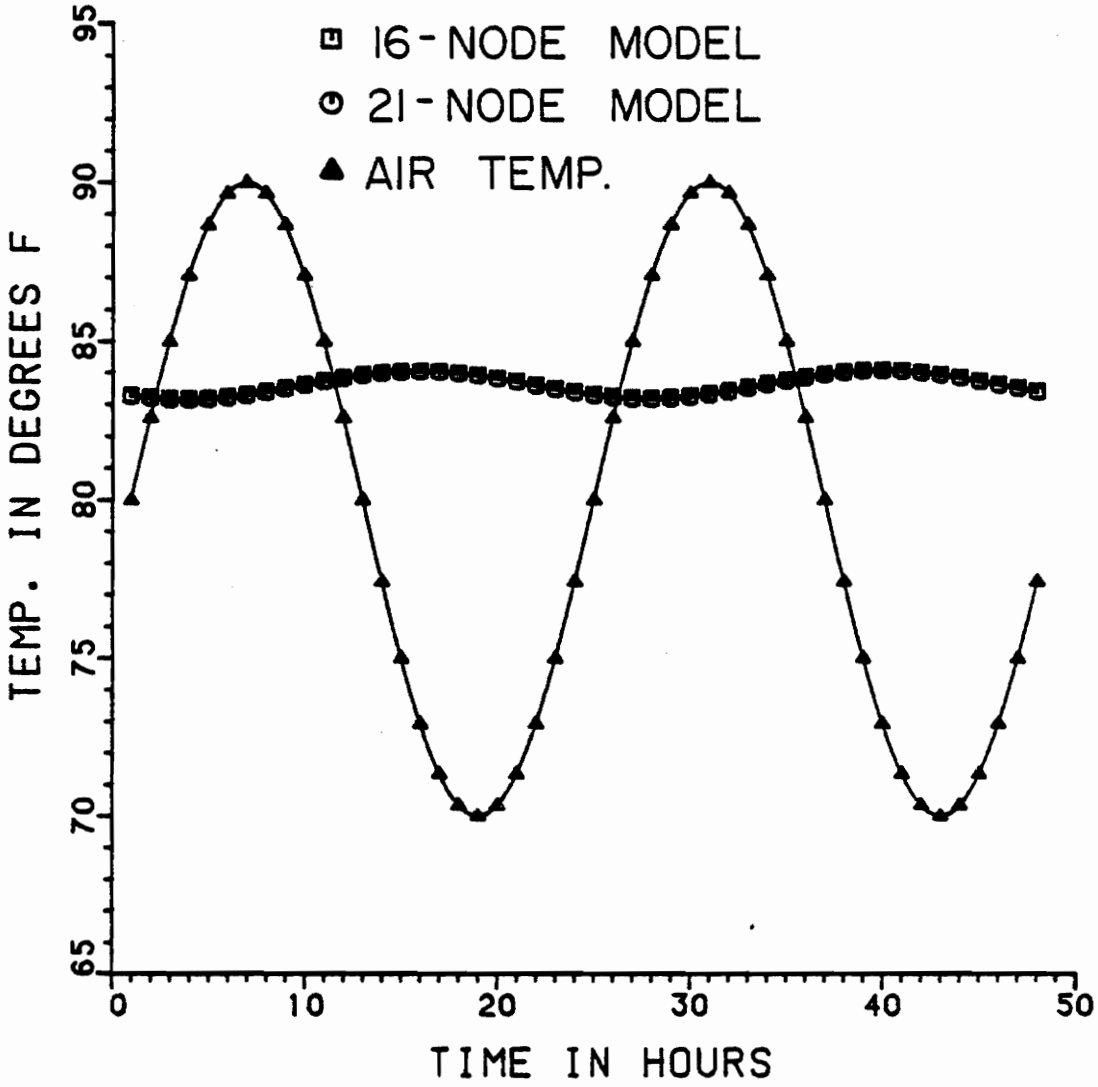

Figure 15. Temperature response at the interface (thick cylinder) of 2 different mesh sizes (sinusoidal input).

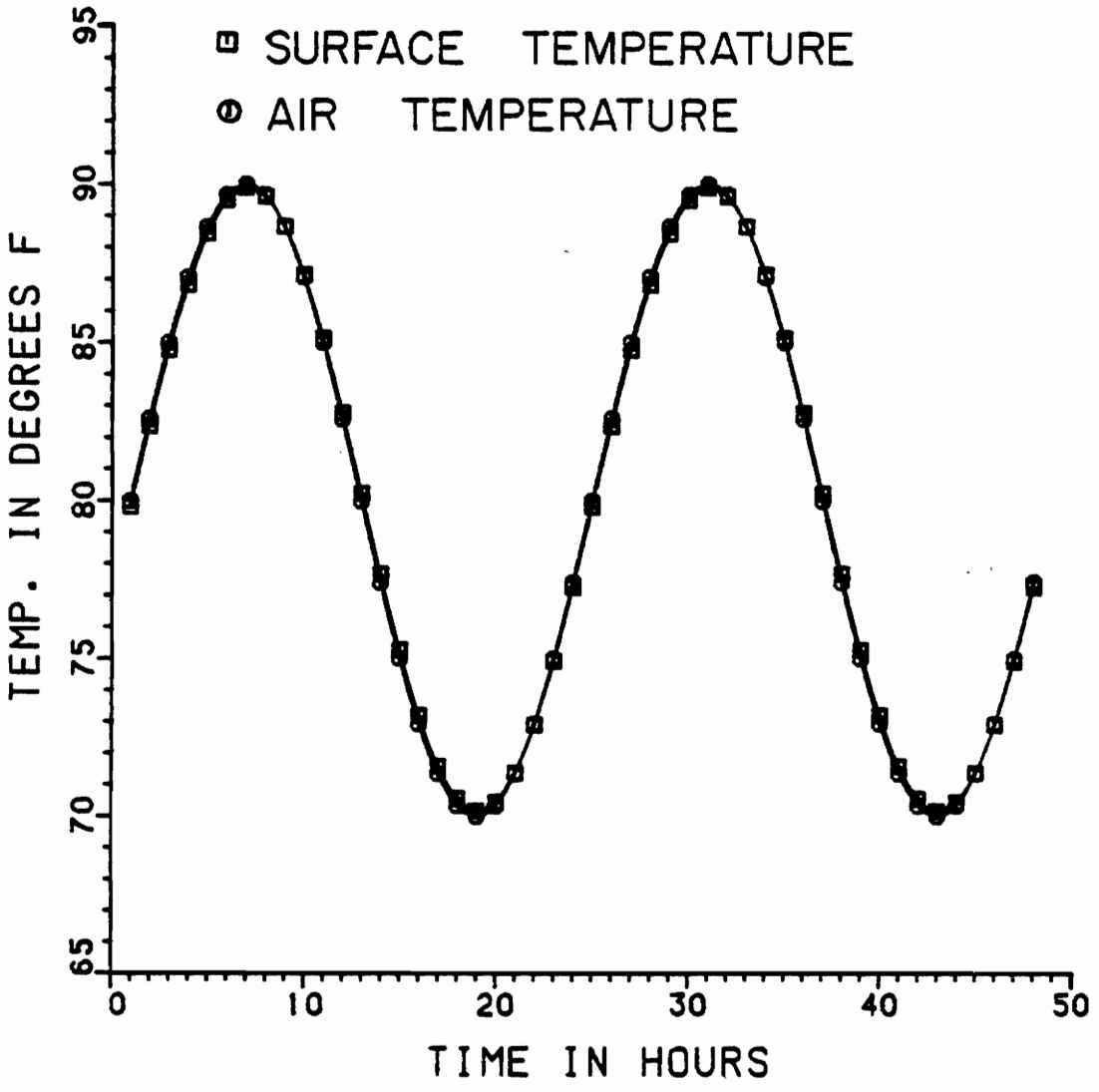

Figure 16. Surface temperature of the thin cylinder (sinusoidal input).

present case. For a sinusoidal input ambient temperature (without solar radiation or convection) ($T = 10 \sin \omega t$, where ω is the daily cycle and t is the time), the finite difference solution with 16 nodes compares very well with Heller's closed form solution [9]. Figure 17 shows the finite difference and closed form solutions for the bore of the cylinder ($h = 1.5$ was used for the finite difference solution).

In the present investigation, solar radiation has been included hence it is of great interest to compare the finite difference solution and closed form solution or experimental data (if available). Experimental measurements for both insulated and uninsulated cylinders are available in [32]. Material properties as well as sizes of the cylinder are the same as those of the thin cylinder. The measured data, however, was obtained for only one day, August 4, 1973.

The measured data include the ambient temperature, solar radiation, wind speed, surface temperature of the steel case and temperature of the air cavity. The measured ambient temperature, solar radiation and wind speed are used to obtain the finite difference solution. The finite difference solution is usually stable sometime after the start of the solution so the same input for August 1 has been repeated for 5 days. The finite difference (16 nodes) solution was obtained. On the 6th day the results compare very well with the measured data. Figs. 18 and 19 show the measured data and finite difference solution for the uninsulated cylinder. Figure 20 shows the measured data and finite difference solution on the surface of the steel case of the insulated cylinder.

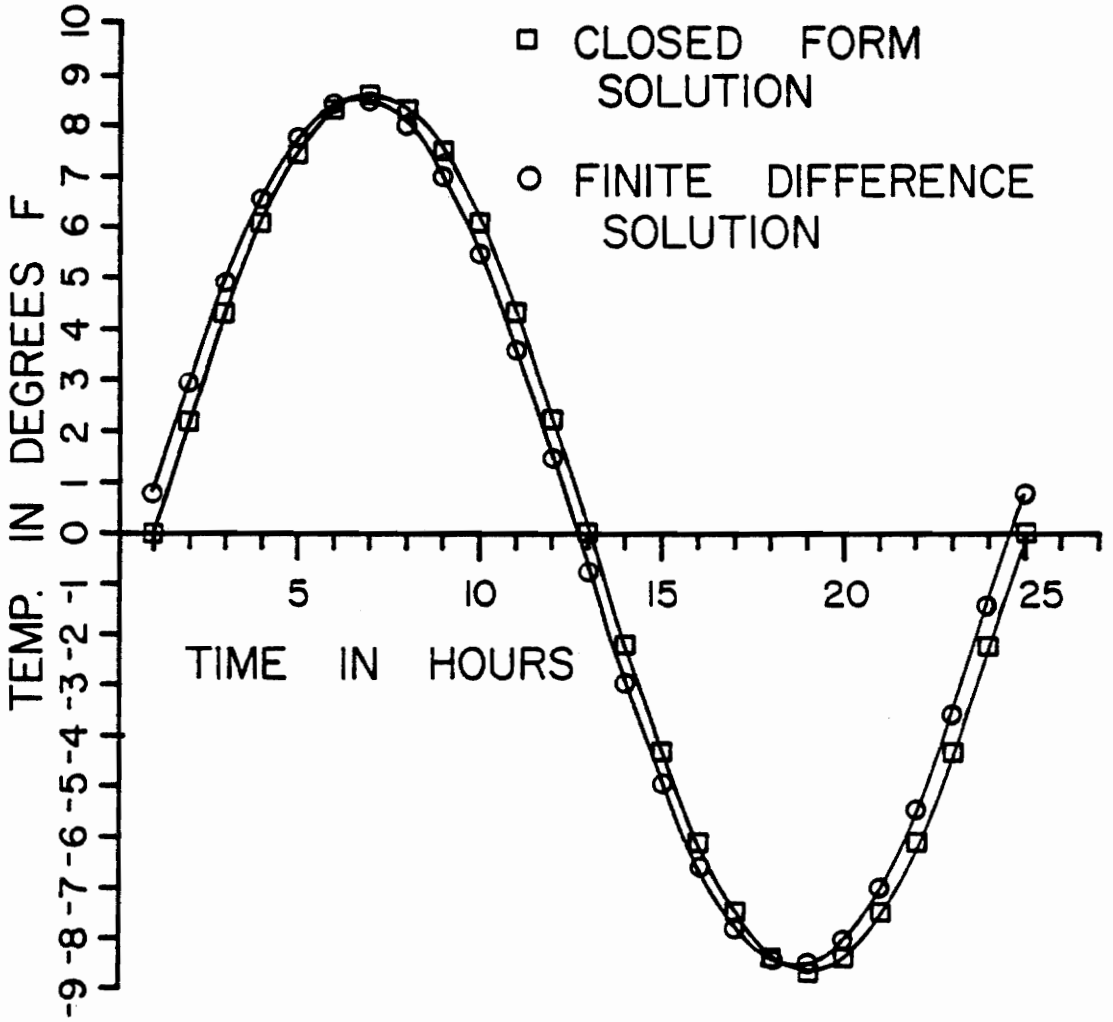

Figure 17. Finite difference and closed form solutions [9] of the thin, uninsulated cylinder (sinusoidal input).

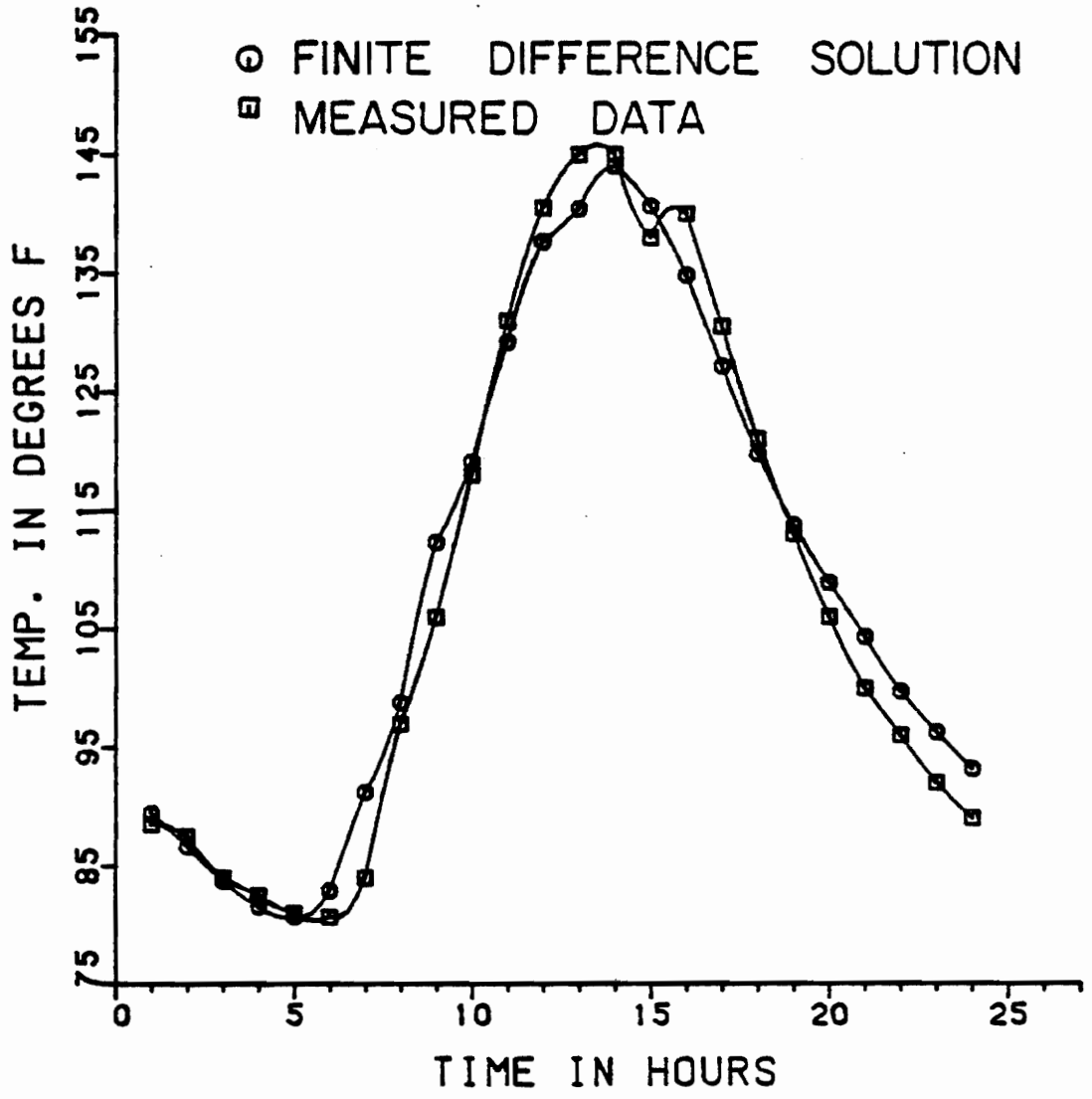

Figure 18. Measured data [32] and finite difference solution on the surface of the uninsulated cylinder (solar radiation and heat convection included).

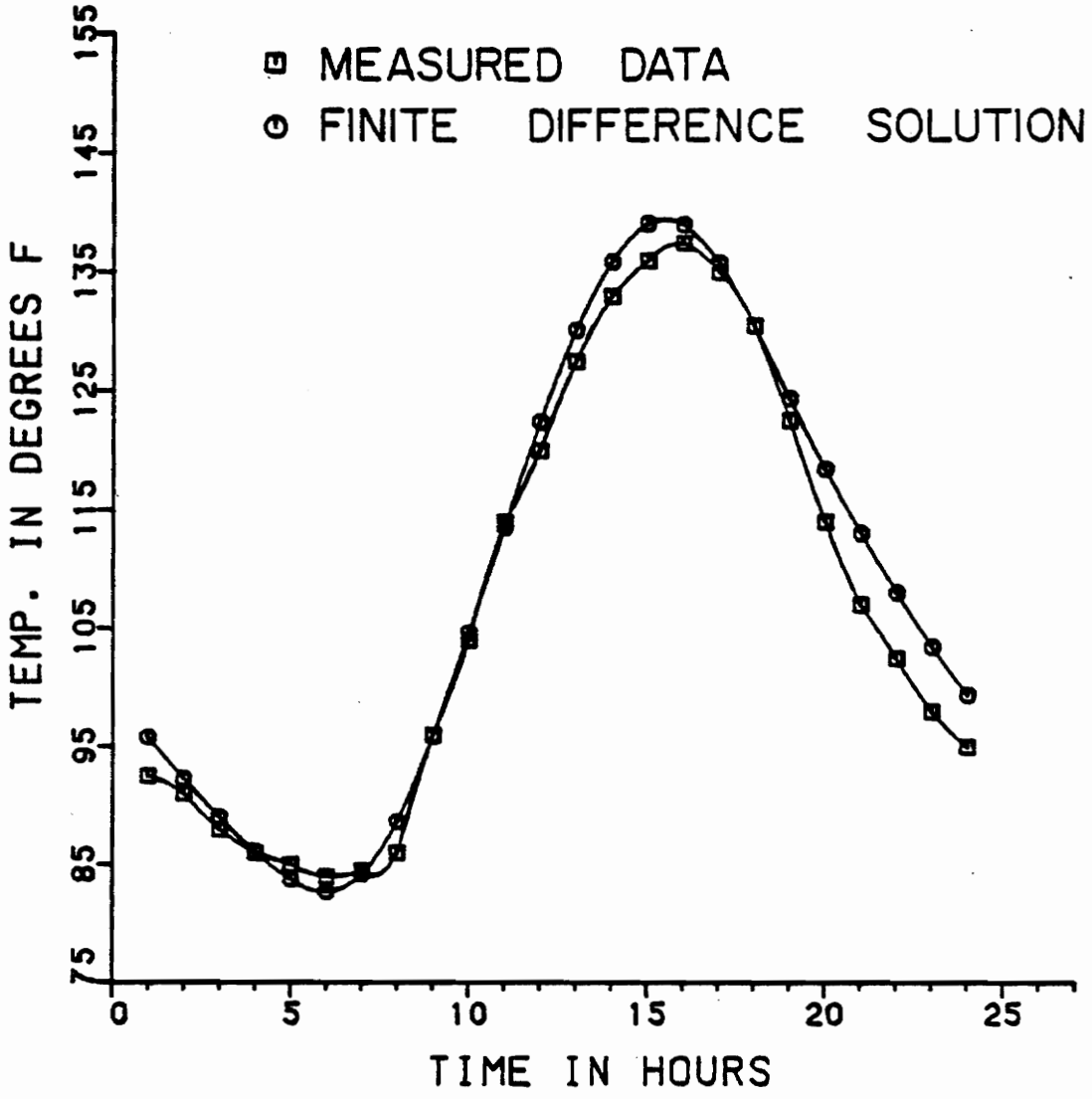

Figure 19. Measured data [32] and finite difference solution at the bore of the uninsulated cylinder.

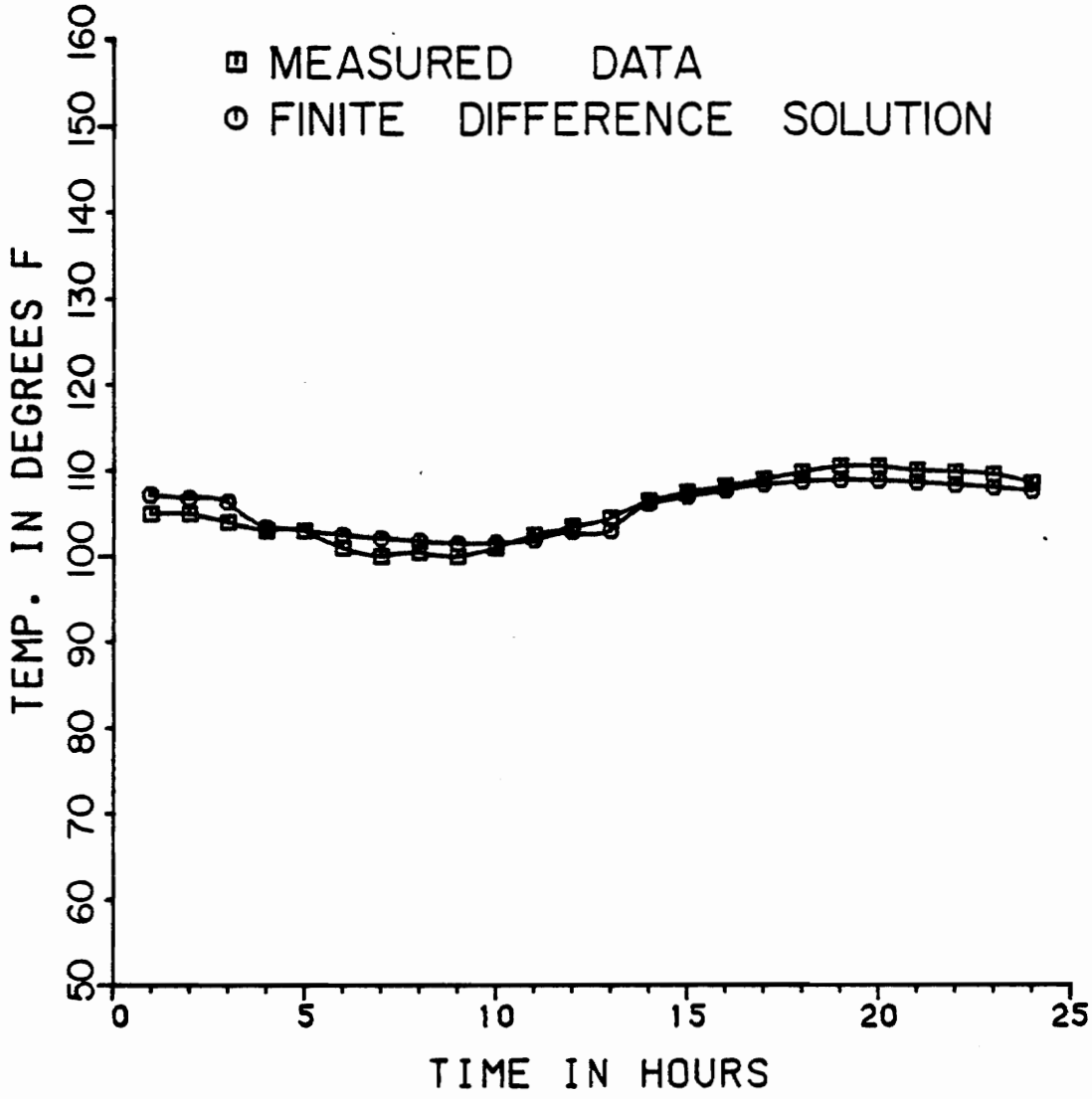

Figure 20. Measured data [32] and finite difference solution on the steel case surface of the insulated cylinder (solar radiation and heat convection included).

The next step is to include solar radiation and a varying heat convective coefficient into the boundary surface of the cylinder. One difficulty is the choice of absorptivity and emissivity values for the insulated surface; there are no available numerical values for the material (polyurethane) considered. A deterministic solar radiation equation based on experimental results has been proposed by some authors which is applicable to the Southwestern region of the United States and has been introduced in Heller's work [11]. By varying the coefficients, a trial and error solution, resulting in a similar response to Heller's results, was carried out. Also from various combinations of the absorptivity and emissivity used previously to compare the measured data with finite difference solution, it has been found that a value of 0.5 for both absorptivity and emissivity might be a reasonable choice. It was also found that within the range of 0.4 to 0.6 the solutions will not change appreciably.

The solutions for both the thin and thick cylinder were obtained for temperature record of a year in Phoenix, Arizona starting on July 1, 1952 and ending on June 31 of 1953. The initial temperature was given a value of 92°F for the thick cylinder and 97°F for the thin cylinder. Since the time interval $\Delta t = 1$ hr, there are 8760 time steps needed for the computations. It is seen from the solutions (Figs. 21 and 22) that temperature responses in the thick cylinder are smaller in amplitude than those of the thin cylinder. In fact, the highest temperature in the propellant of the thick cylinder is about 3°F lower than in the thin cylinder and in the winter the

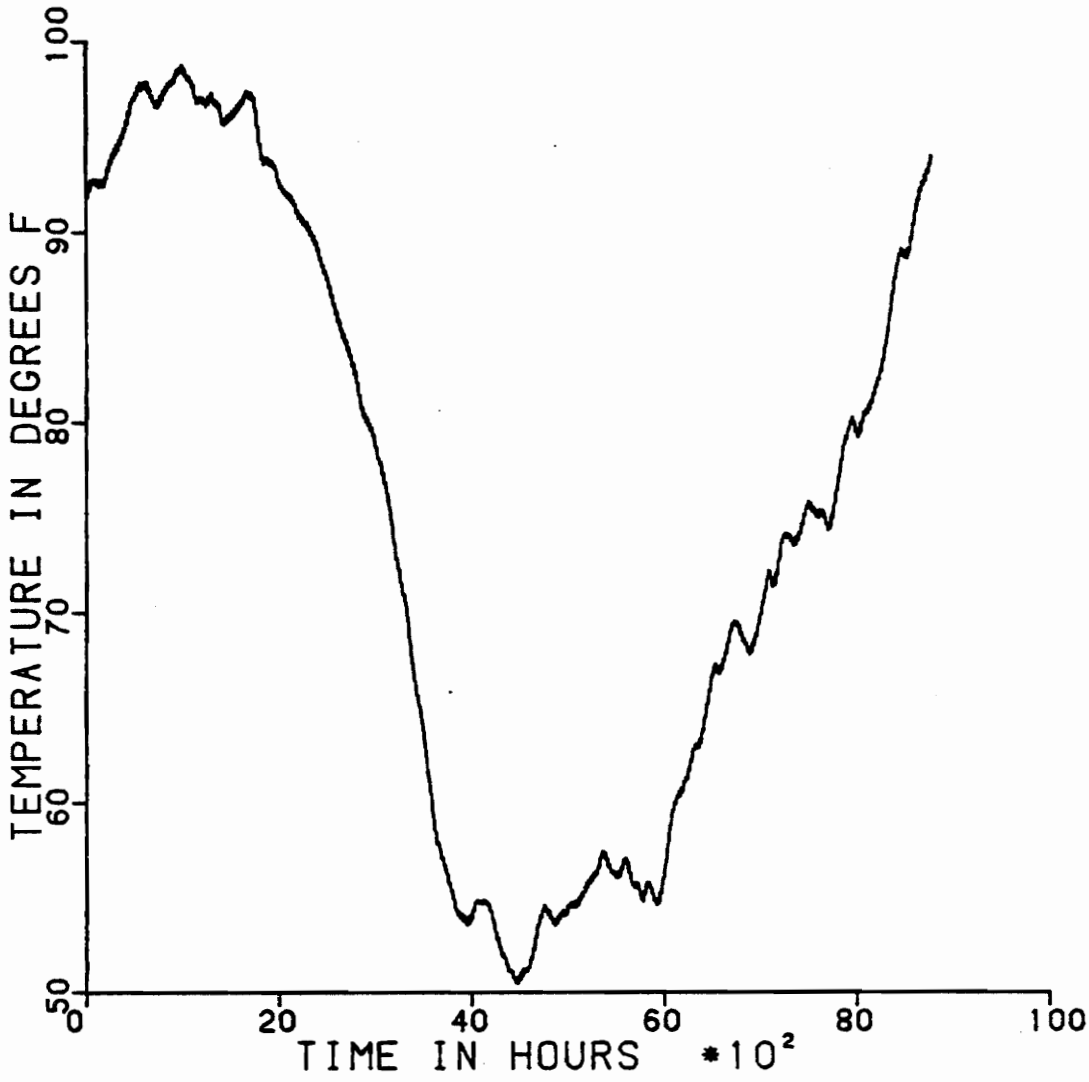

Figure 21. Bore temperature of the thick cylinder in one year (for inputs see Figs. 27, 28, 29).

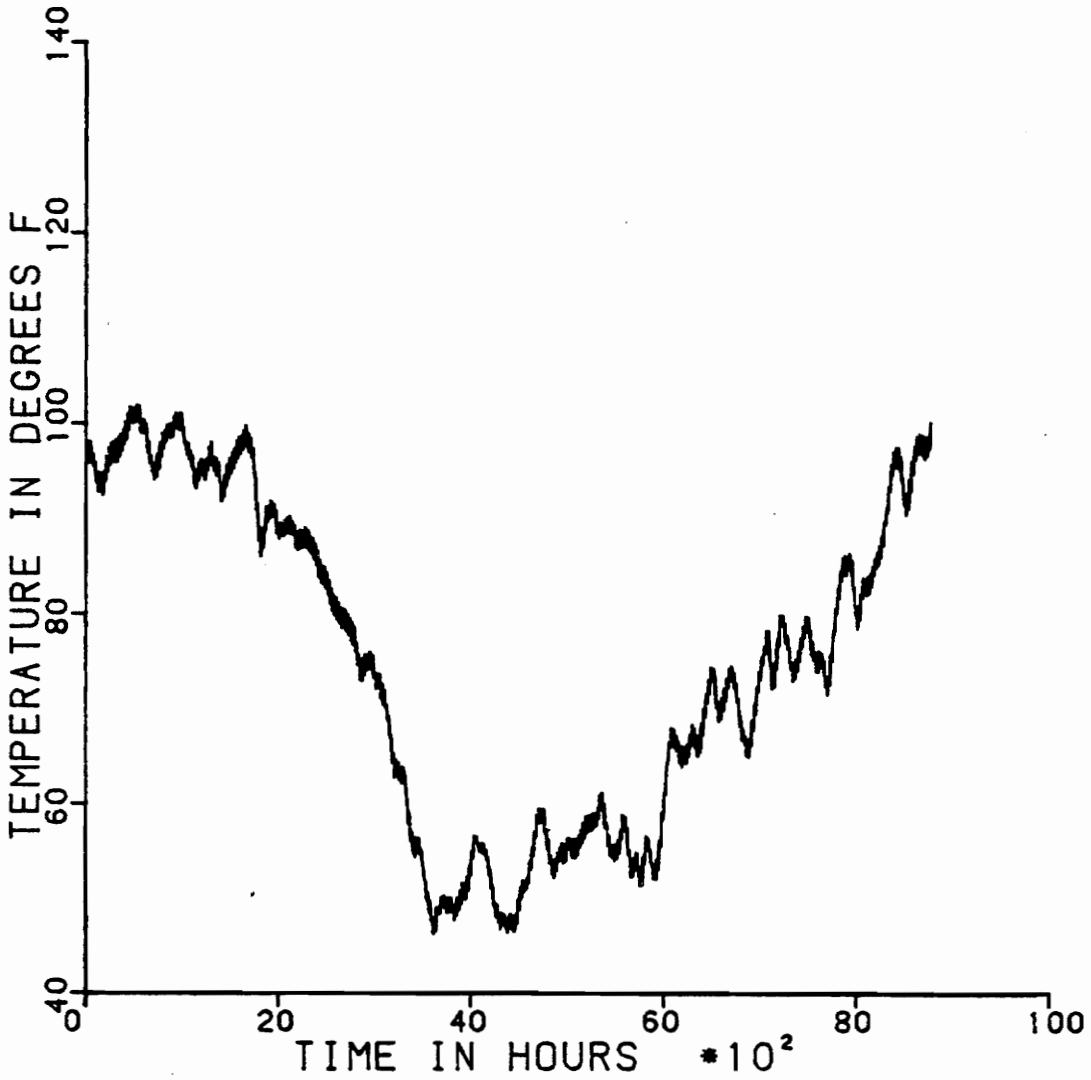

Figure 22. Bore temperature of the thin cylinder in one year (for inputs see Figs. 27, 28, 29).

lowest temperature in the propellant is about 5°F higher in the thick cylinder. Based upon these findings, it will be shown later that induced thermal stresses and strains in the thick cylinder are smaller than in the thin one and so is the probability of failure.

To illustrate thermal responses of the cylinder, Figs. 23 and 24 show temperatures at the bore and on the surface in addition to the ambient temperature for the thin and thicker cylinder respectively. Results are shown for the first two days of August 1952 and obtained after the temperature responses have stabilized (solutions are carried out since July 1, 1952).

It is seen that the temperature on the surface of the cylinder is much higher than the air temperature during noon time and drops below the air temperature during the night. This explains the important role solar radiation plays in shaping the temperature on the surface of the cylinder. Figs. 3, 25 and 26 show the hourly solar (global) radiation, ambient temperature and wind speed on the same two days.

Figures 27, 28 and 29 show the ambient temperature, solar radiation and wind speed for the whole year at the location of interest. As a result, Figs. 21 and 22 illustrate temperature response of the bore of the thick and thin cylinders throughout the year.

As mentioned in part II of this study, several authors have assumed the surface temperature to be identical to the ambient temperature. It is of great interest to develop a deterministic solar radiation model that could be added to the ambient temperature. In fact, such a model has been proposed by some authors as already mentioned earlier.

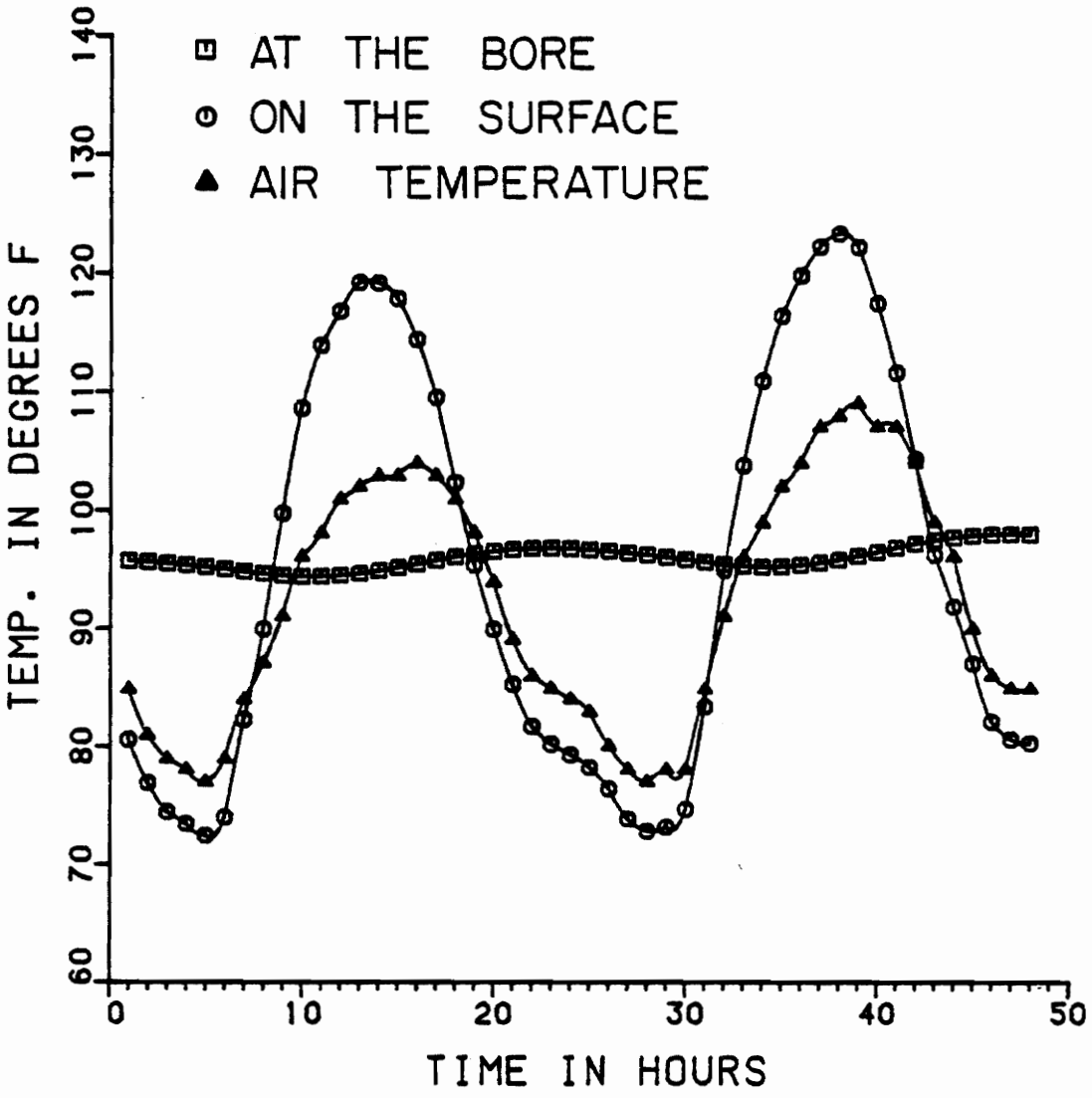

Figure 23. Bore and surface temperature of the thin cylinder in 48 hours (for inputs see Figs. 3, 25, 26).

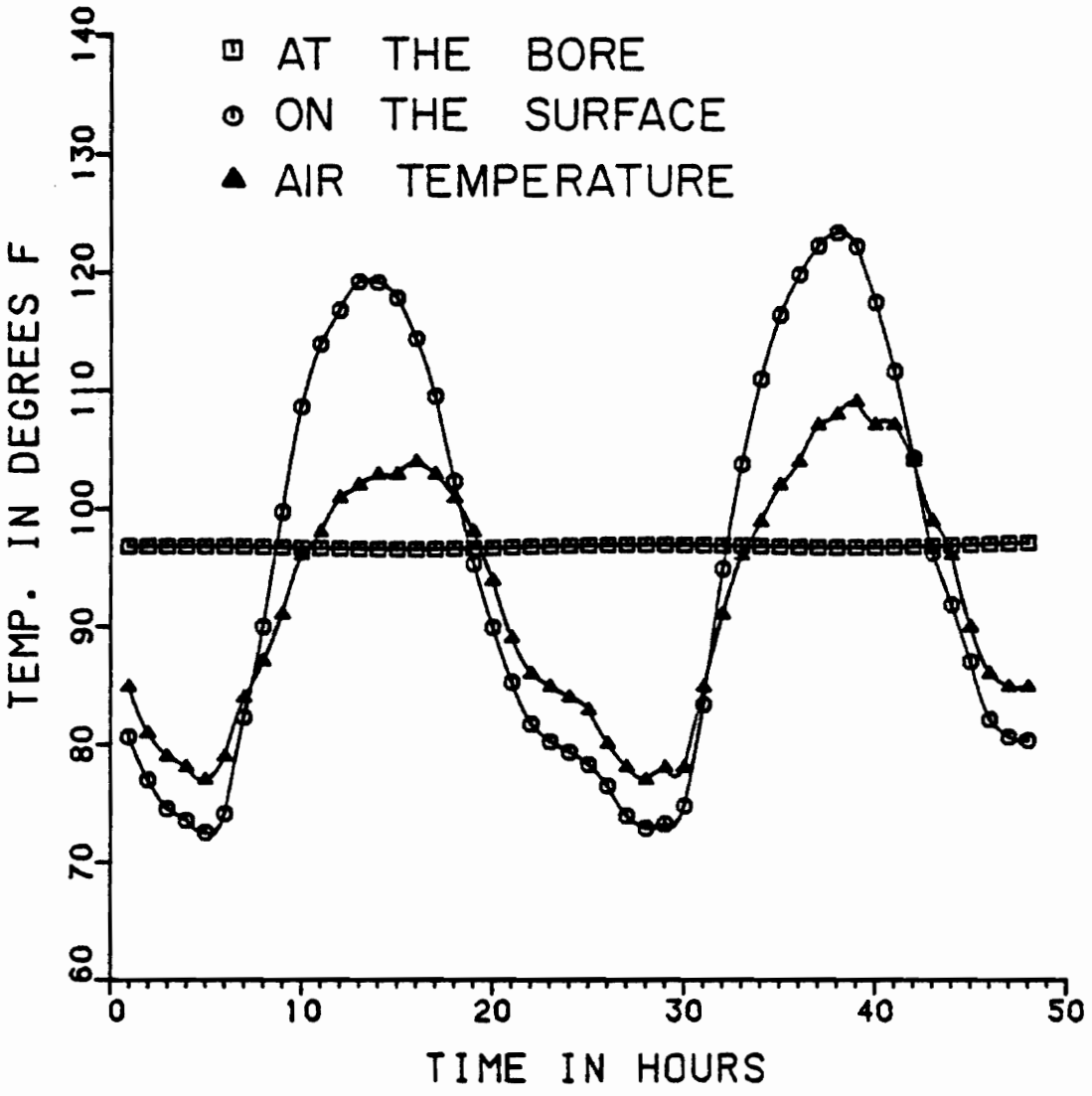

Figure 24. Bore and surface temperature of the thick cylinder in 48 hours (for inputs see Figs. 3, 25, 26).

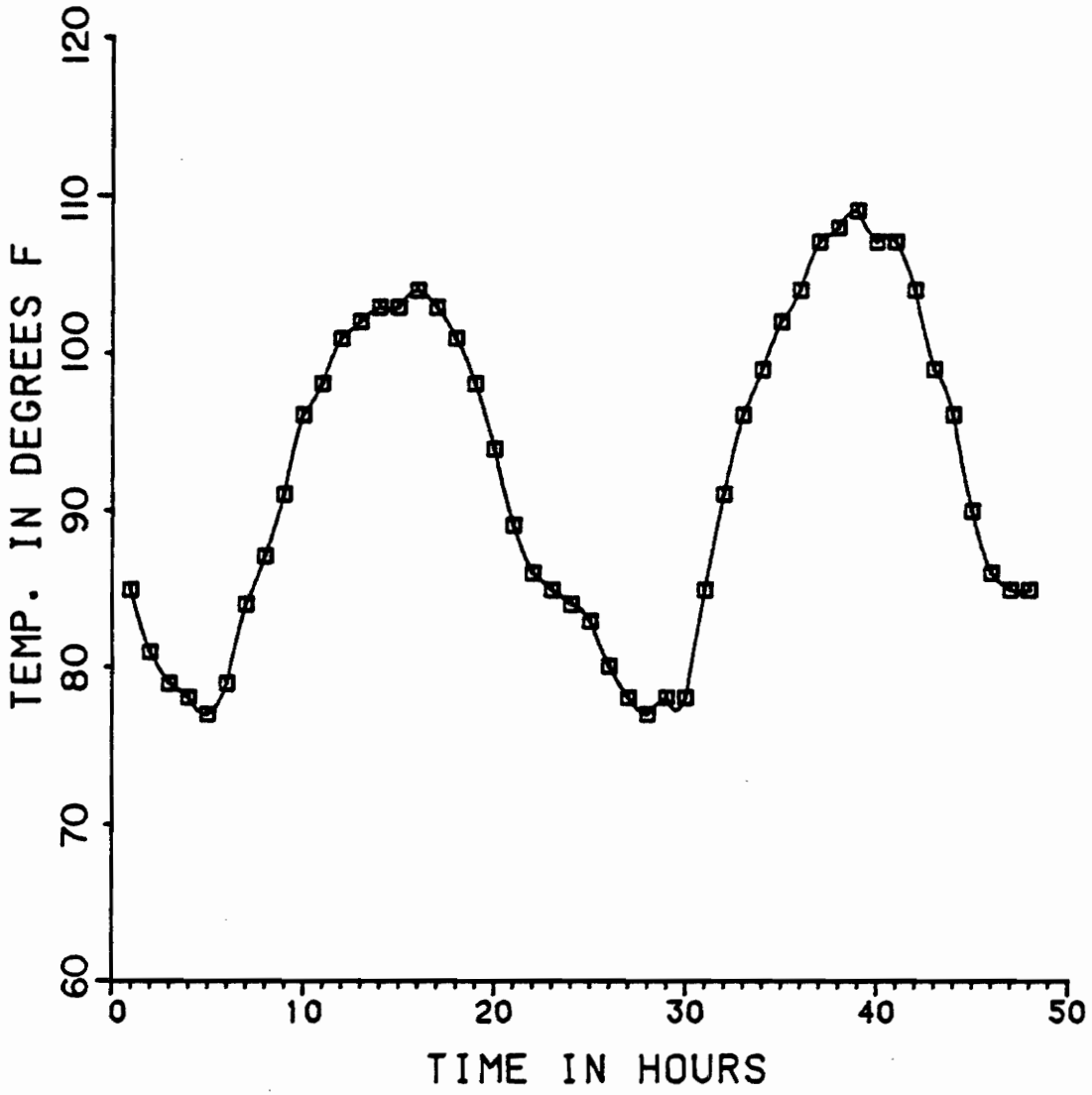

Figure 25. Typical air temperature.

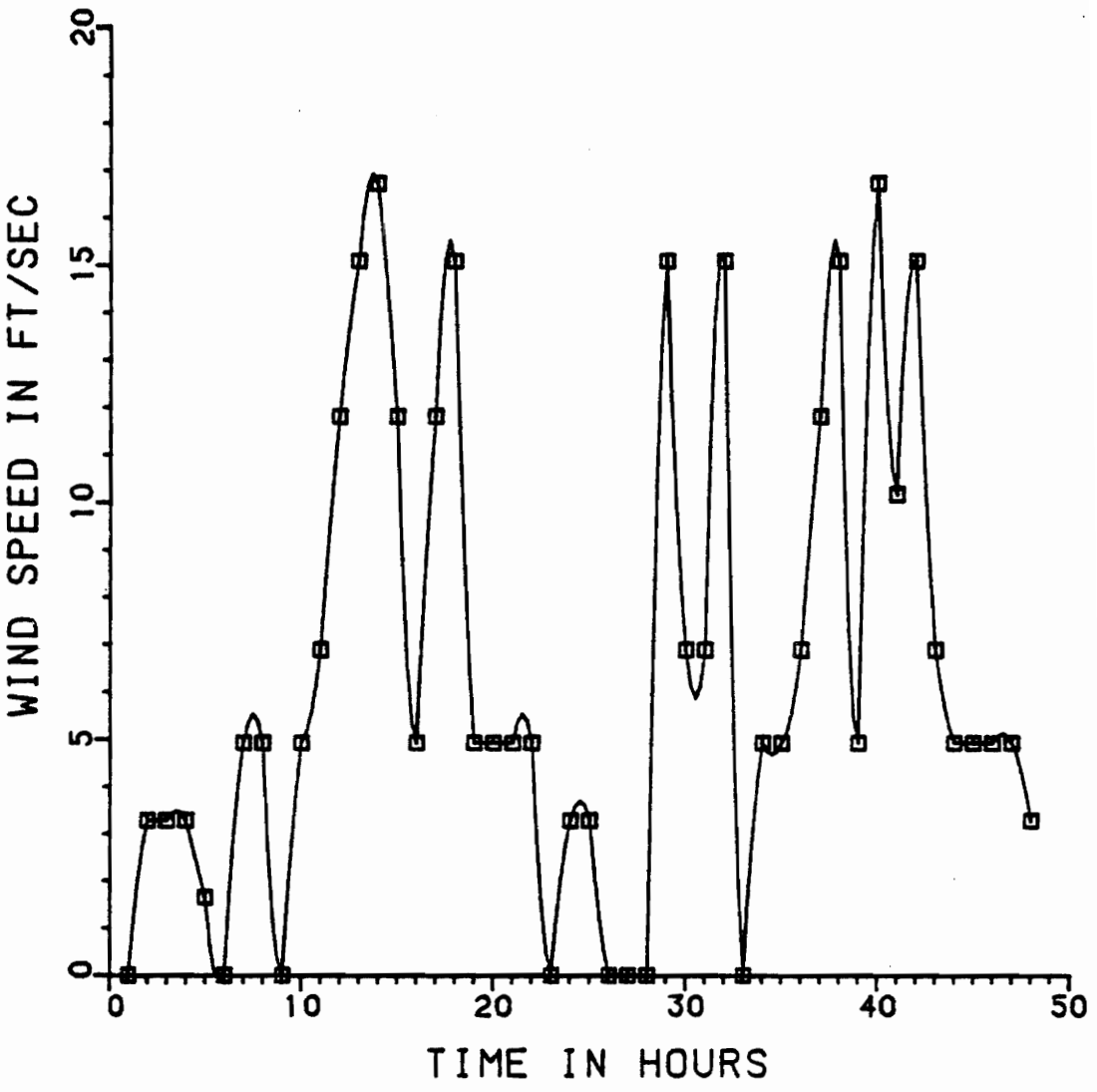

Figure 26. Typical wind speed.

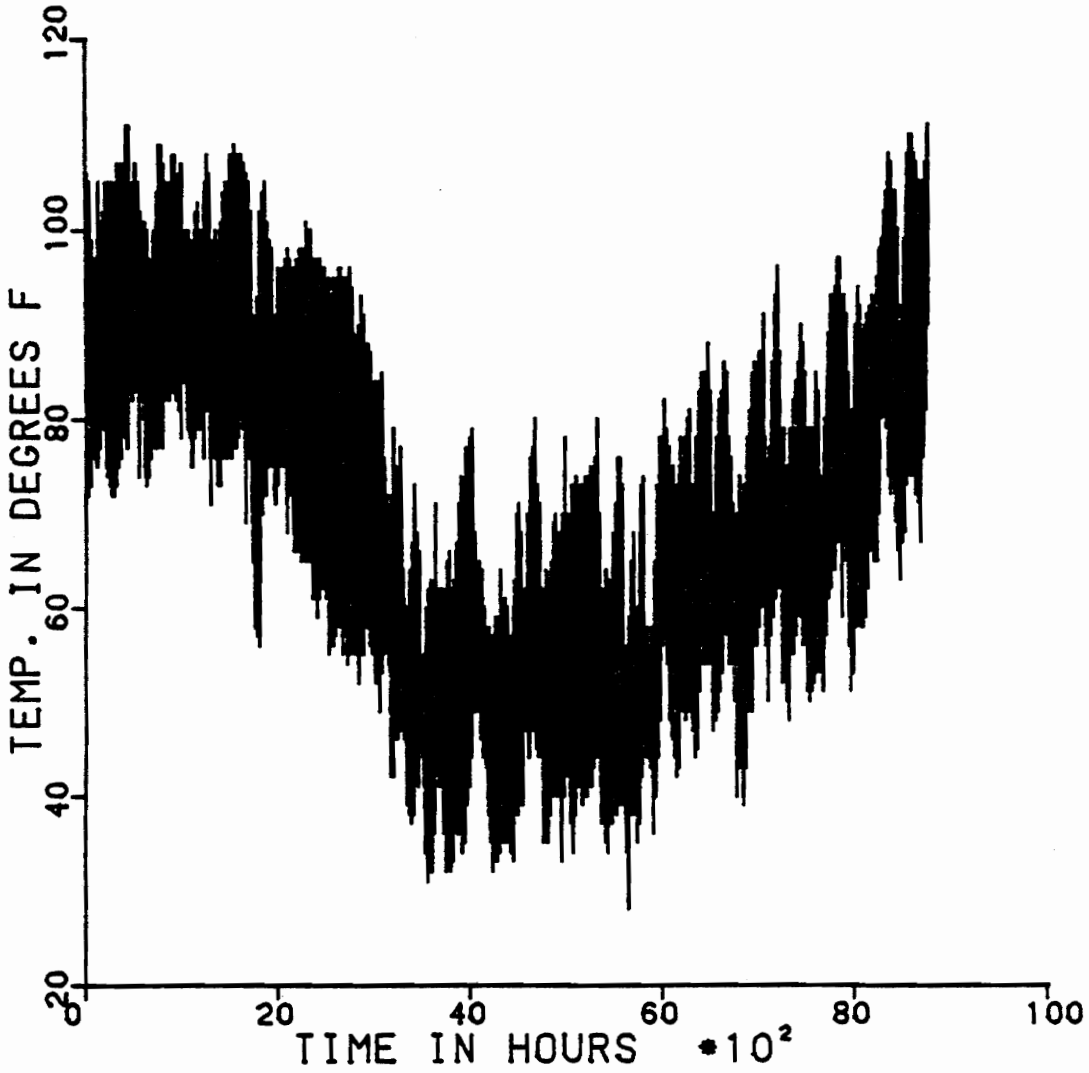

Figure 27. Air temperature in Phoenix, Arizona (7/1/1952-6/30/1953).

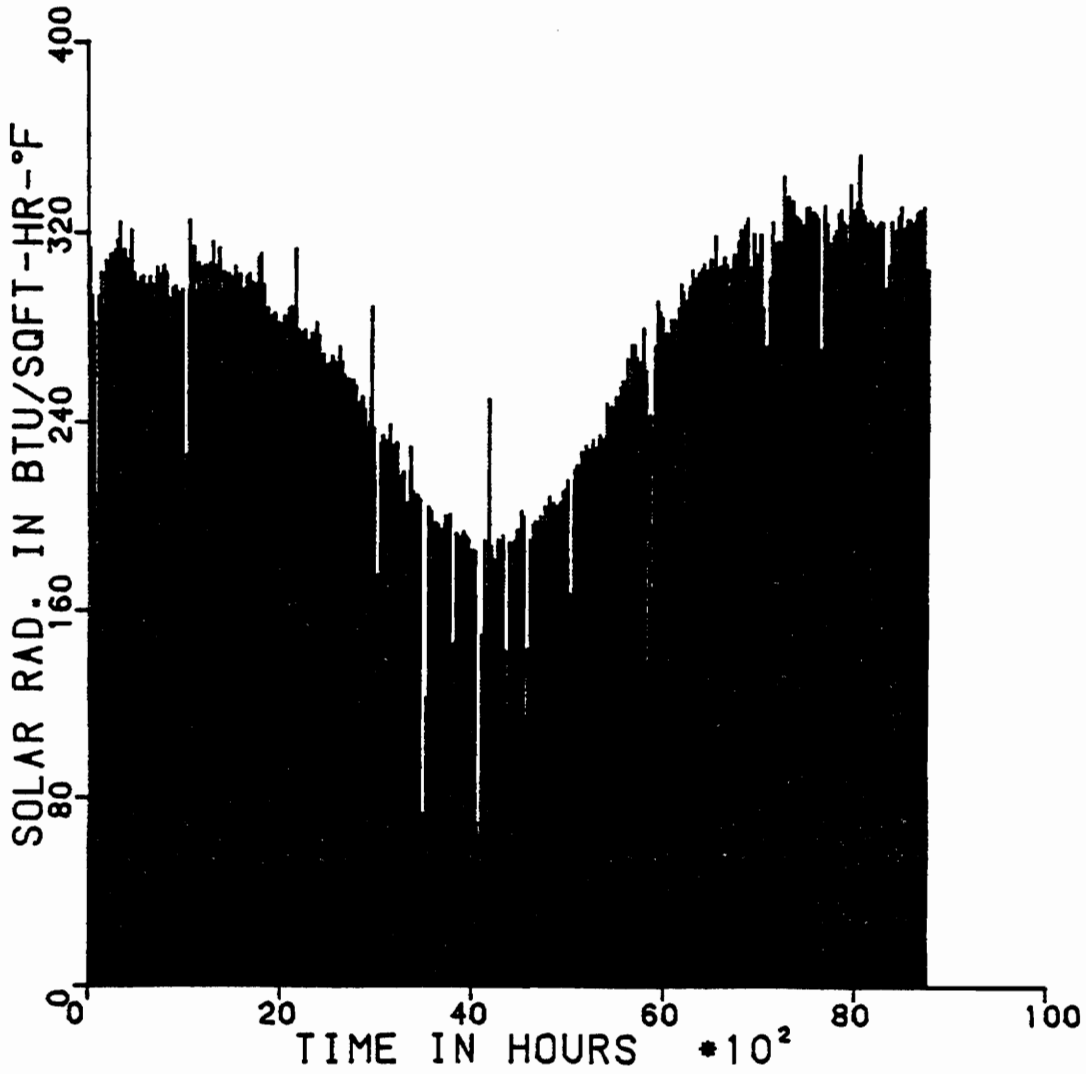

Figure 28. Solar radiation in Phoenix, Arizona (7/1/1952 - 6/30/1953).

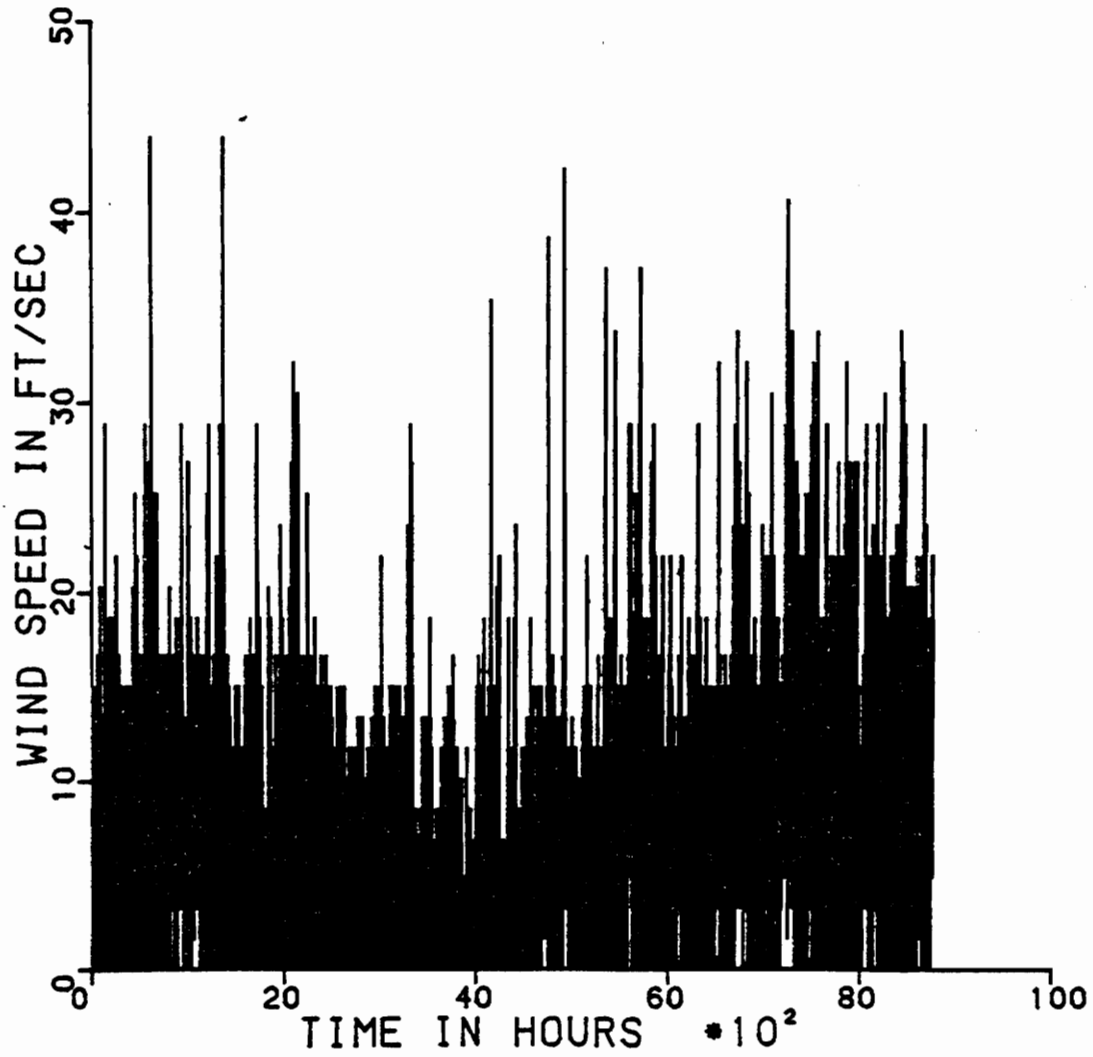

Figure 29. Wind speed in Phoenix, Arizona (7/1/1952 — 6/30/1953).

In the present situation, given the surface temperature (by finite difference solution) of the cylinder, it is possible to develop an additional temperature model which is equivalent to solar radiation transmitted through the surface of the cylinder. This model together with the ambient temperature provide the surface temperature in some approximate sense.

The proposed model is expressed as

*For $165 < t < 215$

$$\Delta T = 7.0 + 0.5 \cos t + 6 \cos 15(h-12) - 12 \cos 5.5(h-12) \quad (6.1)$$

*For $t < 165$ and $t > 215$

$$\Delta T = 7.0 + 0.5 \cos t + 6 \cos 15(h-12), \quad 6 < h < 18 \quad (6.2)$$

$$\Delta T = 7.0 + 0.5 \cos t + 6 \cos 15(h-12) - 12 \cos 5.5(h-12), \quad 18 < h < 6 \quad (6.3)$$

In which the first term of Eq. (6.1) represents the annual mean, the second term represents the seasonal cycle, the third term is the daily cycle and the last term can be considered as the "reradiation" term. T is in °F, t is the day of the year (365 days), starts from 1 (July 1), h is the hour of the day, starts from 1 (1 A.M.). In fact, this model can start from any day of the year. Suppose if one wishes to start on January 1 which is about 180 days from July 1 then the second term of Eq. (6.1) must be (-0.5 cost) and the equation is good for $0 < t < 50$. The second term of Eqs. (6.2) and (6.3) also becomes negative and the equations are good for $365 > t > 50$.

The model has been tested for the year of interest (1952 in Phoenix, Arizona). The results compared relatively well with the finite difference solution. Figures 30 and 31 show a typical day in the summer and winter respectively.

6.2 Stress Response

The next task is to obtain stress and strain responses of the propellant. In part V of this study, it was shown that given the temperatures across the propellant of a given time, a numerical integration technique can evaluate stress and strain across the propellant at that time.

The integration is performed within certain space limits. In this case only stress and strain across the propellant are of interest, so the limit of integration is from the bore (r_1) to the interface (r_2). In principle, within the range of the integration more space intervals give better results, but of course at the expense of increased labor in computation because more nodes are needed for the finite difference solutions. To start out, a 21 node model is used in which the propellant is divided into 5 equal intervals with a total of 6 nodes including 2 nodes shared by the other two layers. A solution is obtained for a sinusoidal input and the product of $T \times r_i$ is plotted vs r_i in Fig. 6. The relation is linear. As such, it is quite possible to use a smaller number of nodes and yet obtain a reasonable solution. In fact given the two lower and upper limit values, the area under the curve $T \times r_i$ can be approximated without large errors being generated. For the present case, the propellant has 3 nodes so

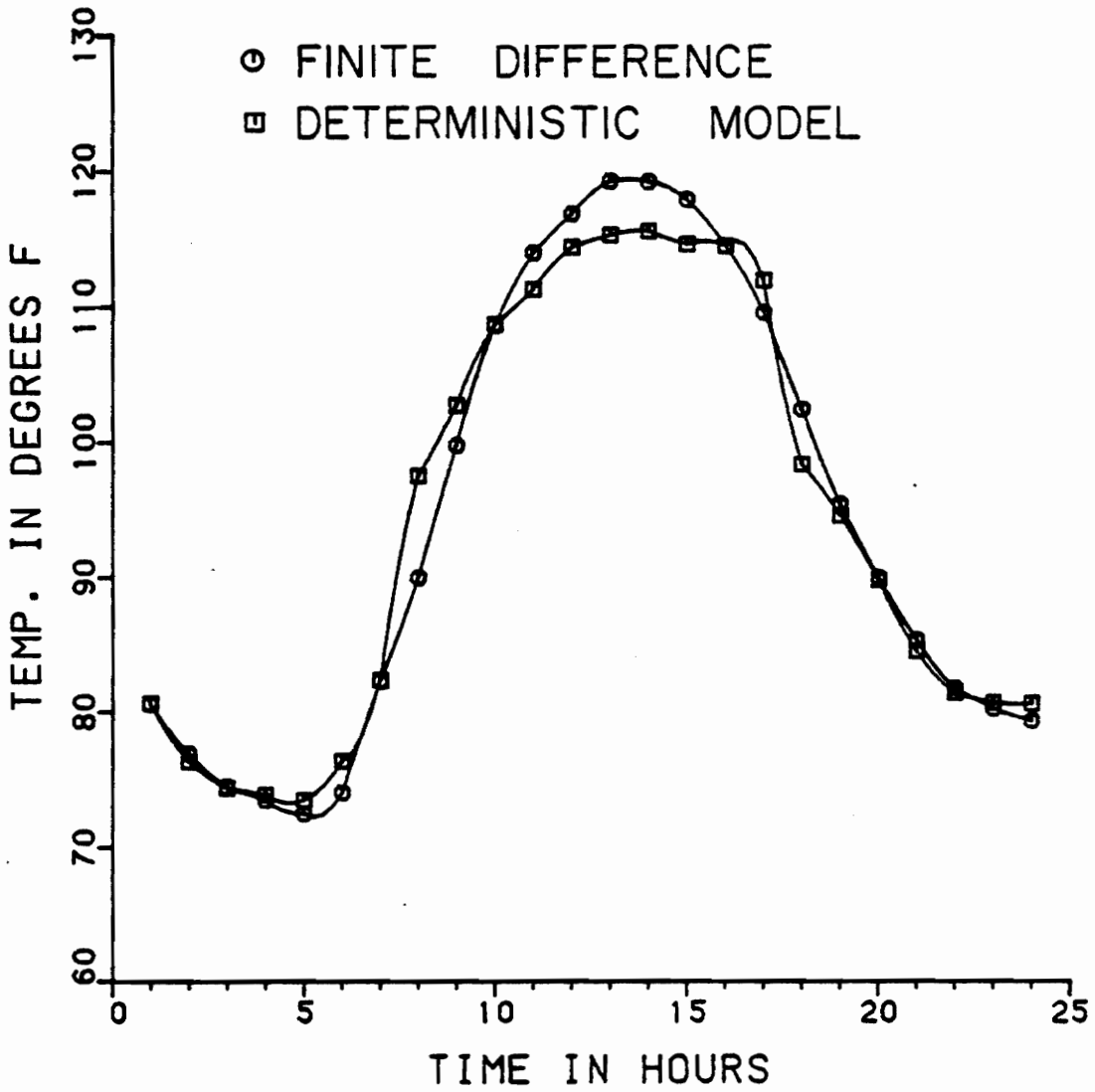

Figure 30. Deterministic model and finite difference solution for the cylinder surface temperature in 24 hours in summer.

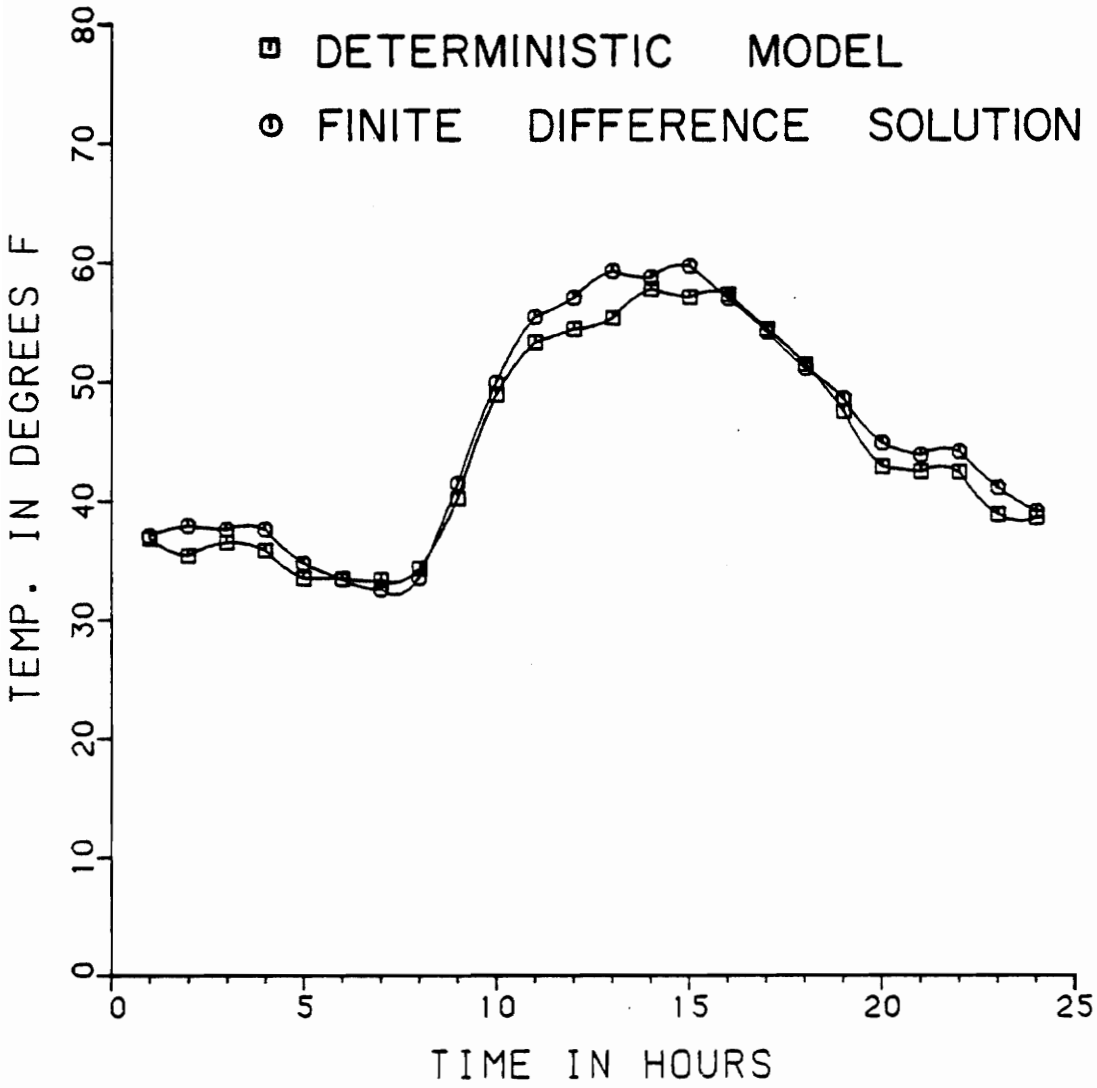

Figure 31. Deterministic model and finite difference solution for the cylinder surface temperature in 24 hours in winter.

one can obtain temperatures at the bore, interface and at the mid-point between them.

Before evaluating stress and strain responses for the real situation, it is important to compare stress responses obtained via the finite difference scheme and the closed form solution. To this end, for a sinusoidal ambient temperature input ($T = 10 \sin \omega t$), temperatures and stresses at various locations across the propellant are calculated. Figure 32 shows the tangential stress obtained by the finite difference technique and the closed form approach. Apparently, they compare quite well.

To illustrate the variations of stress and strain, the same 48 hours used for obtaining temperatures, presented in Figures 33-40, show the variations of radial stress, tangential stress, radial strain and tangential strain for the thin and thick cylinders respectively.

As discussed earlier in Part V the propellant grain tends to expand and contract but is restrained by the motor case. The induced thermal stresses resulting from the interaction between the propellant grain and the case are of interest. In fact, the tangential stress is greatest at the bore of the cylinder and hence likely to become the main cause of failure. Radial stress at the interface although significant is still much less severe than the tangential bore stress.

Tangential strain also shows significant values at the bore. Although radial strain is largest at the bore, it is compressive and hence will not contribute to propellant failure.

Figures 41 and 42 show the tangential stress for one year at the bore of the thin and thick cylinders respectively. Again, it

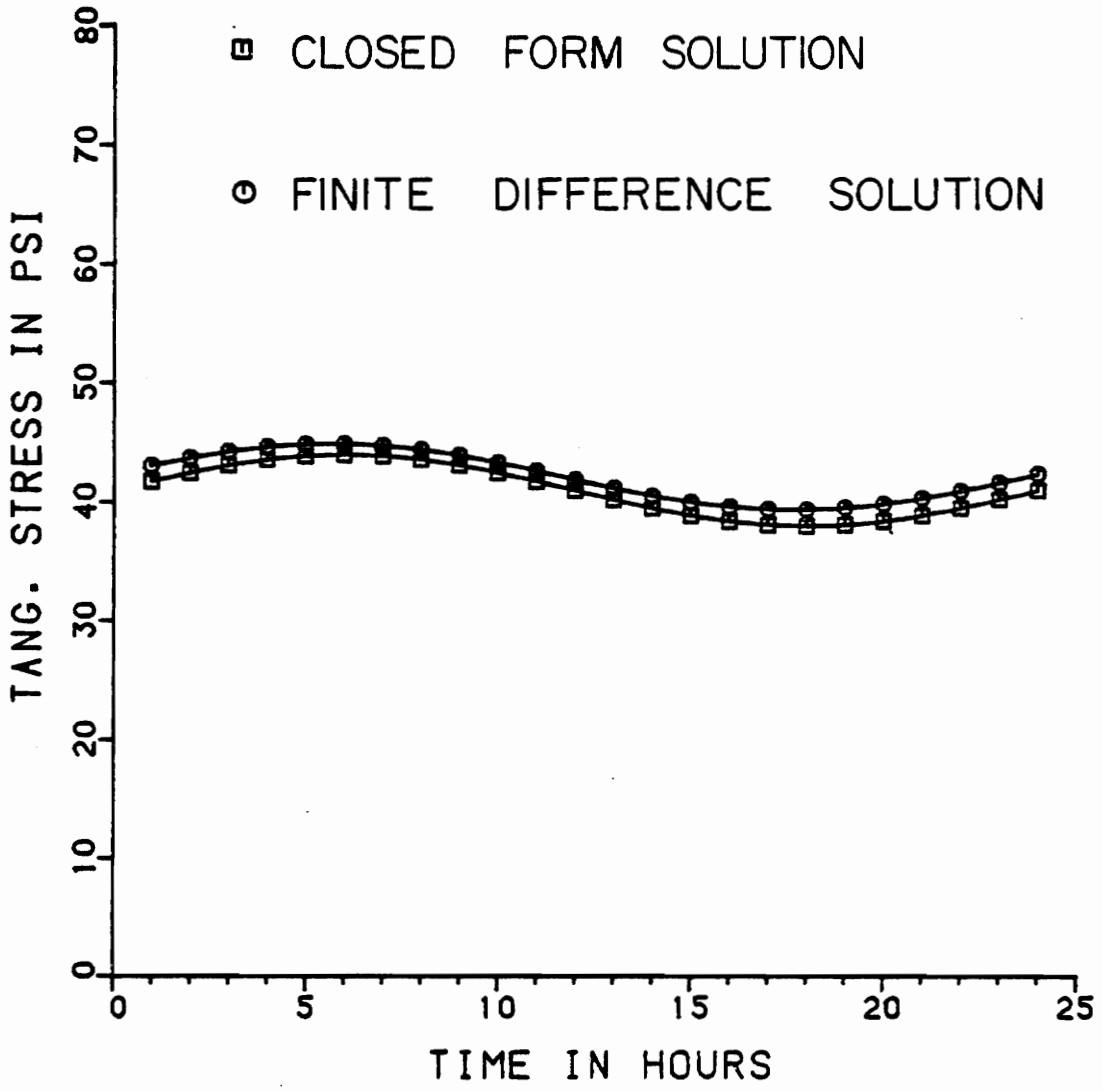

Figure 32. Tangential stress at the bore of the uninsulated cylinder by closed form and finite difference solution (for input see Fig. 17).

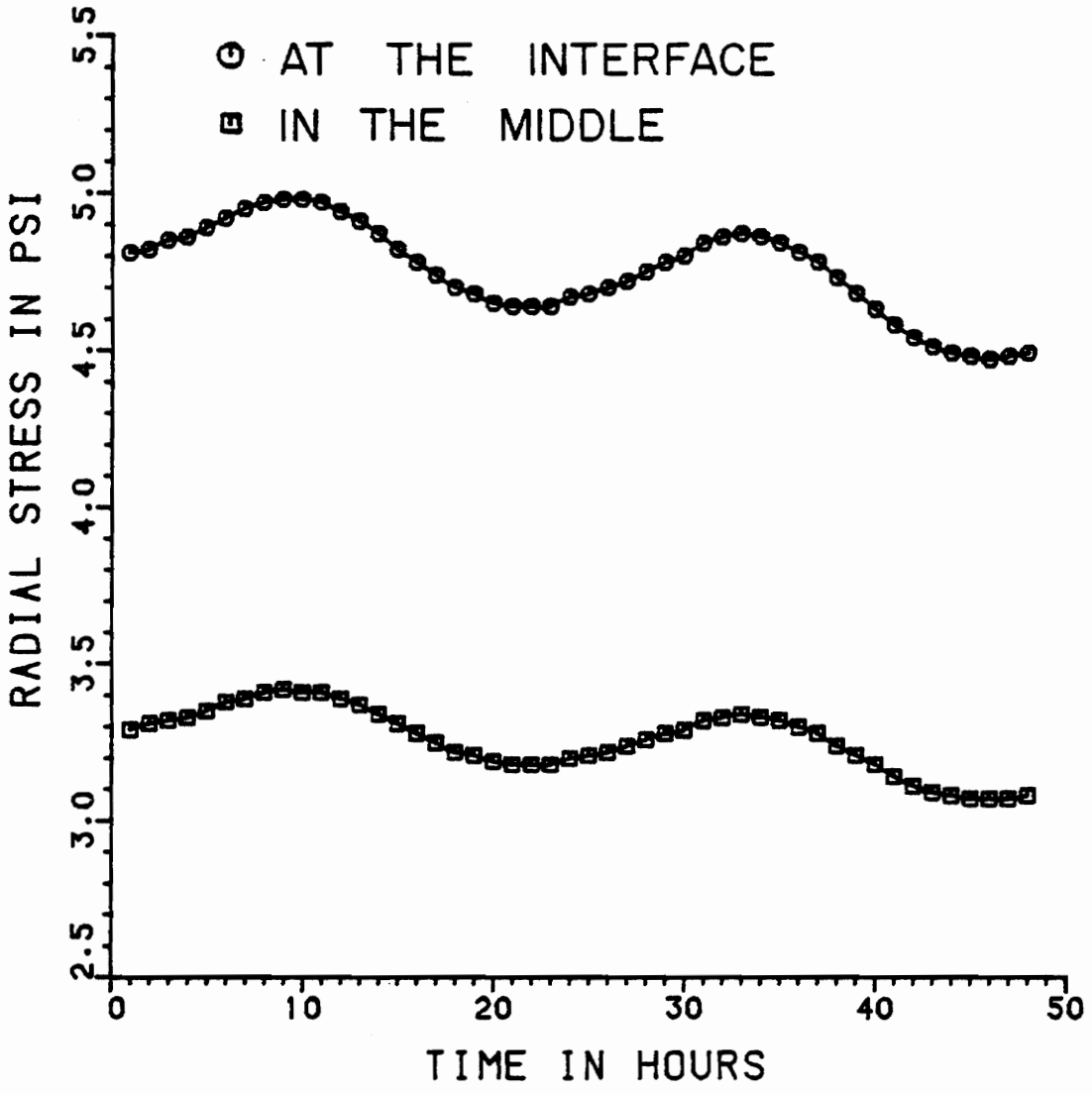

Figure 33. Radial stress in the propellant (thin cylinder) in 48 hours (for inputs see Figs. 3, 25, 26).

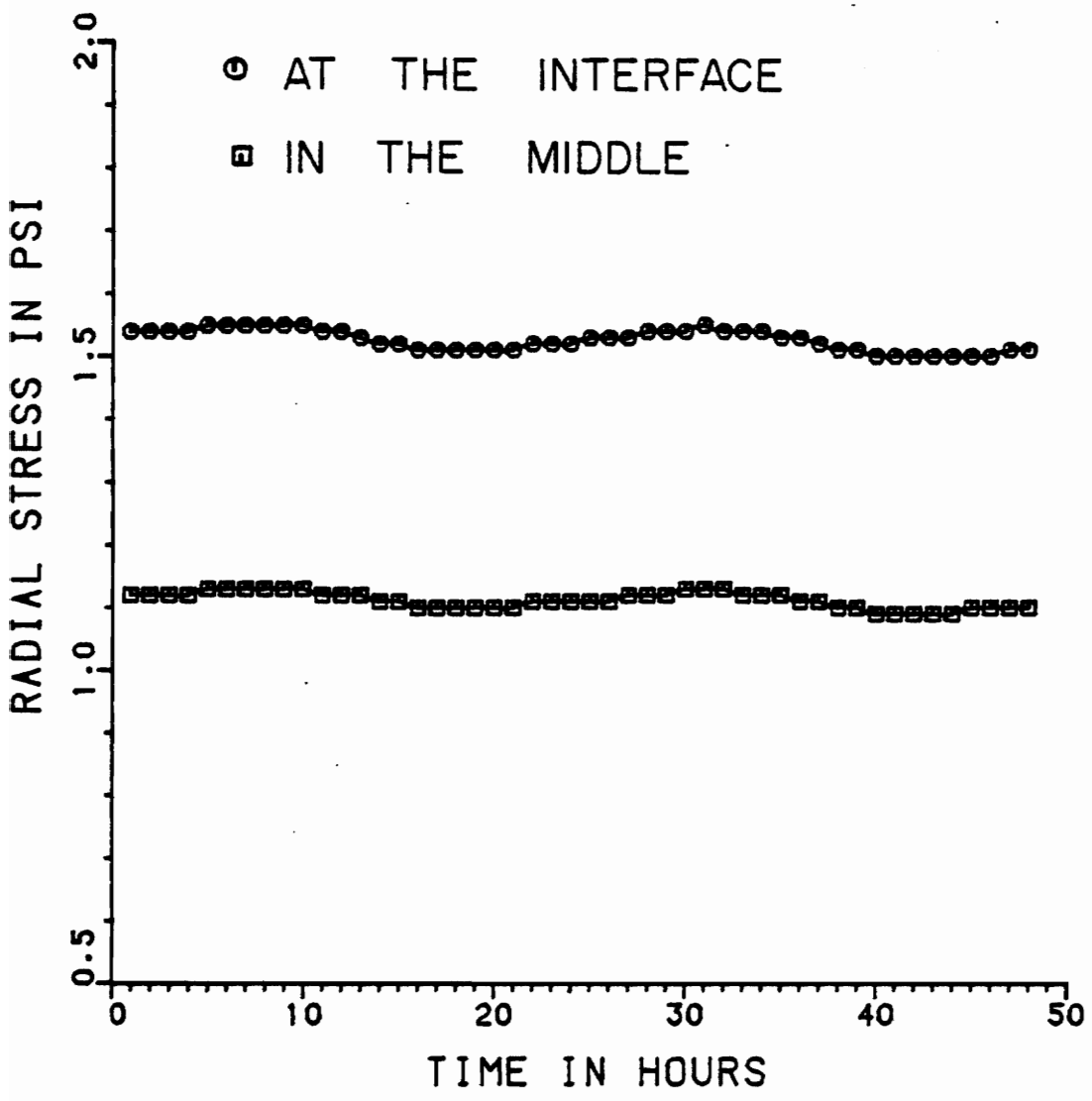

Figure 34. Radial stress in the propellant (thick cylinder) in 48 hours (for inputs see Figs. 3, 25, 26).

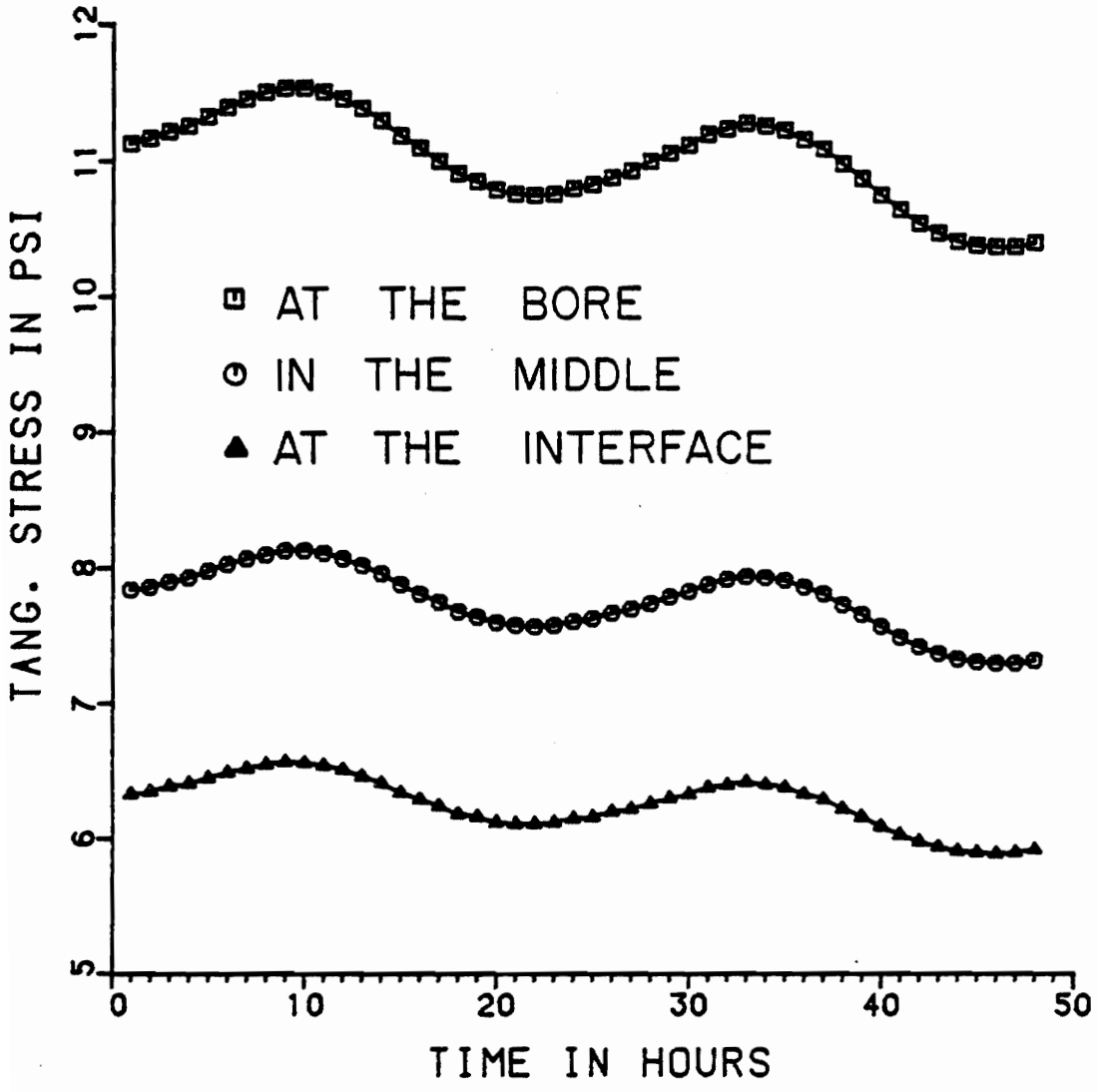

Figure 35. Tangential stress in the propellant (thin cylinder) in 48 hours (for inputs see Figs. 3, 25, 26).

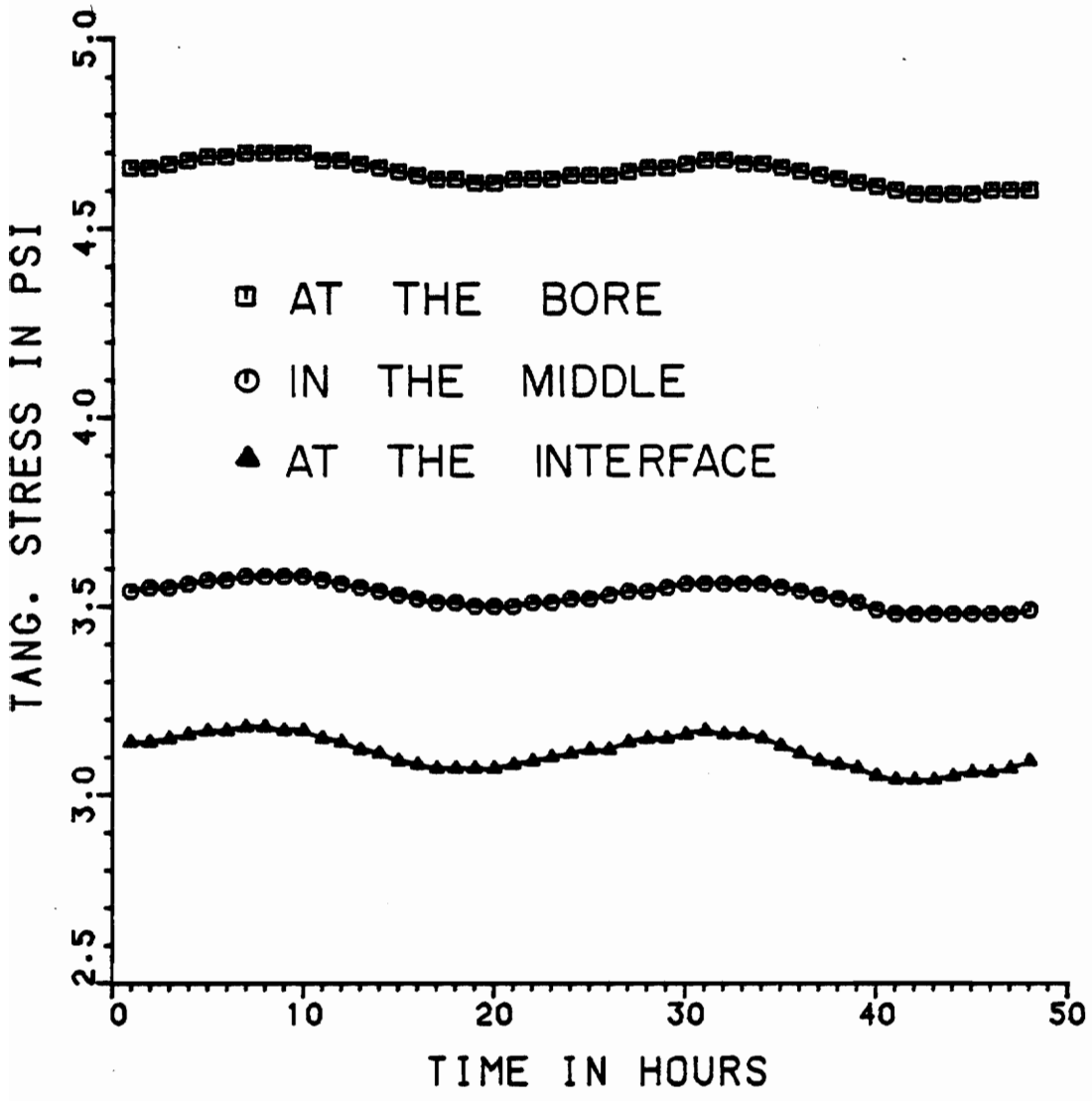

Figure 36. Tangential stress in the propellant (thick cylinder) in 48 hours (for inputs see Figs. 3, 25, 26).

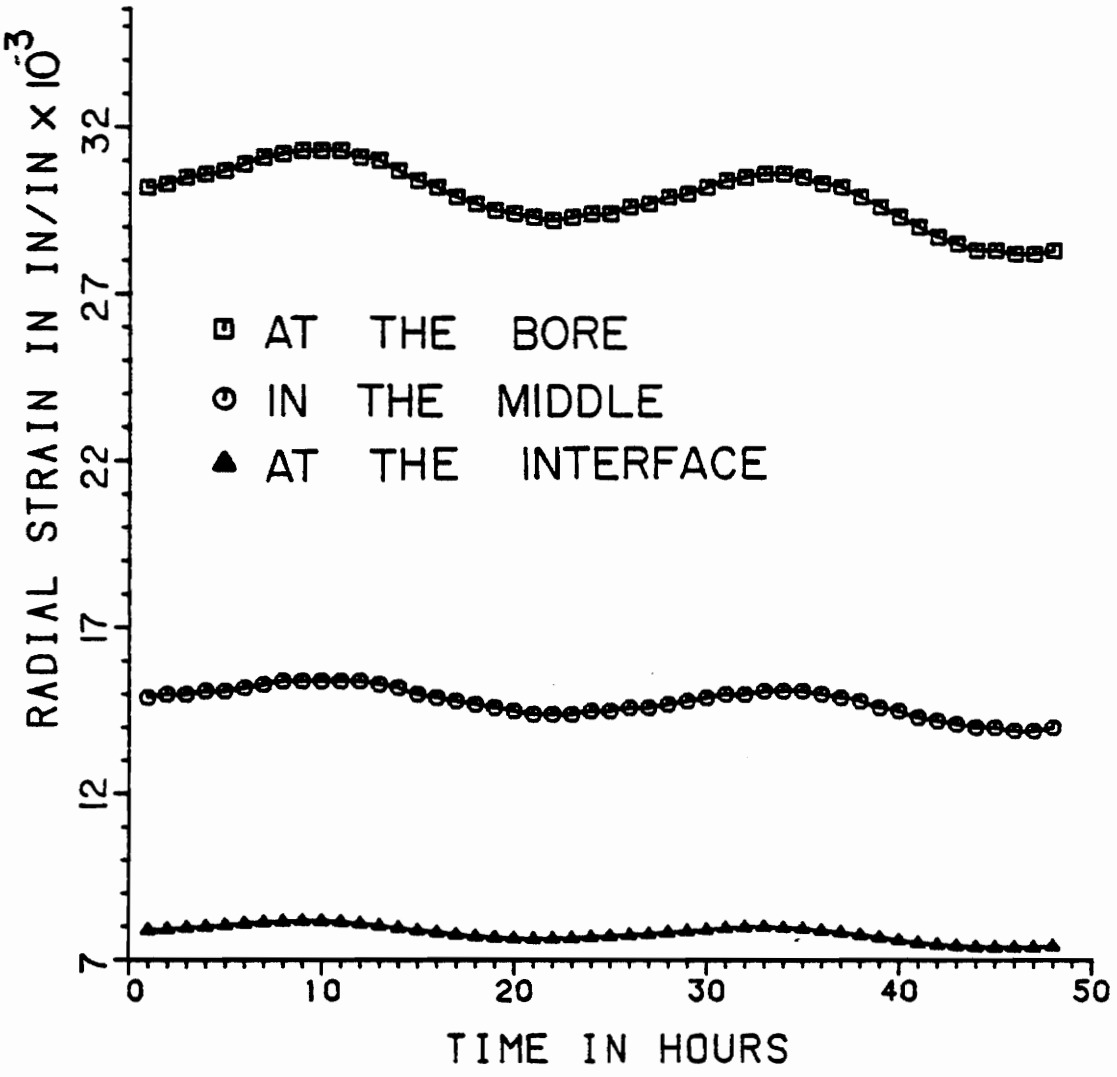

Figure 37. Radial strain in the propellant (thin cylinder) in 48 hours (for inputs see Figs. 3, 25, 26).

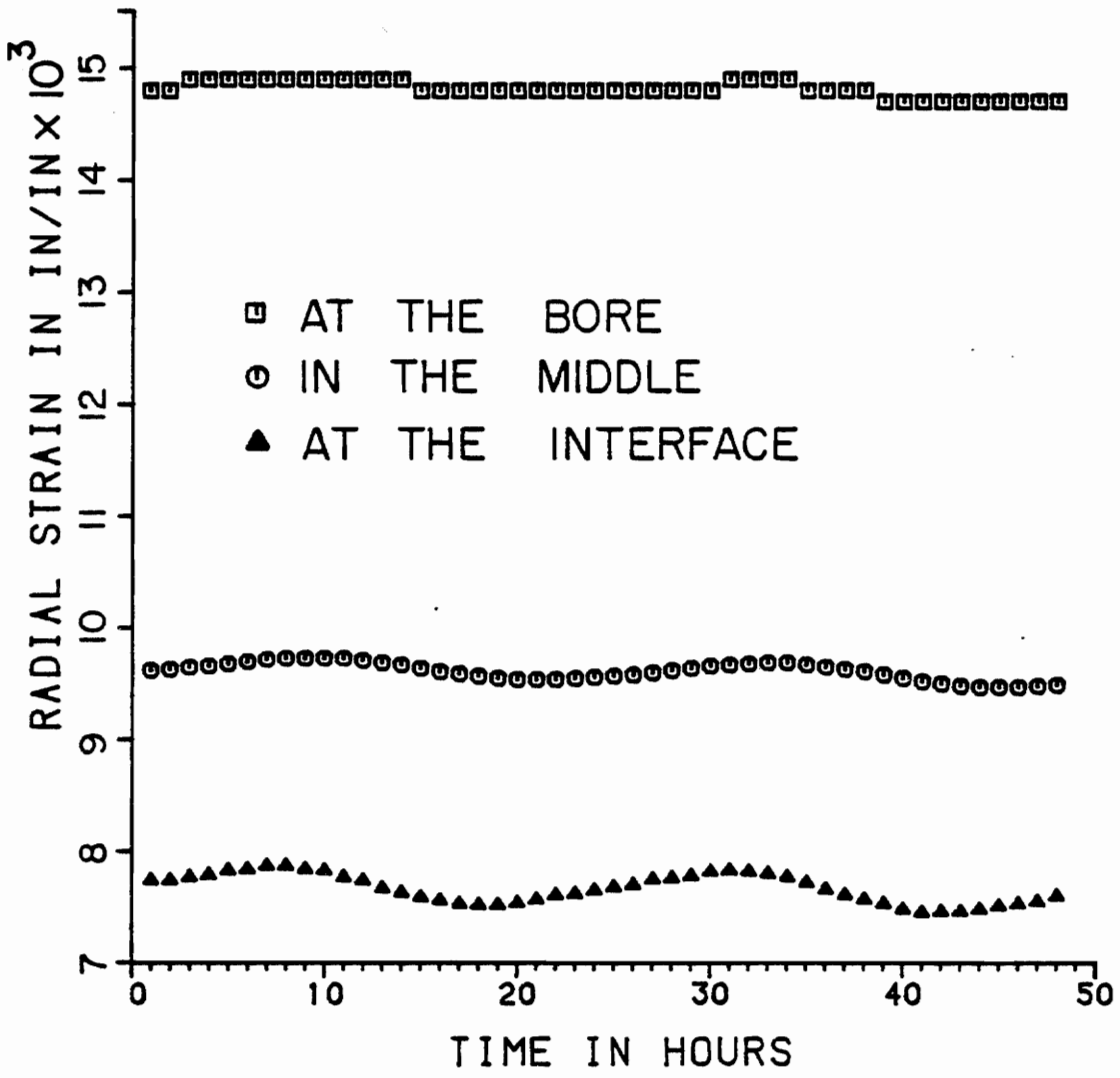

Figure 38. Radial strain in the propellant (thick cylinder) in 48 hours (for inputs see Figs. 3, 25, 26).

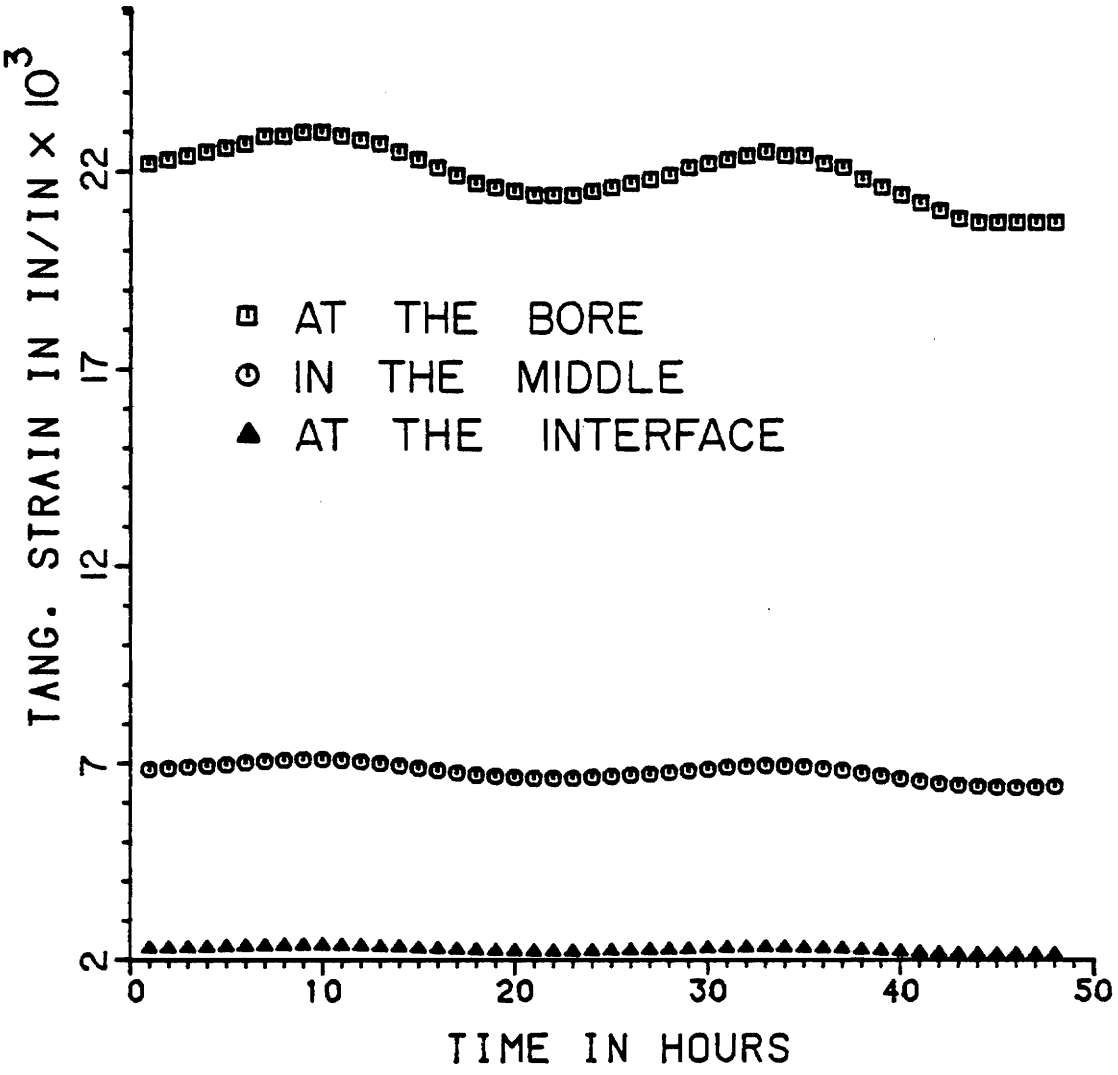

Figure 39. Tangential strain in the propellant (thin cylinder) in 48 hours (for inputs see Figs. 3, 25, 26).

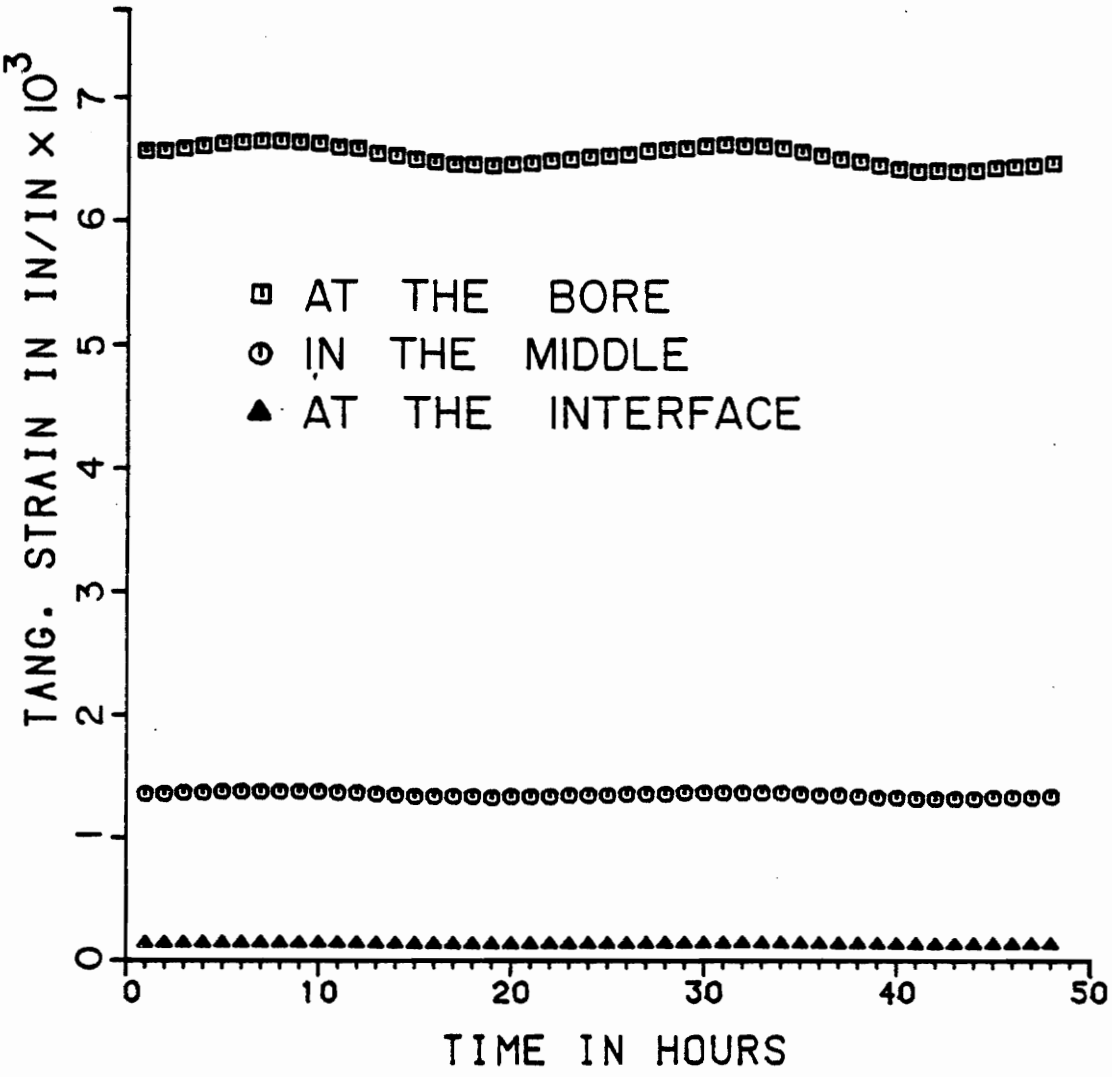

Figure 40. Tangential strain in the propellant (thick cylinder) in 48 hours (for inputs see Figs. 3, 25, 26).

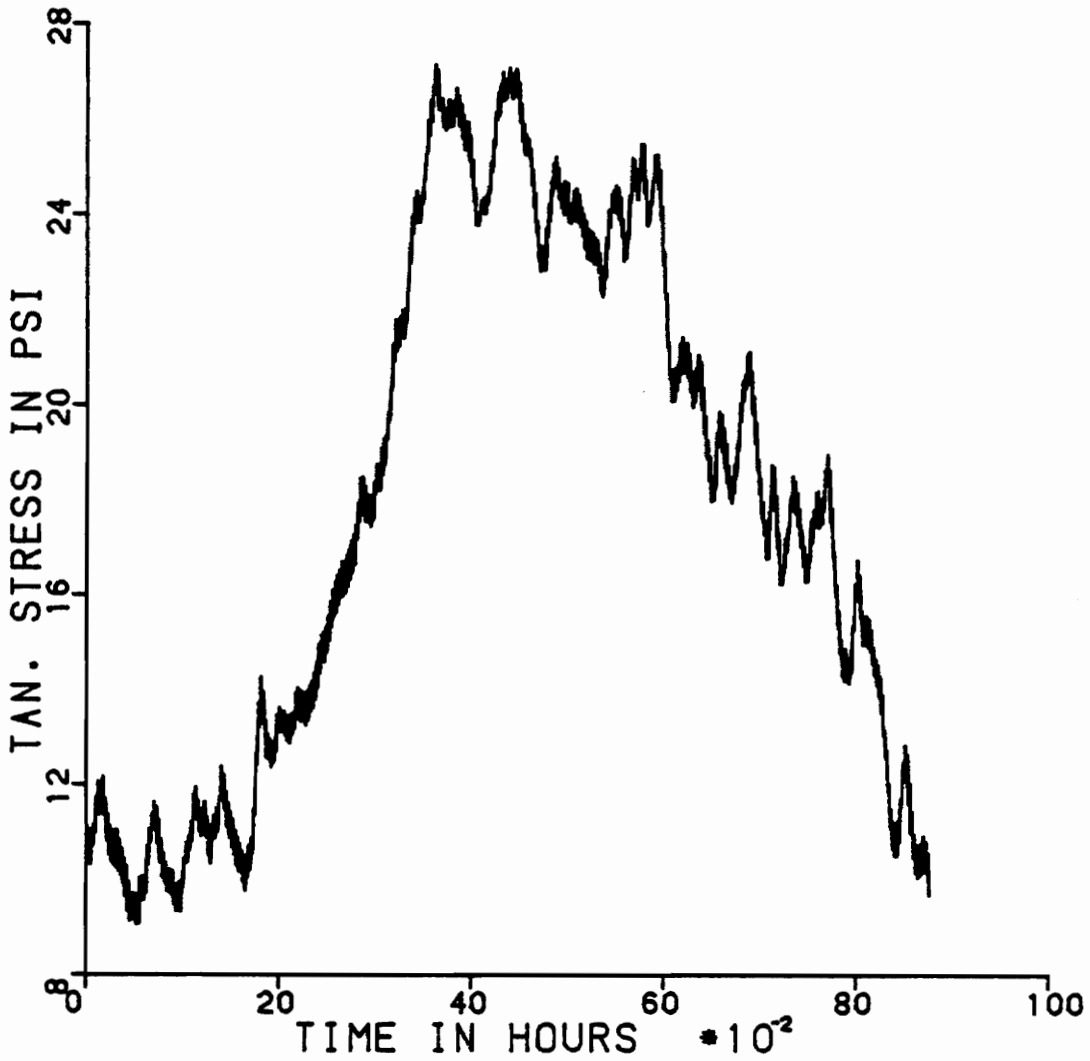

Figure 41. Tangential stress at the bore (thin cylinder) in one year (for inputs see Figs. 27, 28, 29).

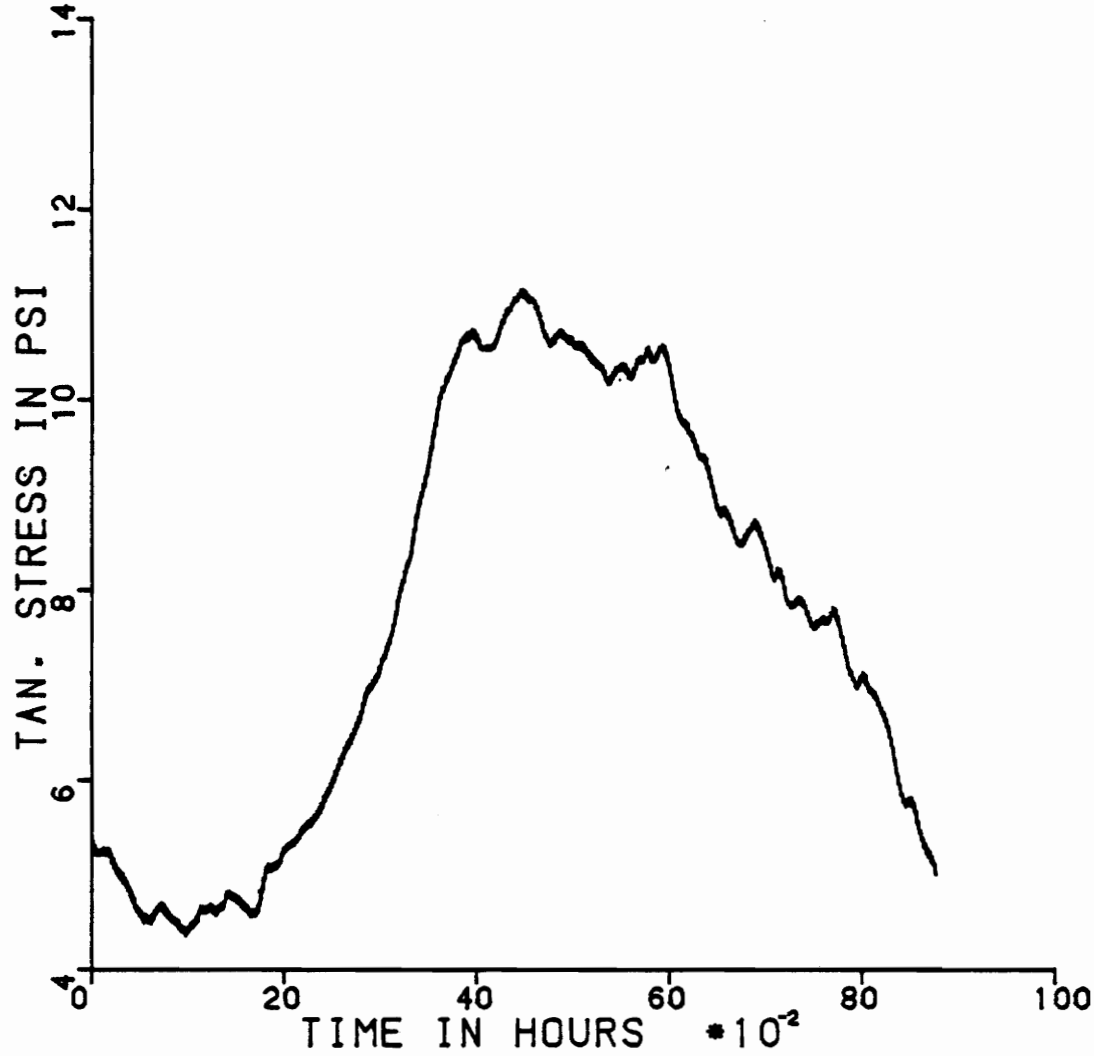

Figure 42. Tangential stress at the bore (thick cylinder) in one year (for inputs see Figs. 27, 28, 29).

should be clear that the induced thermal stress in the thin cylinder is higher than that of the thick cylinder throughout the year.

With reference to Part V earlier, the probability of failure can be obtained from the given strength and strain capacity of the materials involved and the induced stress and strain. It is found that the tangential stress at the bore is the largest tensile stress of all the stress components. Although other components of stress and strain at the bore and interface exist, they are insignificant compared to the tangential stress at the bore. By using the method presented in Part V the probability of failure of the propellant at the bore is calculated first for each day and then for each month. Figs. 43 and 44 illustrate the daily probability of failure for the thin and thick cylinders. Figs. 45 and 46 illustrate the progressive daily probability of failure for two cylinders. Again, as expected, the probability of failure of the thin cylinder is higher than that for the thicker one.

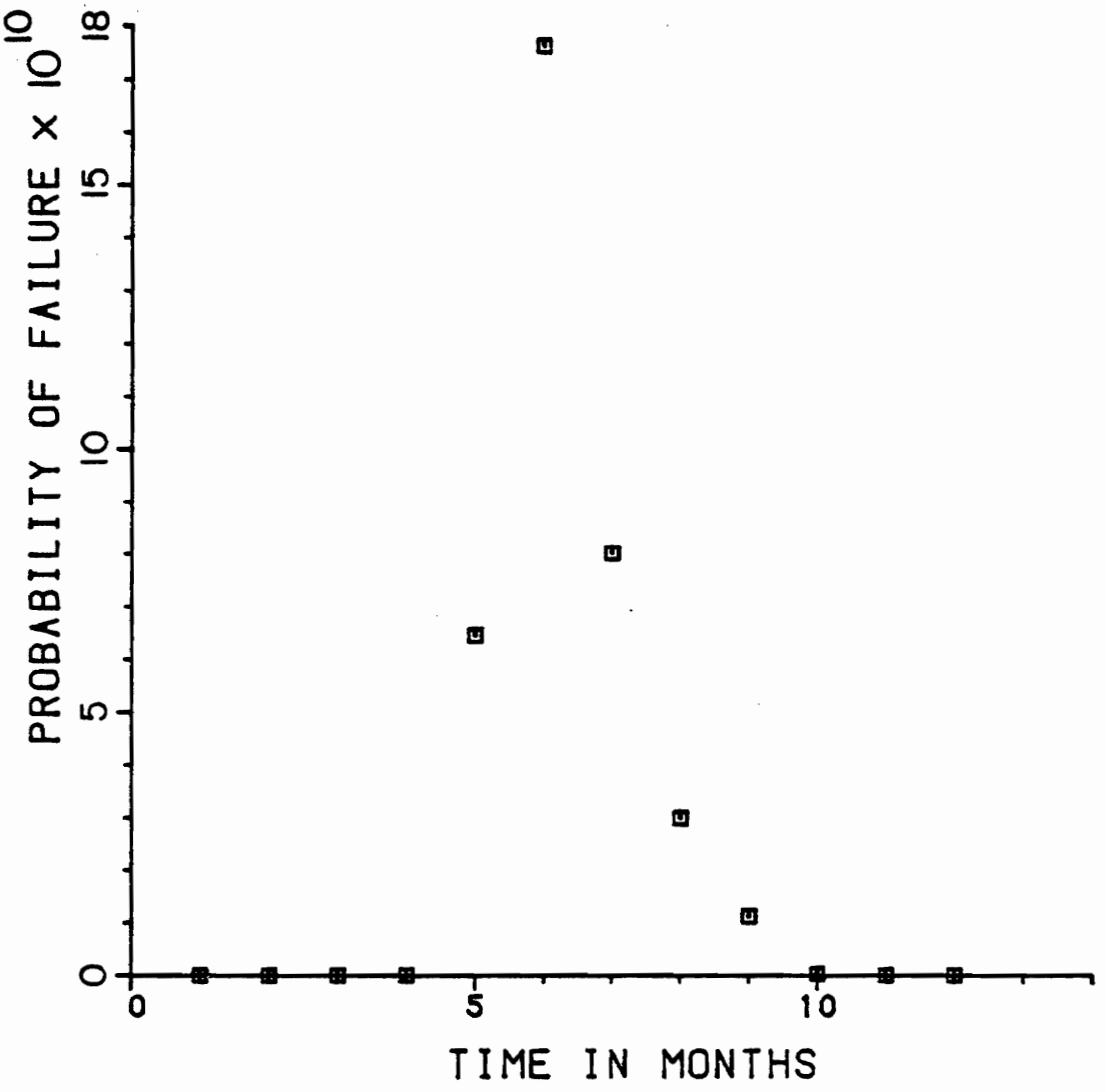

Figure 43. Daily probability of failure due to tangential stress at the bore (thin cylinder).

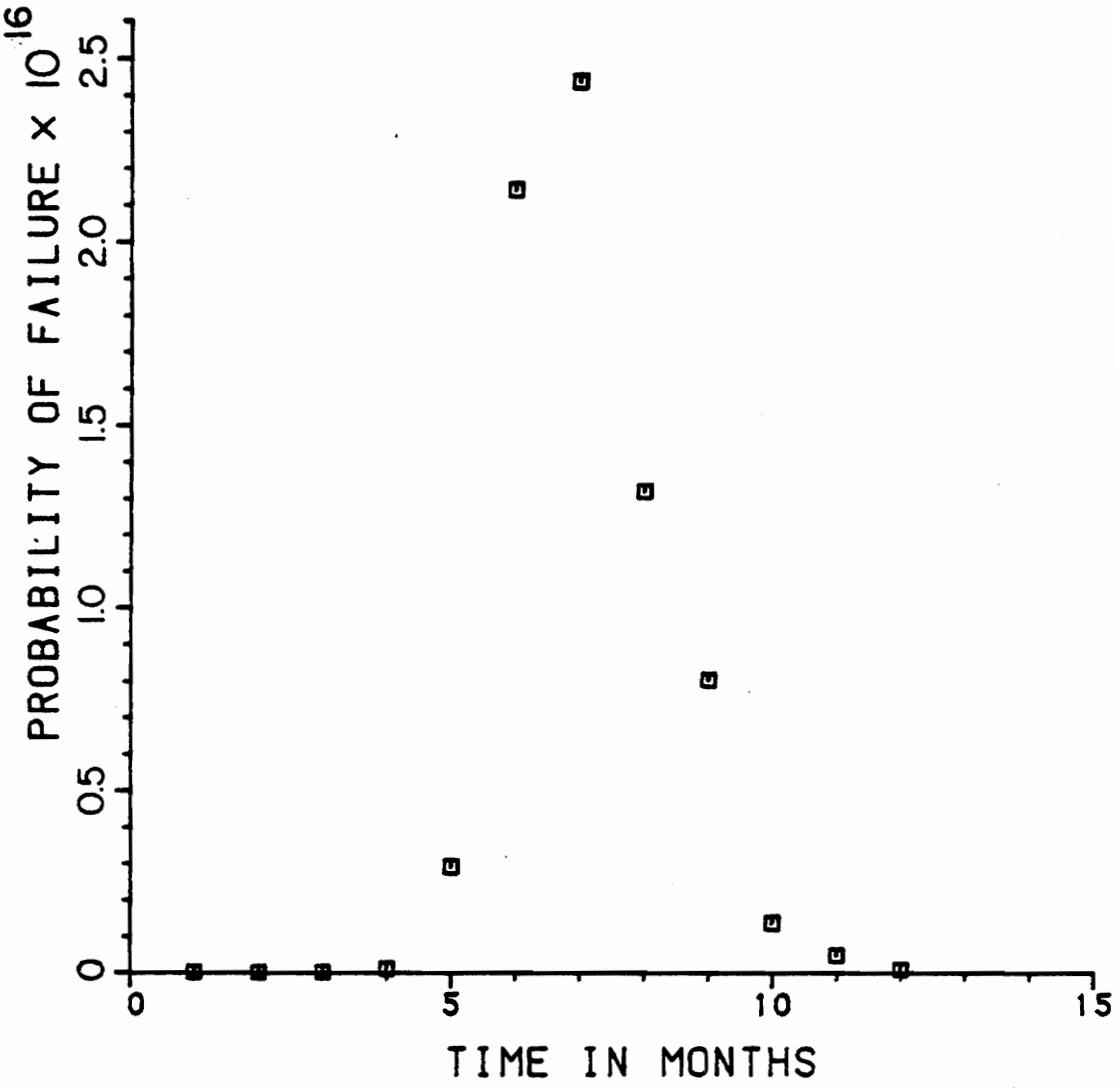

Figure 44. Daily probability of failure due to tangential stress at the bore (thick cylinder).

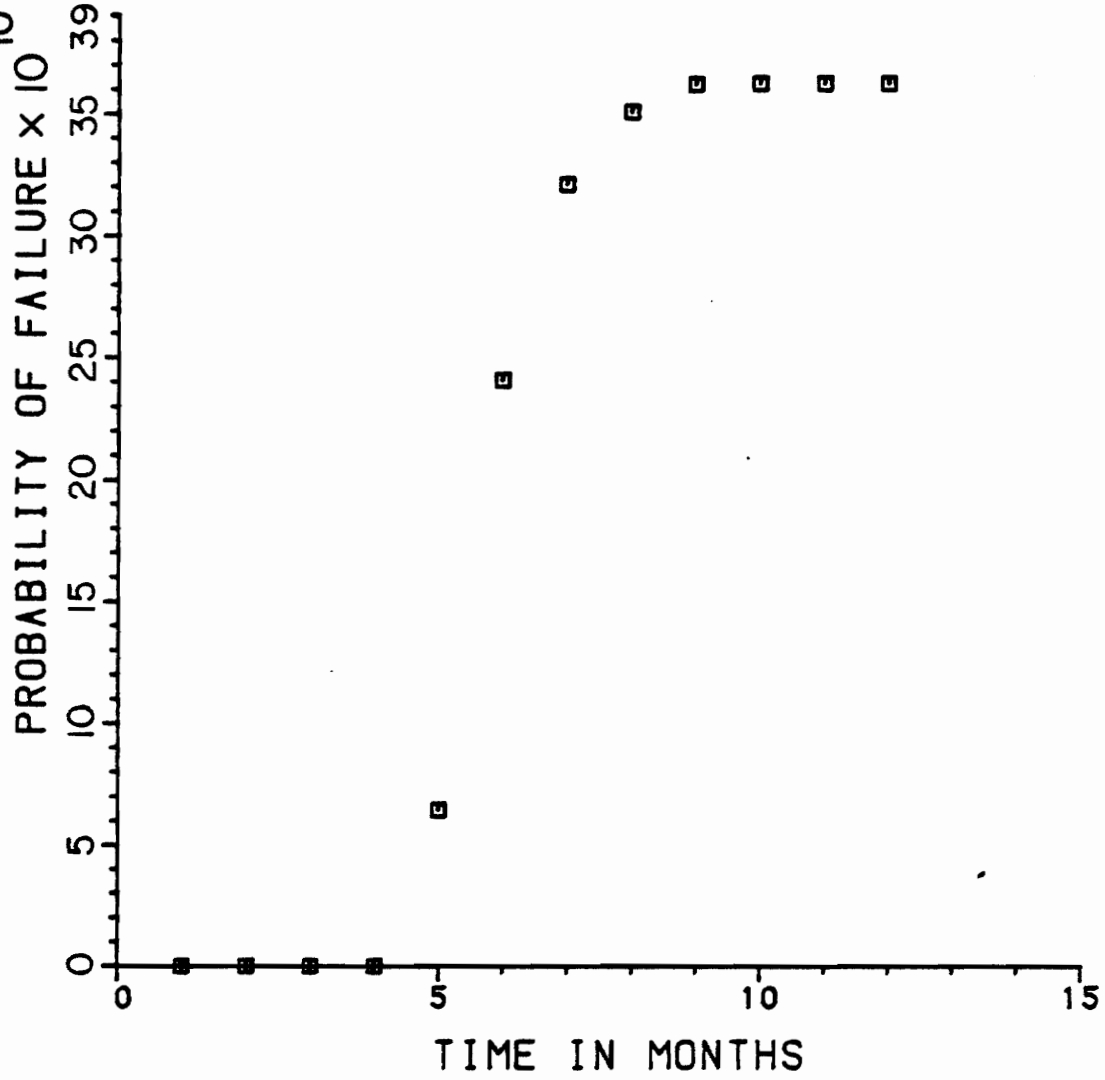

Figure 45. Yearly probability of failure due to tangential stress at the bore (thin cylinder).

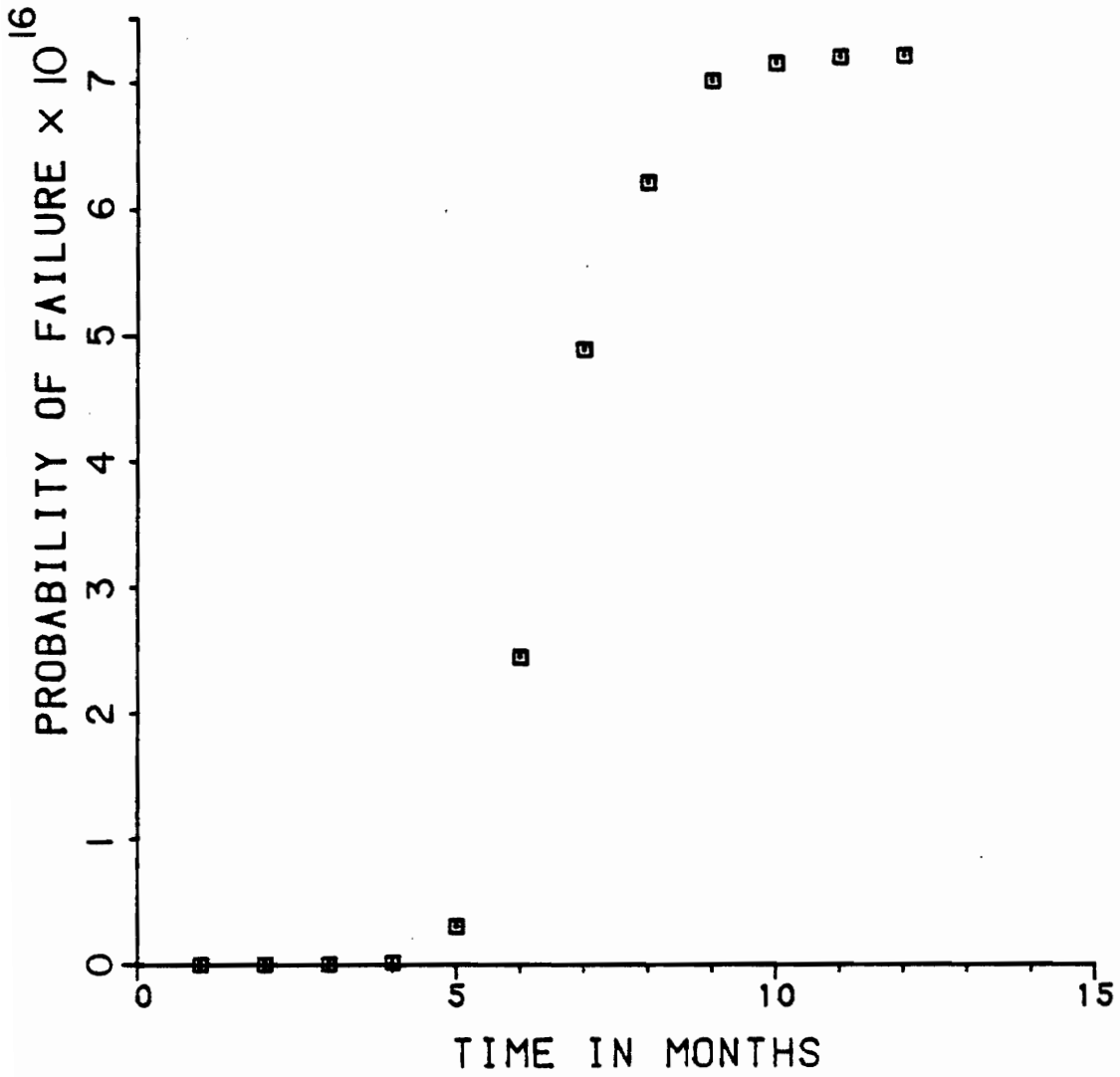

Figure 46. Yearly probability of failure due to tangential stress at the bore (thick cylinder).

VII. DISCUSSION AND CONCLUSION

A cylinder with 5 layers which is subjected to complex boundary conditions where air temperature, solar radiation and wind speed have been included as inputs, has been analyzed. It is known that, for a similar problem, other investigators [10,12,13] assumed that the surface temperature is identical to the air temperature. In this analysis, the surface temperature was evaluated from given environmental conditions.

It has been found that the proposed finite difference scheme has provided a satisfactory means of obtaining temperature responses at various locations across the cylinder. Other investigators [12,13] used the finite element method to obtain solutions for a simpler case (uninsulated cylinder). It has been seen that the implicit scheme used in this investigation provided a close agreement with the closed form solution, when the same inputs were used, as well as with experimental data.

The difference between the curing and current temperature produces stresses and strains in the propellant. A numerical integration has been used to obtain these induced stresses and strains for an elastic motor.

A statistical analysis permitted the evaluation of the probability of failure of the propellant for the year of interest. Of all the stress and strain components, the tangential stress at the bore was found to be the most likely cause of failure. Although other

components exist but contribute only a very small portion (as compared to the tangential stress at the bore) to the probability of failure.

REFERENCES

1. Dahl, O. G. C., "Temperature and Stress Distribution in Hollow Cylinders," Transactions, American Society of Mechanical Engineers, Vol. 46, 1924, pp. 161-208.

2. Kent, C. H., "Thermal Stresses in Spheres and Cylinders," Trans. A.S.M.E., Vol. 54, 1932, pp. 185-196.

3. Poritsky, H., "Analysis of Thermal Stresses in Sealed Cylinders, and the Effect of Viscous Flow during Annealing," Physics, Vol. 5, 1934, pp. 406-411.

4. Gatewood, B. E., "Note on the Thermal Stresses in a Long Cylinder of (m + 1) Concentric Materials," Quart. Appl. Math., Vol. 6, April 1948, p. 84.

5. Williams, M. L., Blatz, P. J., and Shapery, R. A., "Fundamental Studies Relating to Systems Analysis of Solid Propellants," GALCIT, SM 61-5, California Institute of Technology, Pasadena, Calif., 1961, pp. 165-166.

6. Heller, R. A., "Temperature Response of an Infinitely Thick Slab to Random Surface Temperatures," Mech. Res. Communications, V. 3, pp. 379-385, 1976.

7. Heller, R. A., "Thermal Stress as a Narrow-Band Random Load," Am. Soc. Civil Eng., EMS. No. 12450, October 1976, pp. 787-805.

8. Heller, R. A., "Life Prediction of Dump Stored Motors with Statistically Varying Strength and Temperature," U.S. Army Missile Command, Redstone Arsenal, Alabama, TR. RK-76-12, April 1976.

9. Heller, R. A., and Kamat, M. P., "Probabilistic Life Prediction for Rocket Motors Subjected to Random Thermal Lods," Chemical Propulsion Information Agency. 14th JANNAF Structures and Mechanical Working Group Meeting. February 15-17, 1977, Laurel, Md.

10. Heller, R. A., and Kamat, M. P., "Service Life Prediction for Solid Propellant Motors," Paper No. 78-486, AIAA 19th S&SDM Conference, April 3-5, 1978, Bethesda, Md.

11. Heller, R. A., and Singh, P., "Probability of Motor Failures due to Environmental Effects," U.S. Army Missile Command, No. T-CR-78-11 (Part I), March 1978.

12. Cost, T. L., "Computer Simulation of Solid Rocket Motor Service Life for Thermal Loads," U.S. Army Missile Command, Redstone Arsenal, Alabama, No. T-CR-78-9, March 1978.

13. Okono, A. J., "Thermal Stress Analysis and Life Prediction of a Time-Temperature Dependent Viscoelastic Hollow Cylinder Subjected to Random Temperature," Ph.D. Thesis, Virginia Polytechnic Institute and State University, December 1978.

14. Dempsey, B. J., and Thompson, M. R., "A Heat-Transfer Model for Evaluating Frost Action and Temperature-Related Effects in Multilayered Pavement Systems," HRR No. 342, 1970, pp. 39-56.

15. Straub, A. L., Schenck, H. N., and Przybycien, F. E., "Bituminous Pavement Temperature Related to Climate," HRR No. 256, 1968, pp. 53-76.

16. Barber, E. S., "Calculation of Maximum Pavement Temperatures from Weather Reports," HRB Bull. 168, 1957, pp. 1-8.

17. Idso, S. B., and Jackson, R. D., "Thermal Radiation from the Atmosphere," Journal of Geophysical Research, Vol. 74, No. 23, 1969.

18. Geiger, R., "The Climate Near the Ground," Harvard University Press, Third Printing, 1971, p. 20.

19. Cooke, N., and Hunt, B., "Thermal Calculations for Bridge Design," Journal of the Structural Division, ST9, pp. 1763-1781, Sept. 1975.

20. Vehrencamp, J. E., "Experimental Investigation of Heat Transfer at an Air-Earth Interface," Trans. Amer. Geophysical Union, Vol. 34, No. 1, 1953, pp. 22-29.

21. Alford, T. S., Ryan, J. E., and Urban, F. O., "Effect of Heat Storage and Variation in Outdoor Temperature and Solar Intensity on Heat Transfer Through Walls," Trans. ASH & VE, Vol. 45, 1939, p. 384.

22. Ulrich, R. D., "Evolution of the NWC Thermal Standard," Part 1, Naval Weapons Center, China Lake, California, NWC TP 4834, Feb. 1970.

23. Scott, R. F., "Estimation of the Heat-Transfer Coefficient Between Air and the Ground Surface," Trans. Amer. Geophysical Union, Washington, D.C., Vol. 38, No. 1, 1957.

24. Berg, R. L., "Energy Balance on a Paved Surface," U.S. Army Terrestrial Science Center, Hanover, N.H., 1968.

FINITE DIFFERENCE APPROACH FOR PREDICTING PROBABILISTIC LIFE OF A COMPOSITE CYLINDER SUBJECTED TO RANDOM THERMAL LOADS

by

Vu N. Con

(ABSTRACT)

A long hollow cylinder with five layers, subjected to a random thermal environment is analyzed.

The random thermal environment includes the ambient air temperature, solar radiation and wind speed. The location of interest is Phoenix, Arizona.

The governing differential equation is the so-called one-dimensional Fourier heat conduction equation in cylindrical coordinates. An implicit finite difference scheme is developed to obtain temperature responses inside the cylinder. Given the linear elastic behavior of materials involved, induced stresses and strains are evaluated at the end of each time step of the finite difference scheme.

A statistical analysis is then carried out to determine the probability of failure of the propellant and hence the service life of the motor can be computed.